Ministry of Water Resources

Bangladesh Water Development Board

Coastal Embankment Improvement Project, Phase-I (CEIP-I)

Long Term Monitoring, Research and Analysis of Bangladesh Coastal Zone (Sustainable Polders Adapted to Coastal Dynamics)

Pussur River: Meso scale bank erosion modelling - current situation & future projections

Joint Venture of DHI The expert in WATER ENVIRONMENTS & Deltares Enabling Delta Life

in association with IWM, Bangladesh and University of Colorado, Boulder and Columbia University

May 2022

Ministry of Water Resources

Bangladesh Water Development Board

Coastal Embankment Improvement Project, Phase-I (CEIP-I)

Long Term Monitoring, Research and Analysis of Bangladesh Coastal Zone (Sustainable Polders Adapted to Coastal Dynamics)

Pussur River: Meso scale bank erosion modelling - current situation & future projections

May 2022

Joint Venture of DHI The expert in WATER ENVIRONMENTS & Deltares Enabling Delta Life

in association with IWM Water Environment & Climate

University of Colorado, Boulder, USA
Columbia University, USA

Bangladesh Water Development Board
Coastal Embankment Improvement Project, Phase-I (CEIP-I)
Long Term Monitoring, Research and Analysis of Bangladesh Coastal Zone
Office: Flat #3/B, House #4, Road #23/A, Banani, Dhaka 1213, BANGLADESH Phone +880 1307 693299

Memo No: CEIP/LTMRA/0622/170 5 June 2022

Project Management Unit
Coastal Embankment Improvement Project, Phase-I (CEIP-I)
Pani Bhaban, Level-10
72, Green Road, Dhaka-1205

Attn: Mr. Syed Hasan Imam, Project Director

Dear Mr Imam,

Subject: Submission of the Pussur River: Meso Scale Bank Erosion Modelling – current situation and future projections (D-4A-2:1,2&3)

It is our pleasure to submit herewith five copies of the Report Titled ***"Pussur River: Meso Scale Bank Erosion Modelling – Current situation & future projections".*** According to the World Bank Tracker, this report falls under component ***D-4A-2:1,2&3.***

This report includes both model development and applications. The model development report titled "Meso scale bank erosion modelling – current situation – interim report" was submitted earlier and was reviewed by the World Bank. DHI revised the interim report to address the review and extended to include future projections.

There are five chapters in this report. Chapter 1 is the introduction chapter describing the background, objective and approach. Chapter 2 gives an overview on the availability of measurement data and how the data was processed. The development and calibration/validation of the model are described in Chapter 3. Model applications are documented in chapter 4, while the report finalizes with conclusions in Chapter 5.

Thanking you,

Yours sincerely,

Dr Ranjit Galappatti
Team Leader

Copies: Engineer Fazlur Rashid, Director General, BWDB
Dr. Zia Uddin Baig, ADG (Planning), BWDB
Dr Kim Wium Olesen, Project Manager, DHI
Ms. Sonja Pans, Deltares Project Manager
Mr Zahirul Haque Khan, Deputy Team Leader
Mr AKM Bodruddoza, Procurement Specialist
Swarna Kazi, Sr. Disaster Risk Management Specialist, World Bank

CONTENTS

FIGURES

TABLES

APPENDICES

ACRONYMS AND ABBREVIATIONS

ADCP	Acoustic Doppler Current Profiler
BDP2100	Bangladesh Delta Plan 2100
BIWTA	Bangladesh Inland Water Transport Authority
BMD	Bangladesh Meteorological Department
BoB	Bay of Bengal
BWDB	Bangladesh Water Development Board
CBA	Coast Benefit Analysis
CCP	Chittagong Coastal Plain
CDMP	Comprehensive Disaster Management Program
CDSP	Char Development Settlement Project
CEA	Cost Effectiveness Analysis
CEGIS	Centre for Environmental and Geographic Information Services
CEIP	Coastal Embankment Improvement Project
CEP	Coastal Embankment Project
CERP	Coastal Embankment Rehabilitation Project
CPA	Chittagong Port Authority
CPP	Cyclone Protection Project
CSPS	Cyclone Shelter Preparatory Study
DDM	Department of Disaster Management
DEM	Digital Elevation Model
DOE	Department of Environment
EDP	Estuary Development Program
EHRM	Eastern Hilly Regional Model
FAP	Flood Action Plan
FM	Flexible Mesh
FFWC	Flood Forecasting and Warning Centre
GBM	Ganges Brahmaputra Meghna
GCM	General Circulation Model

GIS	Geographical Information System
GRRP	Gorai River Restoration Project
GTPE	Ganges Tidal Plain East
GTPW	Ganges Tidal Plain West
HD	Hydrodynamic
InSAR	Interferometric Synthetic Aperture Radar
IPCC	Intergovernmental Panel for Climate Change
IPSWAM	Integrated Planning for Sustainable Water Management
IWM	Institute of Water Modelling
LCC	Life Cycle Costs
LGED	Local Government Engineering Department
LGI	local Government Institute
LRP	Land Reclamation Project
MCA	Multi Criteria Analysis
MES	Meghna Estuary Study
MIKE 11	DHI's 1-dimensional hydraulic model
MIKE 21C	DHI's 2-dimensional model made specifically for river morphology
MIKE FM	DHI's 2-dimensional flexible mesh flow model
MoWR	Ministry of Water Resources
MPA	Mongla Port Authority
MSL	Mean Sea Level
NAM	Nedbor Afstromnings Model
PPMM	Participatory Polder Management Model
PSD	Particle Size Distribution
PWD	Public Works Datum
RCP	Representative Concentration Pathways
RTK	Real-Time Kinematic
SET-MH	Surface Elevation Tables – Marker Horizons
SLR	Sea Level Rise
SOB	Survey of Bangladesh
SSC	Suspended Sediment Concentration
SWMC	Surface Water Modelling Centre

SWRM	South West Region Model
TBM	Temporary Bench Mark
TRM	Tidal River Management
ToR	Terms of Reference
UTM	Universal Transverse Mercator
WARPO	Water Resources Planning Organization
WL	Water Level

EXECUTIVE SUMMARY

DHI and IWM studied five rivers in the coastal zone of Bangladesh as part of the project "Long Term Monitoring, Research and Analysis of Bangladesh Coastal Zone (Sustainable Polders Adapted to Coastal Dynamics)".

This Executive Summary applies to all meso-scale bank erosion models and reports developed during the study. The same Executive Summary can be found in all five model reports.

The main objectives of the modelling study were to develop predictive bank erosion tools for selected rivers and to estimate future bank line changes under different scenarios.

The five rivers were studied with emphasis on meso-scale bank erosion, and the rivers listed from west to east are: Sibsa, Pussur, Baleswar, Bishkhali and Sangu. The four rivers in the SW region of Bangladesh are all tidally dominated, while the Sangu in morphological terms is dominated by the monsoon hydrograph.

One report was issued for each of the studied rivers. The same overall modelling approach was used for all five rivers, and therefore all the reports followed the same template.

The overall approach can be summarized into:

- Preliminary study of historical bank erosion in the larger tidal rivers by using satellite imagery
- Digitization of historical bank lines (Landsat) for the selected rivers
- Review of publications related to bank erosion with the emphasis on identifying the most suited bank erosion description for the tidal rivers in Bangladesh
- Setup, calibration, and validation of the model with field measurements and remote sensing data
- Morphological hindcast – reproduce historical bathymetric and bank line shifting
- Scenario runs - study future changes in the morphological processes based on possible scenarios, e.g. climate change, upstream development and subsidence
- Output - geospatial datasets of present erosion and sedimentation in the river system for various seasons and for possible scenarios

The following data were required for each model:

- Bathymetries
- Hydrometric data (water levels and discharges)
- Sediment bed samples
- Sediment bank material samples
- Suspended sediment concentrations
- Suspended sediment particle size distributions
- Historical bank lines from satellite imagery

All meso-scale bank erosion reports follow this template:

- Introduction
- Data
- Model development
- Model application
- Conclusions

Bank erosion
Bank erosion patterns in Bangladesh vary significantly from the monsoon dominated fluvial rivers to the tidally dominated muddy rivers. Two main reasons were identified in the study:

Firstly, tidal flow: The monsoon dominated rivers exhibit large imbalances between the dry season and monsoon, while the tidally dominated rivers do not show this imbalance, but instead exhibit similar discharge amplitudes during the dry season and monsoon. Due to this, the monsoon dominated rivers will experience very high morphological activity during the monsoon, which will be followed by high bank erosion rates, while the tidal rivers are better adjusted morphologically to the hydraulic conditions all year. In practice, monsoon dominated rivers are morphologically inactive during the dry season.

Secondly, cohesion: The tidally dominated rivers have cohesive banks, which are erosion resistant, while the sandy banks in most inland fluvial rivers have much higher erodibility.

The difference between fluvial and tidal rivers is significant and can also be followed along the coastal zone with strong tidal dominance in the west and monsoon dominance in the east. The increase in erosion from west to east can even be followed gradually from the Baleswar to the Bishkhali and increases further in the Sangu River.

Bank erosion rates in the tidally dominated muddy rivers are typically 5-10 m/year, while the rivers are kilometres wide, hence annual erosion is less than 1% of the width. Further to the east, bank erosion increased markedly in the Bishkhali and increases dramatically in the Lower Meghna and Sangu when measured relatively to the width (the absolute erosion rates in Lower Meghna are measured in hundreds of meters per year, while Sangu is narrow).

<u>The value of Landsat data in Bangladesh</u>
In most countries, Landsat data (30 m satellite imagery) is of little use for determining bank line movements due to the lack of resolution in the images compared to bank erosion rates. However, in Bangladesh, Landsat imagery is extremely useful because bank erosion rates are high. Although annual bank erosion cannot be followed in the tidal rivers from Landsat images, bank erosion over 5-10 years can be tracked accurately in the Landsat imagery. The Landsat data hence became a prism through which bank erosion in the past could be identified accurately.

The relatively slow bank erosion in the tidally dominated rivers was also found through data analysis to be systematic, such that a bank eroding in 1988 is extremely likely also to be eroding in 2019, and more or less with the same rate.

<u>Model development template</u>
The model development followed this template:

- Select model extent
- Develop curvilinear grid
- Interpolate bathymetry data to the curvilinear grid
- Extract hydrometric boundary conditions from e.g. the South West Regional Model (SWRM)
- Develop sediment transport boundary conditions
- Calibrate hydrodynamic model to observed water levels
- Calibrate sediment transport and morphological model to observed bed level changes
- Calibrate bank erosion model to observed bank line changes

The models were developed as hydro-morphological models with bank erosion included and physically moving the curvilinear grids to account for bank line changes. Model calibration was performed in depth by using the period 2011-2019 as hindcast, which was found ideal due to the two bathymetry datasets typically collected in 2011 and 2019 by IWM with almost identical resolution and accuracy. The value of such data cannot be overstated, and by combining with bank erosion obtained from Landsat data in the same period, the models could be calibrated in depth. There are exceptions to this, namely that no 2011 bathymetry was available for Bishkhali River, while Sangu River was calibrated to 2018-2020 for which good data was available.

The calibration of the tidally dominated rivers resulted in very similar calibration parameters, especially the silt transport models and bank erosion formulas were almost identical in the rivers.

Bank erosion mechanics and formula

The bank erosion formula is central to the simulated behaviour of the rivers. Several bank erosion descriptions were investigated in detail in the models, and the optimal choice was found to be a formula derived from Hasegawa (1989). The Hasegawa model is based on a near-bank excess velocity approach, which means that bank erosion occurs when the near-bank flow speed is higher than the cross-section average flow speed. This could in principle have been adopted in the model engine, but it was found to give some practical problems because the Hasegawa formula was developed for meandering rivers with an outer bend and associated bend scour, which is not always the layout for the tidal rivers. Hence, the formula was modified by estimating the excess flow speed from the near-bank flow speed and an estimated average flow depth using the Manning formula. This resulted in bank erosion derived from the near-bank flow speed and water depth, notably bank erosion is proportional to the near-bank flow speed and a function of the water depth, such that the water depth must exceed a characteristic average depth for bank erosion to occur and then it will increase with depth beyond this limit.

Several bank erosion expressions were found calibratable to observed bank erosion, even with significant variations in the described mechanics. The best calibration was obtained by simply using a critical bank height (Mosselman, 1995) beyond which bank erosion increases with the exceedance of the bank height beyond the critical height. However, this was found mechanistically problematic because it does not state anything about erosive fluid forces along the bank, and hence bank erosion would continue along any bank independent of the flow along the bank, if the bank height exceeded the critical limit.

Bank erosion calibration using the Hasegawa derived formula is only slightly less accurate than for the critical height formulation, and Hasegawa has a solid theoretical foundation in addition to its inclusion of the flow speed along the bank. Hence, all taken into consideration, there was no doubt that Hasegawa was the correct choice.

Several traditional bank erosion descriptions were tested without success. For instance, a simple bank erosion description is to derive bank erosion from near-bank scouring; however, this does not work in the tidal rivers because the description is only valid for sandy banks. Surprisingly, relating the bank erosion rate to the shear stress was initially found to give a bad description of bank erosion. This was also the case when relating bank erosion rate to the flow speed without considering water depth.

It is important to understand that in addition to being able to describe the bank line changes over time, the bank erosion formula also needs to describe the physical processes in a lumped manner. The adopted Hasegawa derived formula derives bank erosion from flow speed and water depth, which proved to be the two most important variables.

Limitations in the models and data

In general, the models developed suffer from similar limitations, which are also related to the lack of specific types of data. The limitations are listed in the order of importance.

In particular, all models show that simulated bar formation is sensitive to flow resistance used in the models and that the flow resistance calibrations adopted in the models are only one variant in a calibration space. Detailed investigations were conducted to show that different resistance models can be developed to yield the same simulated water levels but resulting in different velocity distributions between bars and channels as well as different sediment transport patterns and hence different bar sizes. Essentially the models have calibration spaces where the true calibration cannot be identified solely by matching water levels. Consequently, the bathymetry and bank erosion behaviours can vary significantly. The best approach for reducing calibration uncertainties is to collect ADCP velocity profiles, but this was not done as part of the present project.

The sensitivity of bar development to the flow resistance model used is very pronounced. For instance, a constant resistance number applied in a model can cause bars to erode in a manner where the deep channel will be located where the bar should be located and vice versa. In turn, this will lead to a simulated bank erosion where the erosion pattern essentially becomes the opposite of the observed. Due to feedback in the river morphology, this can also cause other bars to behave incorrectly. The implication of this sensitivity is that when the model simulates the right morphological development, this is a strong indication that the right resistance model has been applied.

The models also suffer from uncertainties in the calibration of sediment concentrations. This comes back to the traditional way of collecting data in Bangladesh, namely the standard collection of total sediment concentrations (i.e. the combined concentration of clay, silt and (fine) sand). The tidal rivers contain significant clay concentrations, which do not contribute morphologically. In the tidal rivers only the silt transport contributes to the morphological development since the sand concentration is negligible. Hence, it is not possible to calibrate silt transport models to the observed concentrations, as the observations generally only show the total concentration. However, observed particle size distribution data was available only in a few cases.

Only a handful of bank sediment samples were available. The erosion resistance of banks depends on the sediment composition of the banks. Bank erosion plays an important role in the river morphology, in some of the rivers contributing significantly to sedimentation, but the particle size distributions in the banks is largely unknown.

Rivers with mixed sediments require many bed samples to identify the particle size distribution in the riverbed. All the tidally dominated rivers are probably characterized by a mixture of sand and silt (while clay is morphologically inactive), but it was only possible for some of the rivers to identify this mixture, and none of the rivers had enough bed samples to determine the spatial distribution of the bed sediment composition.

The limitations of the available dataset have probably impacted the quality of the calibration of the models. However, the fact that the models all predict the overall morphology of the rivers quite well, including bank line migration and erosion/deposition pattern of the riverbeds, gives some confidence that also flow distribution, sediment transport etc. are well represented in the final model calibrations. Further model improvements can be made at a later stage if/when additional data collection is carried out. IWM has the capacity to conduct the necessary data collection.

<u>Model applications</u>
Model applications included the following:

- Projection of bank lines 30 years into the future
- Impact of climate change
- Impacts of bank protection on bank erosion and bed levels
- Dredging of shoals to mitigate or eliminate bank erosion
- Access to Mongla Port

Projection of bank lines 30 years into the future
The most important deliverable of the project was projected bank lines 30 years into the future for the four tidally dominated rivers in the west (Sibsa, Pussur, Baleswar and Bishkhali). The future projections showed that most of the banks currently eroding will continue eroding in the future with more or less the same rates. Hence, the future development was essentially projected to be similar to the 1988-2019 development. This is a very important finding that can be utilized for planning and managing polders and embankments. There are deviations from the overall systematic behaviour, but these are few in numbers. The projected future bank lines were also submitted to the CEIP-2 feasibility study in digital format (line themes) in order to maximize the value to planners and decision makers. Projection of bank erosion 30 years into the future is not meaningful for the Sangu River because the erosion rates are too high compared to the river width for projections on such timescale and was therefore not conducted.

Impact of climate change
In most of the models, climate change increases the tidal flow amplitude slightly, leading to a small increase in bank erosion. However, the impact of climate change is small compared to the absolute future bank line changes. Hence, the impact of climate change on future bank lines is modest.

Impacts of bank protection on bank erosion and bed levels
Bank protection was also shown to induce scouring due to the removal of sediment sources associated with bank erosion. The effect on bed levels is not insignificant, while bank erosion impacts are small. The models do not suggest that local bank protection will cause significant changes to the erosion of other banks, which is an important conclusion to keep in mind for management purposes, i.e. eroding banks do not seem to significantly influence each other in the tidal rivers.

Dredging of shoals to mitigate or eliminate bank erosion
The use of dredging of shoals located opposite of eroding banks was tested in the Baleswar River. The model results suggest that shoal dredging is potentially very effective at reducing bank erosion, especially if combined with backfilling of dredged spoils in the deep channel along the eroding bank. Unfortunately, this cannot be conducted simply by dumping the spoils in the deep channel due to the settling length for the silt exceeding the length of the eroding bank. However, the impact of shoals dredging combined with filling the deep channel essentially eliminates bank erosion over a long timescale and should be studied further, assuming that the filling problem can be addressed. A simple approach using geotextile (e.g. jute) bags to secure sedimentation in the deep channels was proposed, but needs to be investigated further and tested.

Access to Mongla Port
A separate investigation was also carried out for Mongla Port. Several scenarios were tested using the model, including quantification of the impact of Ganges Barrage, bank protection, closing and/or regulating upstream connections to Sibsa, guide bunds at Mongla, and TRM applied to Pussur or Sibsa. The investigation confirmed that the fundamental problem with Mongla Port is that the Sibsa incoming flood tide occupies (captures) most of the tidal prism located upstream of Mongla Port, preventing the incoming slower tide in the shallower Pussur River from occupying the tidal prism. The Pussur flood tide hence stagnates at Mongla Port, making the port susceptible to sedimentation, and model results show that Mongla Port indeed has the highest sedimentation rate in the Pussur River. The only way to really fix the sedimentation problem is to prevent the Sibsa from capturing tidal prism from the Pussur, while other schemes do not really solve the underlying problem, although they can act to mitigate. Schemes involving attempts to add tidal prism to the Pussur are remarkably ineffective due to the always faster flood tide in Sibsa, which will occupy tidal storage before Pussur. In effect adding tidal basins to Pussur downstream of Mongla Port just causes the Sibsa to capture more of the upstream tidal prism.

Conclusions
The conclusions from the study can be summarized into the following.

Bank erosion in the tidally dominated rivers of Bangladesh is slow and systematic, and therefore the predictability is very good, even over decades. This is a very important finding that can be utilized for planning and managing polders and embankments, for instance, designing embankments in safe distance from the eroding rivers, planning future retirement of embankments or when to implement bank erosion measures. On the contrary, fluvial systems in Bangladesh are known to have good predictability only over relatively short timescale, if even that.

The five developed models reflect the bank erosion predictability. For the four tidally dominated rivers, the bank erosion model was applied for projections 30 years into the future, while this is not meaningful for the Sangu River.

Although one should never take morphological predictions as accurate, the project team is confident that the future bank lines projected 30 years into the future are reliable enough for decision-making purposes. The predictable planform development should be exploited when managing polders and banks.

Dredging of shoals located opposite of eroding banks shows promising results, although only tested conceptually. The best outcome is achieved by combining dredging with dumping of the spoils into the deep channel flowing along the eroding bank, which will give two synergizing effects, namely attracting flow to the dredged flow path through the shoal and attracting less flow to the deep outer channel. There is a major practical issue with the approach, namely that it is not easy to dump the spoils into the outer channel. One proposal for handling this is to fill the spoils into geotextile bags and dump them in the outer channel, which is similar to the approach followed in some meandering rivers for navigation purposes (by preventing deep bend scour), but here done to prevent bank erosion (by also preventing deep bend scour).

For the Sangu and other fluvial systems, managing polders via predictable future bank lines is not meaningful. However, a river like the Sangu has a meander belt, which has good predictability, even if the bank lines themselves are difficult to predict. However, this may require allowing the Sangu River to move within its meander belt, which means accepting a loss of land area behind polders.

The model shows that Mongla Port has the highest sedimentation rate in the Pussur River model. In other words, Mongla Port happens to be located at the worst possible location for a port.

The Pussur River model was also applied to scenario testing at Mongla Port. The fundamental problem with Mongla Port is that it is located just south of the tidal meeting point between the Pussur and Sibsa tides, which has been understood for decades, and indeed some of the scenarios addressing this problem have been tested before. Several mitigation schemes were tested, and it was found that the most effective solution is to increase the Pussur tidal prism located upstream of Mongla Port. Getting the Pussur flood tide to flow north from Mongla can only be done by preventing the faster Sibsa flood tide from occupying the prism. Closing the three upstream connections to the Sibsa River was proposed and tested almost 30 years ago by DHI (1993), and the present study reverified the validity of this scheme. However, the scheme can be further developed by using regulators on the connection rivers to enhance the outgoing tide (ebb) at Monga Port, which is the driver for keeping the Mongla Port water depths sufficiently large. It was shown that closing the connections appears neutral in the Mongla Port bed levels, while significant scouring can be achieved with regulators, opening up for managing the Monga Port bathymetry by using the regulators to adjust the hydraulic dredging driven by the ebb flows.

The use of guide bunds at Mongla Port, proposed before, was investigated by using the MIKE 21C model. It was found that this scheme can sustain deep channels at Mongla Port, but it will also induce sedimentation further downstream due to the slightly reduced tidal discharges associated with the added flow resistance from the guide bunds. This suggests that the guide bund scheme cannot stand alone in solving the Mongla Port problem.

Various other schemes were also investigated, in particular increasing the tidal prism of the Pussur downstream of the tidal meeting point located upstream of Mongla Port. Schemes involving an increase in the Pussur tidal prism downstream of the tidal meeting point are problematic because they ultimately leave more tidal prism for the Sibsa flood tide to occupy from the Pussur upstream of Mongla Port.

A real solution to the Mongla Port problem must address the ability of the faster Sibsa flood tide to capture (from the Pussur) tidal prism upstream of Mongla Port, which is the fundamental problem. Mitigation schemes that do not address the fundamental problem do not seem to be able to stand alone.

1 Introduction

1.1 Background

Bangladesh is situated at the confluence of three great trans-Himalayan rivers, the Ganges, the Brahmaputra or Jamuna, and the Meghna, which form the Bengal (or GBM) Delta. While over 90 percent of the catchment of the GBM system lies outside of Bangladesh, more than 200 rivers and tributaries and distributaries of the GBM system drain through the country via a constantly changing network of channels, tidal inlets and creeks, forming the most active large delta on the planet. The coastal land mass is shaped by the interaction of large volumes of sediment laden water with the moderate to high tides of the Bay of Bengal.

Land in the coastal zone is built up by the deposition of river sediments in the tidal delta, including the mangroves of the Sundarbans, the largest mangrove forest in the world. The deposits of sand, silt, clay, and organic material form the land mass which, despite subsidence due to continuous consolidation of layers many kilometres deep, is kept around the level of the highest tides by the continuing deposition of sediments.

The coastal zone of Bangladesh spans over 710 km of coastline and is subject to multiple threats. Sixty-two percent of the coastal land has an elevation less than 3 meters above mean see level. With a sediment supply of 1 billion tons per year, this is the delta with the largest sediment supply in the world. This leads to continuing accretion of the land area in the coastal zone (5-10 km^2/year), mainly in the Meghna Estuary, but also erosion of the coast farther west. It has been observed that the land subsidence rate may vary from place to place due to anthropogenic factors such as drainage and ground water extraction as well as the properties and depth of underlying strata. On top of this there are tectonic plate movements, particularly in the eastern delta, that give rise to other changes in ground level.

The coastal lands, particularly in SW Bangladesh, being subject to regular flooding by saline water during high tides, could not be used for normal agricultural production in a country with a very high demand for land. The Coastal Embankment Project (CEP) was initiated in the 1950s and 1960s to build polders surrounded by embankments preventing the spilling of saline water onto the land at high tides. These embankments were built along the larger rivers and across the smaller rivers and creeks which then formed the drainage system within each polder and connected to the peripheral rivers via appropriately sized flap gate regulators, that open at low tide to let the drainage water out.

The Coastal Embankment Project enabled the reclamation of large tracts of land for agriculture from 1960 onwards. Polder building proceeded continuously until today. Up till now, 1.2 million hectares have been reclaimed in 139 active polders in the coastal zone of Bangladesh.

In over half a century of its existence, a number of challenges have surfaced that threaten the long-term safety and even the very existence of the polder system as a viable and sustainable resource. These are:

- Sea level rise and changes in precipitation and water discharge due to climate change
- Threats of damming and diversion to the delivery of river sediments from upstream
- Subsidence of lands (except where it has been allowed to be rebuilt by tidal flooding) and structures founded on existing land
- Drainage congestion due to accumulation of silt in some peripheral waterways around polders
- Changes in tidal hydrodynamics and related river erosion and siltation in the peripheral rivers of polders
- Increasing vulnerability to cyclones and storm surges

The main objective of the “Long-term monitoring, research and analysis of Bangladesh coastal zone” project is to create a framework for polder design, based on understanding of the long-term and large-scale dynamics of the delta and sustainable polder concepts. The field and modelling work within the project is carried out to improve understanding of the long-term and large-scale dynamics of the Ganges-Brahmaputra-Meghna (GBM) delta. There is insufficient knowledge about sediment budget in the delta involving sediment transport within the estuaries, sediment sources and sediment distribution into the river system. Sediment and tidal dynamics are important for river and coastal erosion, land reclamation, and delta development. Subsidence of the land alters the topography and hydrodynamics and increases flooding, coastal erosion and salinization. The knowledge of sediment dynamics, distribution, subsidence, erosion-deposition processes, sediment management at present and in the future under climate change, land use changes and proposed interventions in the upstream reaches of the Ganges Brahmaputra River systems is essential for the framework of polder design.

In the coastal zone of Bangladesh – both in the major estuaries and in the peripheral rivers of the polders – bank erosion is a significant problem even though the erosion rates are normally smaller than those encountered further upstream in the non-tidal main rivers (e.g. Padma, Brahmaputra). Failure of embankments in the coastal zone during storms has not always been as the result of overtopping. There have been many failures as a result of undermining of the toes of the embankment due to riverbank erosion. In fact, unexpectedly high levels of bank erosion have already been encountered in the execution of CEIP-1. This matter was highlighted in the Inception Workshop of this project leading to the recommendation that a special meso-scale study of “Bank Erosion Hindcasting” should be undertaken to analyse the bank erosion processes that have taken place in the large tidal estuaries in the last 20 or more years in areas where large and often intensive data collection programmes have been mounted for various projects. Improved guidelines for predicting medium term bank erosion are supposed to emerge from this study.

Figure 1-1 Revetment along Baleswar River (photo 11 February 2019).

1.2 Objective and Approach

The main objective of the modelling presented in this report is to develop a predictive bank erosion tool for the Pussur River and to estimate future bank line changes under different scenarios.

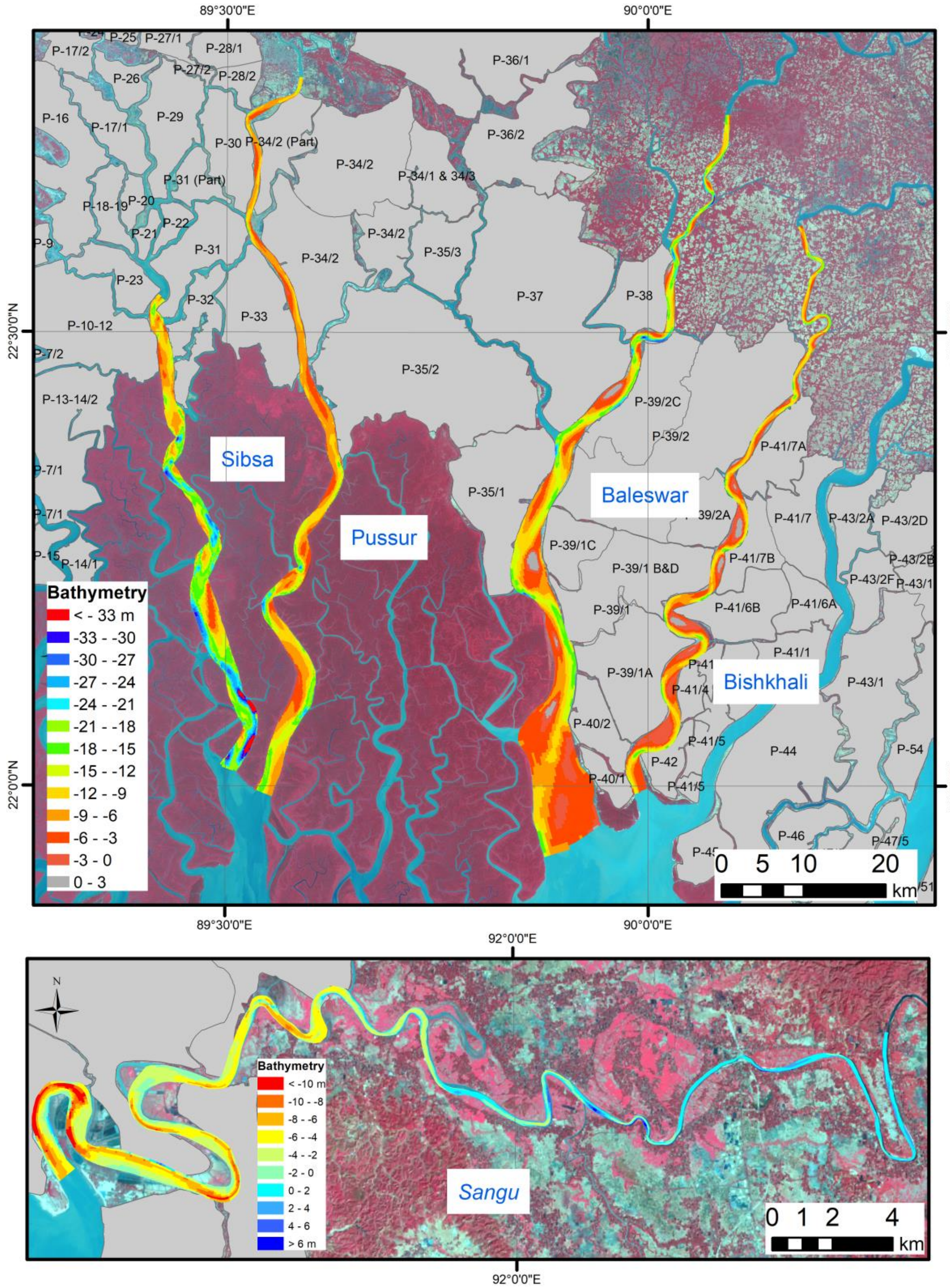

Figure 1-2 The five MIKE 21C models developed for the project.

The general approach for this modelling is the following:

- Preliminary study of historical bank erosion in the larger tidal rivers by using satellite imagery
- Digitization of historical bank lines (Landsat) for the selected rivers
- Review of publications related to bank erosion with the emphasis on identifying the most suited bank erosion description for the tidal rivers in Bangladesh
- Setup, calibration, and validation of the model with field measurements and remote sensing data
- Morphological hindcast – reproduce historical bathymetric and bank line shifting
- Scenario runs - study future changes in the morphological processes based on possible scenarios, e.g. climate change, upstream development and subsidence
- Output - geospatial datasets of present erosion and sedimentation in the river system for various seasons and for possible scenarios 25, 50 and 100 years from now, for various seasons and circumstances

The modelling is carried out using MIKE 21C. The key features of this modelling system are:

- Curvilinear boundary conforming grids allowing accurate representation of the river planform with relatively few grid points
- 2D Saint-Venant equations with a parallelized and optimized solver allowing time-true simulations covering several years
- Helical flow
- Multi-fraction sediment framework covering mixtures of clay, silt, sand, gravel
- Bed-load calculated with inclusion of helical flow and bed slope
- Suspended load calculated from advection-dispersion with helical flow included
- Morphological updating of the bed levels
- N-layer substrate model
- Bank erosion with optional inclusion of eroded material in the sediment budget
- Dynamic updating of the curvilinear grid to account for bank line changes

Waves are not included in any of the MIKE 21C models. The fetch is generally small within the estuaries of the delta, and the modelled rivers are very deep, usually at least 10 m and often up to 40 m water depth along eroding banks, which means that the small surface waves will not penetrate to the lower water column, hence it may be assumed that waves have little influence on the sediment transport in the areas modelled.

1.3 This report

An interim report describing the model development for the current situation was submitted earlier in the study and reviewed by the World Bank. The interim report was titled:

"Meso scale bank erosion modelling - current situation - interim report"

DHI revised the interim report to address the review, and the report was extended to include future projections. The final report was titled:

"Meso scale bank erosion modelling – current situation & future projections"

The interim report is included already in the final report and not submitted separately.

The five modelling reports are organised in a similar manner with the following chapters: Chapter 2 gives an overview on the availability of measurement data, as well as how the data was processed. These data are used in Chapter 3, which describes the development and calibration/validation of the model used to study the river morphology and bank erosion. Model applications are documented in Chapter 4, while the report finalizes with conclusions in Chapter 5.

1.4 General definitions

It is useful to provide some general definitions and explanations for the terminology used in this report.

The projection is always BTM, and the vertical datum is always mPWD. In some cases, data was made available in UTM and MSL. Such data was converted to BTM and mPWD.

All MIKE 21C models were developed with the grid direction going in the direction of the river from upstream. This means that the discharge sign convention is that ebb flow is positive and flood flow is negative in all models.

The term “mud” is defined as a mixture of mainly fine-grained sediments, organic matter and water where the cohesive properties of the clay fraction, enhanced by the properties of the organic matter, dominate the overall behaviour of the sediment mixture.

Several figures present results in ways that can seem confusing if the reader is not aware:

- Some figures show Pussur River divided into upstream and downstream
- Some figures show several Pussur River maps side-by-side

The MIKE 21C models are very long, and to avoid narrow graphics, some 2D figures are made by splitting the river into upstream and downstream parts shown side by side, with the upstream part to the left and the downstream part to the right. Grids and bathymetries are shown in this manner.

The plots with several Pussur River 2D maps shown next to each other are useful for showing several results together because they belong together. Examples include time-series of bathymetries that need to be compared as well as bed level changes shown together with the bathymetries. When showing these, the 2D maps are displaced 5 km in eastern direction (to the right), and the easting coordinates are hence only correct for the first 2D maps shown to the left. When showing more 2D variations together in this manner, there can be several colour scales in a figure, and the reader is notified in the caption.

For one-dimensional variations, the fact that the Pussur River runs almost north to south makes it convenient to use the BTM northing as coordinate in the graphics. This cannot be done for all MIKE 21C models (e.g. Baleswar River has a sharp bend where the northing coordinate hardly changes over some kilometres). For models where the BTM northing cannot be used as unique longitudinal coordinate, a chainage coordinate was applied.

1.5 Important note regarding MIKE 21C version

The developed MIKE 21C models take advantage of the most recent developments of the modelling software, hence it is important that MIKE 21C version 2022.1 or later is used. This version is installed on the project computers.

2 Data

This section documents all the data that was used for the model development.

The projection is BTM, and the vertical datum is mPWD.

2.1 Bathymetry

A very detailed bathymetry survey was conducted in 2011 for the Pussur-Sibsa river system as part of the Gorai River Restoration Project (GRRP). For the present project, a similarly detailed survey was conducted in the Pussur-Sibsa system in 2019. In addition, several older sets of cross-sectional data were available for the two rivers, which are tabulated for the sake of completeness. However, these old cross-sectional datasets do not have the required density to generate reliable 2D model bathymetries and are therefore not used in the present project.

Table 2-1 Bathymetry data for Pussur River. The two recent datasets have similar spatial resolution with cross-sections typically spaced 1 km longitudinally and with 3 m spacing across the river. The older bathymetry datasets were available in cross-section databases but were not used in the 2D model due to too low resolution for 2D contouring.

Bathymetry data collection year	Sources
1990/1992 (dates not available)	SWMC
2003 (dates not available)	IWM
2011 (dates not available)	IWM (GRRP)
2019 (17-24 March)	Primary data (present project)

Table 2-1 summarises the bathymetry datasets used, while the contoured bathymetries and bed level changes (difference plot) are shown in Figure 2-1. The plot of bed level changes shows that the Pussur River experienced significant deposition in the period 2011-2019, particularly in the central part.

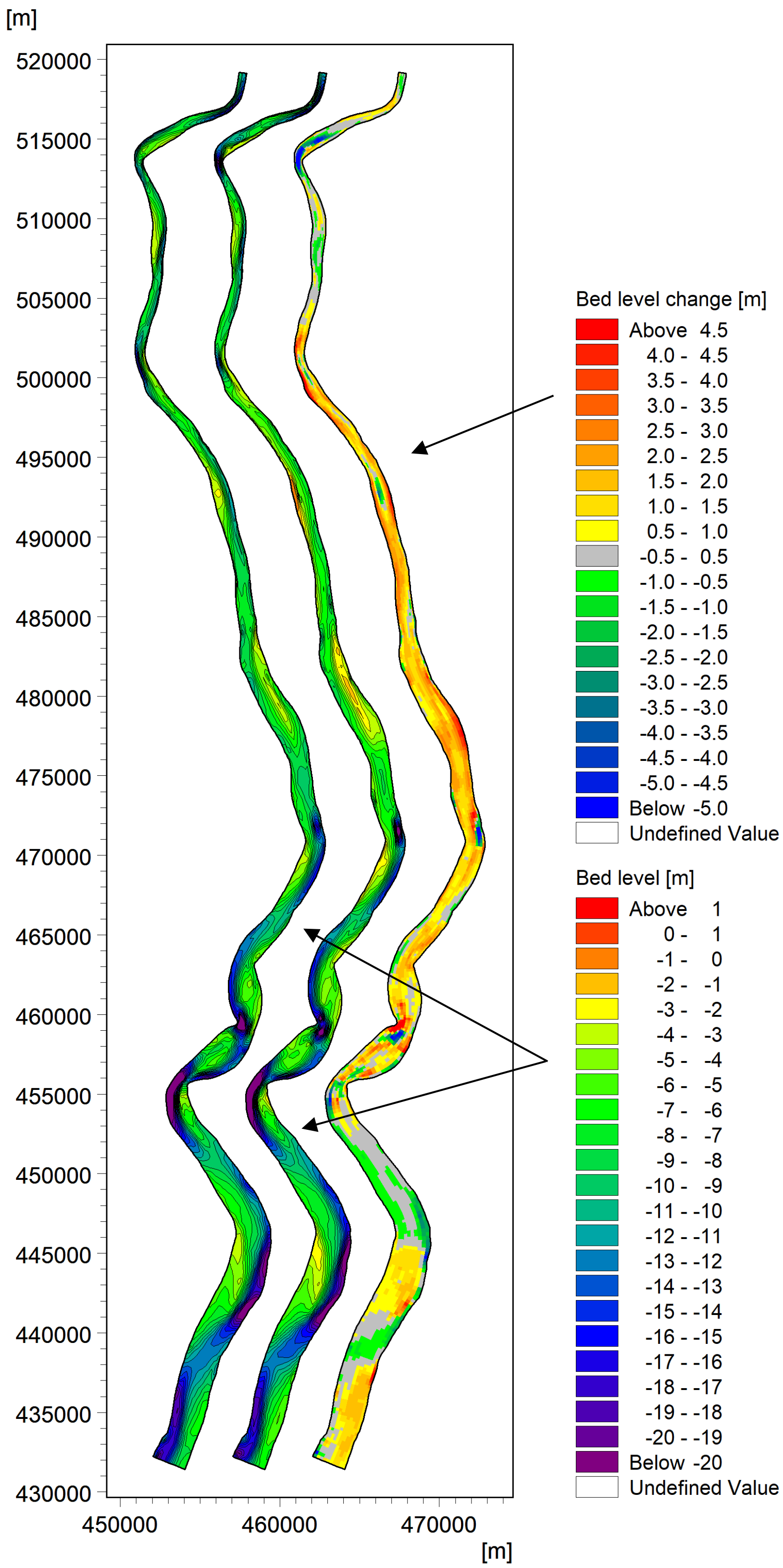

Figure 2-1 From left: 1) 2011 bathymetry, 2) 2019 bathymetry and 3) bed level changes 2011-2019. Only the leftmost bathymetry is displayed with correct coordinates. The easting coordinate is shifted 5 km for each of the subsequent plots. Also note the different colour scales.

2.2 Hydrometric time-series

Hydrometric data includes water levels and discharges.

Observations of water levels are available at numerous stations in Bangladesh from two primary sources, viz. Bangladesh Water Development Boards (BWDB) and Bangladesh Inland Water Transportation Authority (BIWTA). In this study, only the data collected in conjunction with the bathymetrical surveys was used along with water levels simulated with the South West Regional Model (SWRM).

Water level and discharges data collected as part of the project during 2019 were not used in the model development process, as they were not available at the time when the model was developed.

Table 2-2 Measured water level data for Pussur River.

Water level collection period	Station Name	Sources
2011 (16-20 September)	Mongla	IWM (GRRP)
2011 (16-29 March)	Mongla	IWM (GRRP)

Time-series of tidal discharges are not measured on a routine basis in Bangladesh. Therefore, only measured data collected in connection with project activities was available. Discharge data was used from the Pussur River at Rupsha, Mongla and Akram Point. The locations of the stations with measured data are shown in Figure 2-2.

Table 2-3 Measured discharge data for Pussur River.

Discharge collection year	Station Name	Sources
2011	Mongla	IWM (GRRP)
	Akram Point	
2016	Rupsha	CEIP-1
	Mongla	
2019		Primary data (present project)

The discharge data was collected by IWM, typically during one day, using tide tables to plan for neap and spring data collection. Water levels were collected at the same time, and often IWM also collects suspended sediment concentration data together with the ADCP/discharge data. Water level stations are often permanent and contain water levels collected every 30 min.

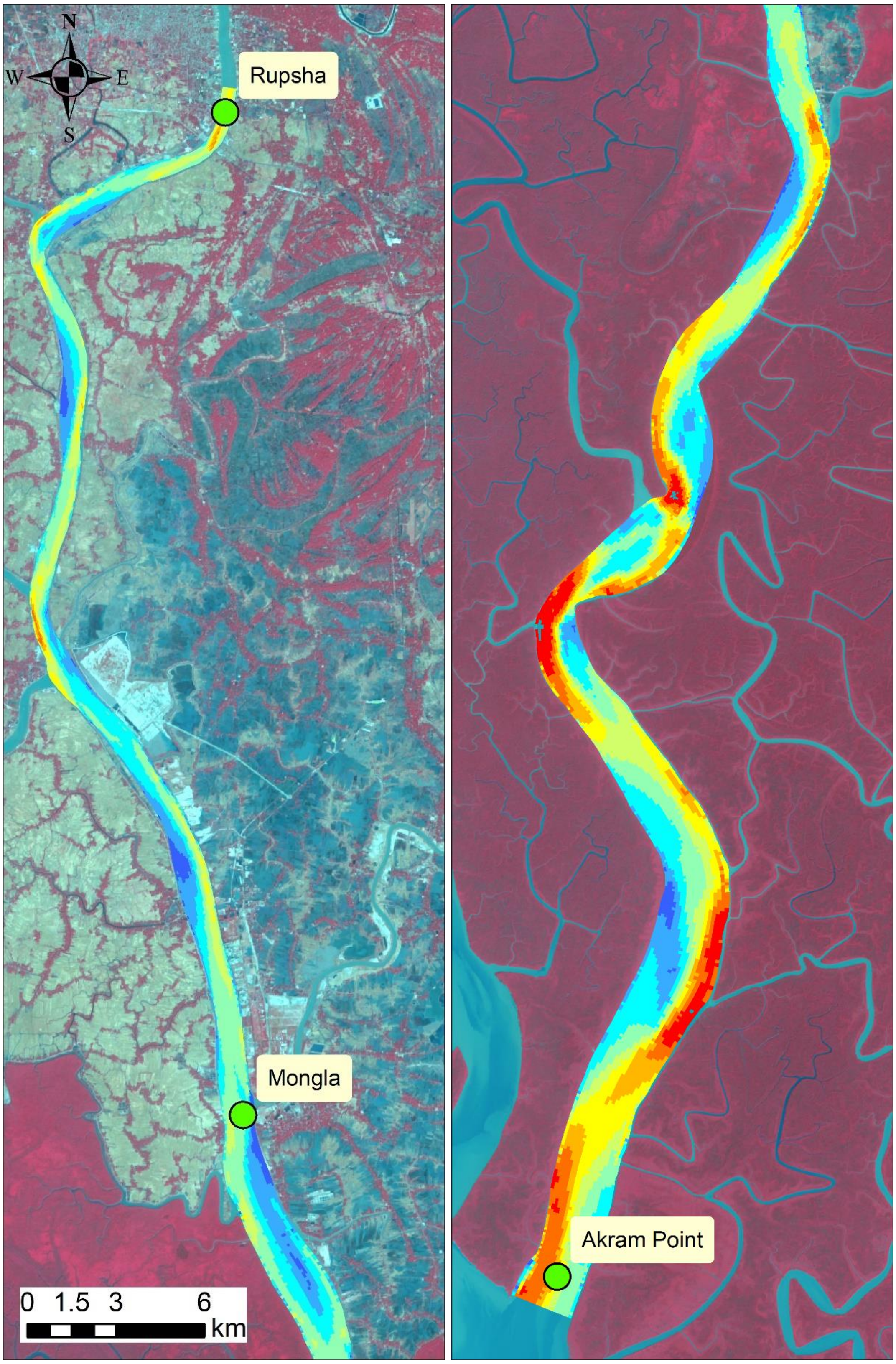

Figure 2-2 Field hydrometric data collection map for 2011 and 2016. All three stations have discharge data, while only Mongla has water level data as well.

2.3 Sediment bed samples

A relatively large number of bed samples data from the Pussur River are available. The data have been collected from various sources, including GRRP (2011), a project conducted by IWM (2016) and this project (2019), see Table 2-4.

Table 2-4 Bed samples data from the Pussur River collected in 2011, 2016 and 2019. The Krumbein (1934) scale for size classes has been used, i.e. VFS = very fine sand, FS = fine sand, MS = medium sand. It is noted that the three samples ending by "395" are from the downstream estuary.

BTM X [m]	BTM Y [m]	Year	Name	Clay <0.005mm [%]	Silt <0.063 mm [%]	VFS <0.125 mm [%]	FS <0.25 mm [%]	MS >0.5 mm [%]
453243	497824	2019	Pusur_2B_CL	5.12	54.53	22.70	14.52	3.13
456727	491480	2011	Pussur_MD_02	8.59	81.35	8.19	1.70	0.17
458421	484070	2011	Pussur_LB	0.00	13.80	52.21	24.67	9.32
458725	481396	2016	Pussur_CL	4.72	89.38	2.90	2.19	0.82
456877	458065	2011	Pussur_MID_182	0.00	11.48	34.68	52.21	1.63
454478	434175	2011	Pussur_MID_318	0.00	12.06	39.05	39.82	9.07
452916	491747	2019	Pusur_1B_RB	5.82	86.88	4.12	2.66	0.52
456190	491349	2011	Pussur_RB_02	9.15	90.29	0.56	0.00	0.00
456190	491349	2011	Pussur_LB_182	14.54	84.76	0.70	0.00	0.00
459415	481365	2016	Pussur_LB	5.68	84.94	4.88	2.97	1.54
456154	458907	2011	Pussur_RB_182	7.61	90.83	1.56	0.00	0.00
454955	433992	2011	Pussur_LB_318	7.52	90.78	1.70	0.00	0.00
453074	497682	2019	Pusur_2B_RB	7.74	77.33	9.43	4.43	1.06
456985	492018	2019	Pusur_1B_LB	8.10	70.51	12.84	6.80	1.75
457115	491756	2011	Pussur_LB_02	7.17	77.95	7.00	6.49	1.40
457536	483888	2011	Pussur_RB	17.17	81.08	1.74	0.00	0.00
458065	480895	2016	Pussur_RB	11.71	85.41	2.88	0.00	0.00
453210	434624	2011	Pussur_RB_318	14.22	85.22	0.56	0.00	0.00
452491	415919	2011	Pussur_LB_395	10.35	87.66	1.99	0	0
449513	415656	2011	Pussur_MID_395	0	7.42	7.55	81.07	3.95
445979	416066	2011	Pussur_RB_395	20.5	77.34	2.16	0	0

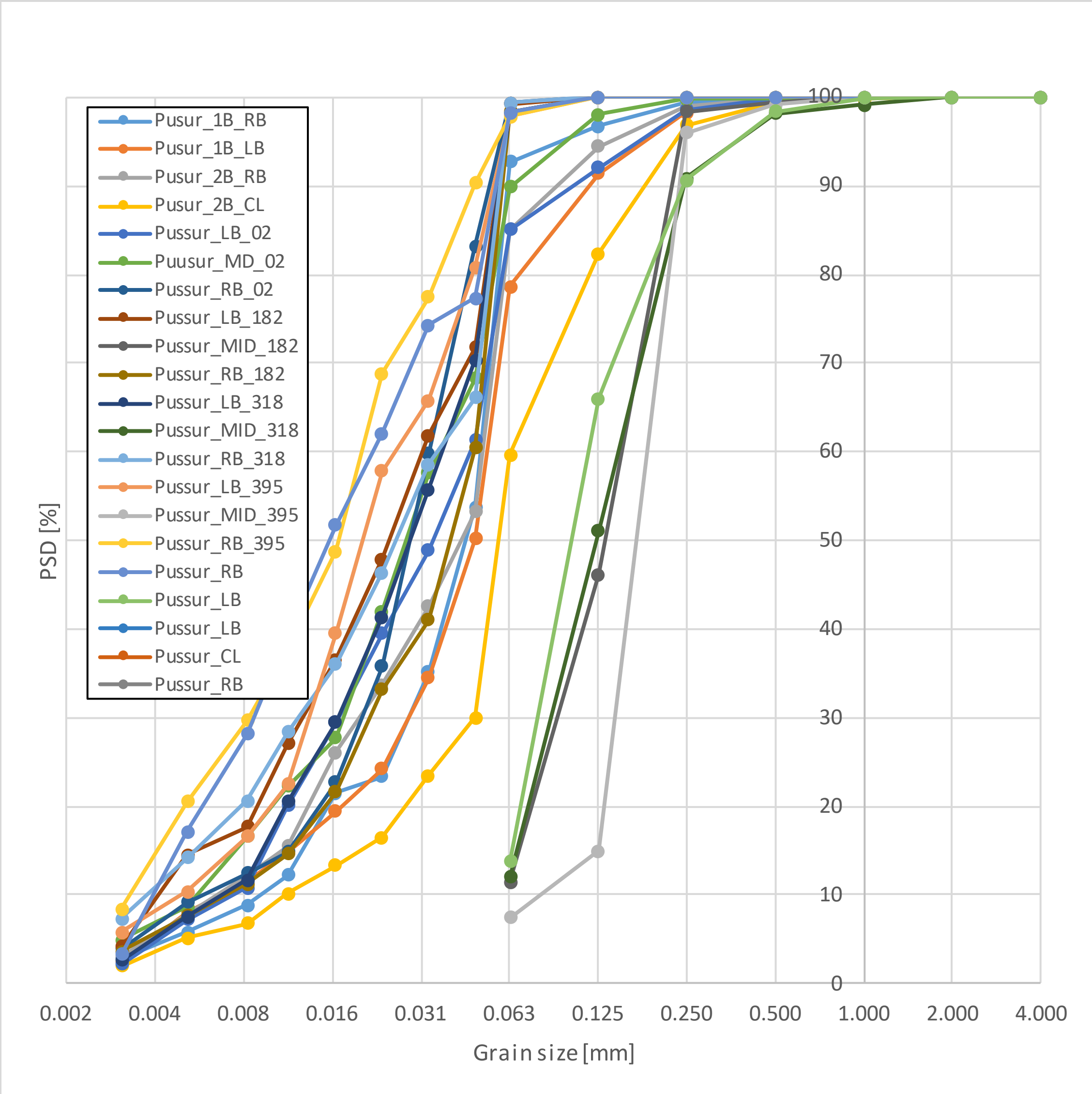

Figure 2-3 Particle size distribution of bed sediment in the Pussur River for 2011, 2016, 2019. Note that the 2016 bed samples are missing from the figure because they were not available in relevant format.

Table 2-4 shows the bed samples processed into the Krumbein (1934) scale for the sand partition and clay/silt for the cohesive partition. The corresponding particle size distribution curves are shown in Figure 2-3. The samples fall into two categories: 1) dominated by sand, and 2) dominated by mud. It is noticed that most of the samples are muddy.

The bed samples are shown in Figure 2-4. While the bathymetry is from 2011, the bed sample are for the period 2011 to 2019. However, no significant changes to the overall pattern of bars and channels will take place during such a limited time span. Hence it is descriptive to use the 2011 bathymetry to represent the general bathymetry in the river for the period 2011-2019.

Generally, the samples collected from the riverbed close to the banks are muddy. Bed samples from the flow channels are also generally muddy

The bed samples suggest that the sandy bed surface is found mostly on the side slopes of the bars, but not really on the bar surface itself. An explanation for this could be the relatively short adaptation length of the sand, so the sand deposits before reaching the top of the bars.

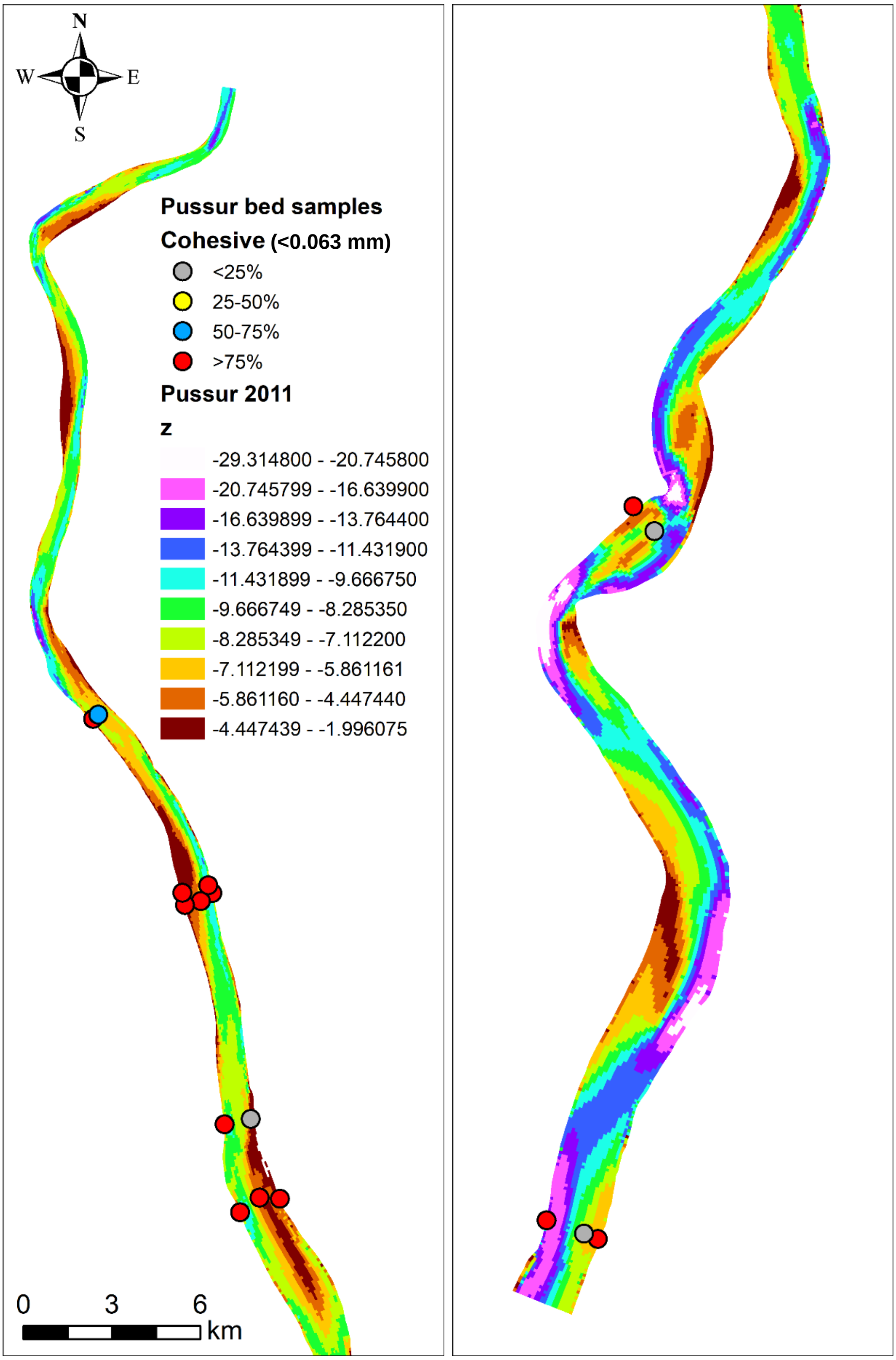

Figure 2-4 Bed samples from the Pussur River shown together with the 2011 bathymetry. Note: There are three bed samples also from the downstream estuary, which show a sandy sample in the middle and cohesive samples at the edges, i.e. same as for Pussur River. Those three samples are of little interest to the modelling study and are not shown in the figure but mentioned for the sake of completeness.

2.4 Particle size distribution of the bank material

No data on the particle size distribution of the sediments in the riverbanks of the Pussur River was collected during the study.

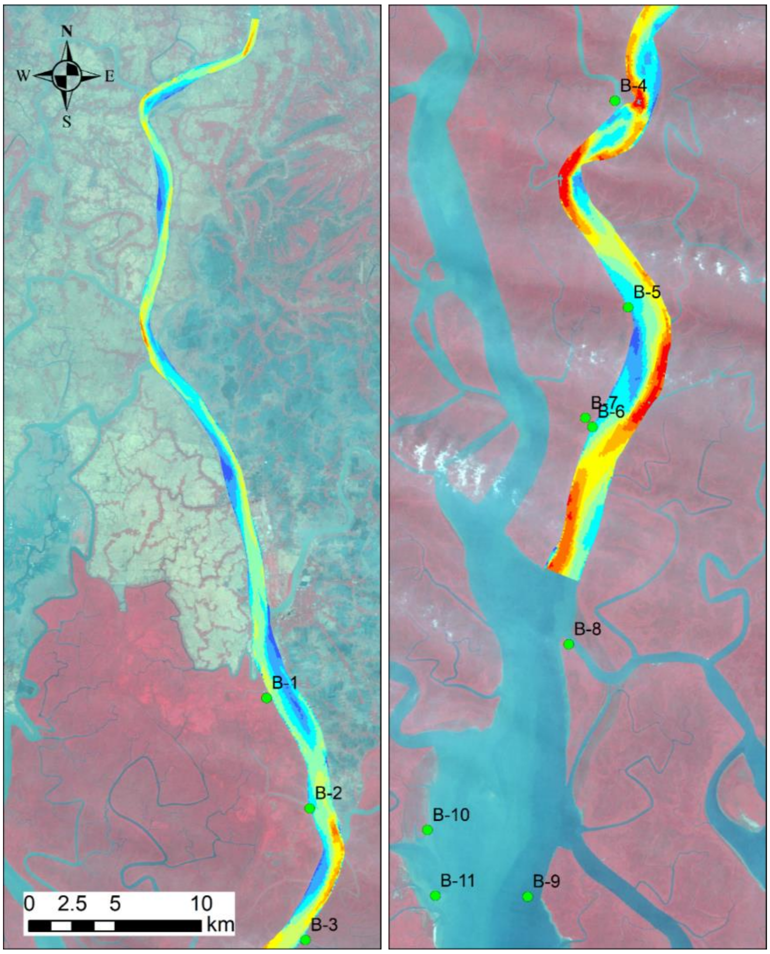

Figure 2-5 Land surface samples around the Pussur River from Kumar et al (2016).

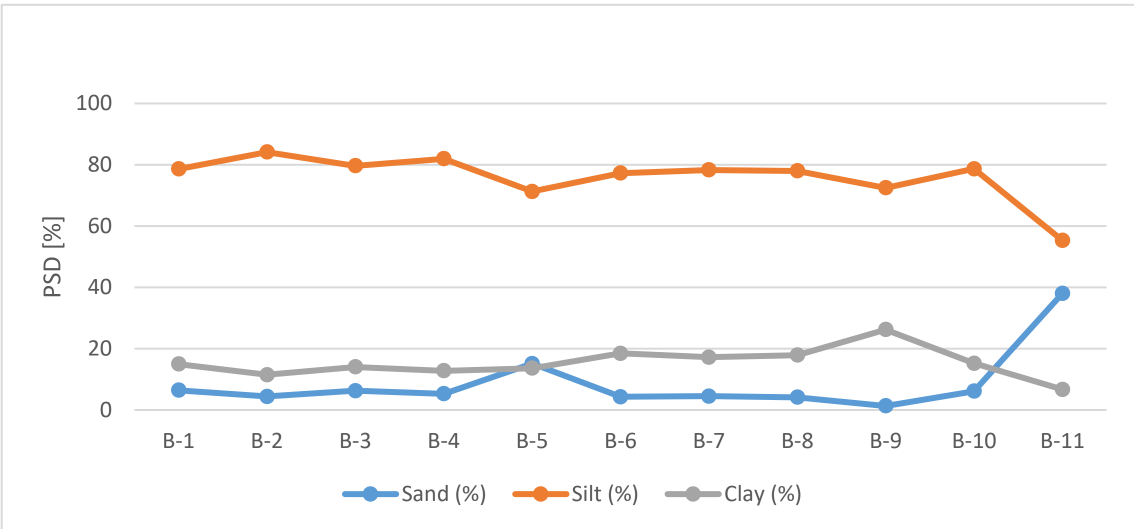

Figure 2-6 Particle size distribution data from Kumar et al. (2016). Samples B-1 to B-7 were collected along the Pussur River model.

However, Kumar et al. (2016) presented data from land surface samples collected adjacent to the riverbank. Eleven samples were collected with seven of the samples within the Pussur River model area, see Figure 2-5. The percentage of clay, silt and sand in the surface samples are shown in Figure 2-6 The average sand content in the riverbank is around 6-7% while the average clay content is about 17-18%. The sand content is lower and the clay content higher than the bed sediment (see Table 2-4), as would be expected from overbank sediments deposited by the river during high stages.

2.5 Suspended sediment data

Suspended sediment data are available from three stations in the Pussur River, i.e. at Rupsha, Mongla and Akram Point. At the same stations hydrometric data were collected simultaneously, see Section 2.2.

In the following sections C(Q) correlations (discharge versus sediment concentration) are presented for the three stations. This is a common approach in fluvial systems where it is used to establish a sediment transport rating curve. In fluvial systems flows and sediment transport will be slowly varying and there will generally be a relation between discharge, water level and bed shear stress, so also a unique sediment rating curve. This contrasts with a tidal system as the present, so a unique relation between discharge and sediment concentration cannot be expected. The plots, however, are useful for developing an understanding of the sediment dynamics and to generate continuous time-series to be used at the model boundaries.

No data on particle size distribution of the suspended sediment was available.

2.5.1 Rupsha suspended sediment concentration as a function of discharge

Rupsha is located at the upstream boundary of the model of the Pussur River.

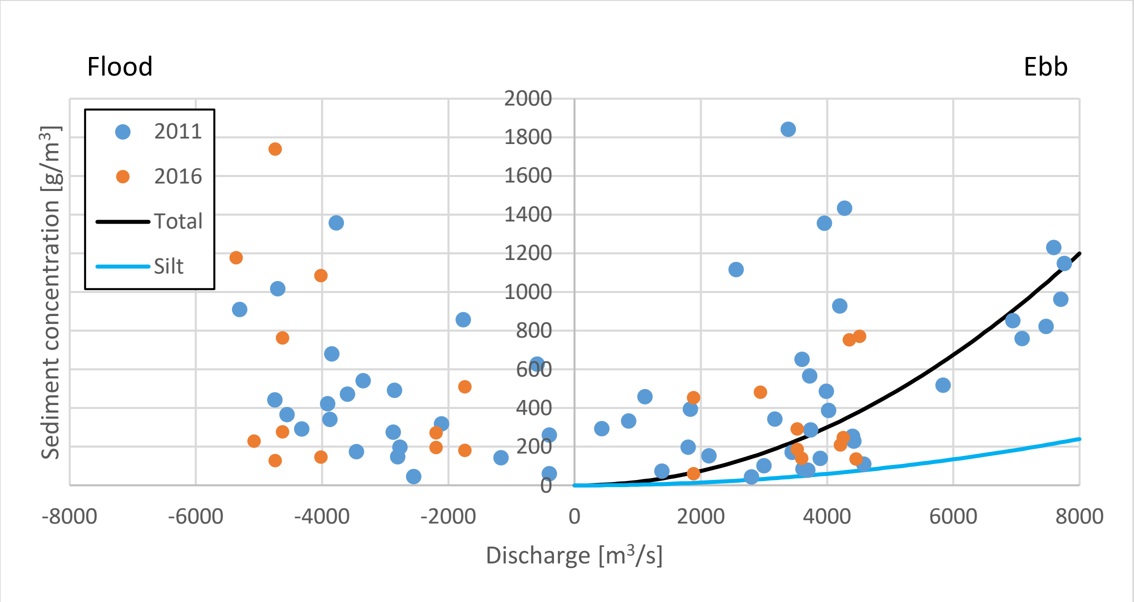

Figure 2-7 Rupsha C(Q) correlation based on sediment concentration data from 2011 and 2016 and simulated discharges from the SWRM. The fitted curves for total and silt concentrations were used for generating boundary conditions, which is described later in the report.

The model needs a boundary condition at this location during ebb flow. The plot of concentration versus discharge is shown in Figure 2-7.

Some of the 2011 Rupsha discharge observations had issues with time-shifts. To circumvent this, the simulated 2011 discharges from the SWRM provided by IWM were used instead of the observed discharges.

The 2016 data was also added with simulated discharge from the SWRM, as there were no observed discharges from 2016.

2.5.2 Akram Point suspended sediment concentration as a function of discharge

The Akram Point Q-SSC data was reprocessed as follows.

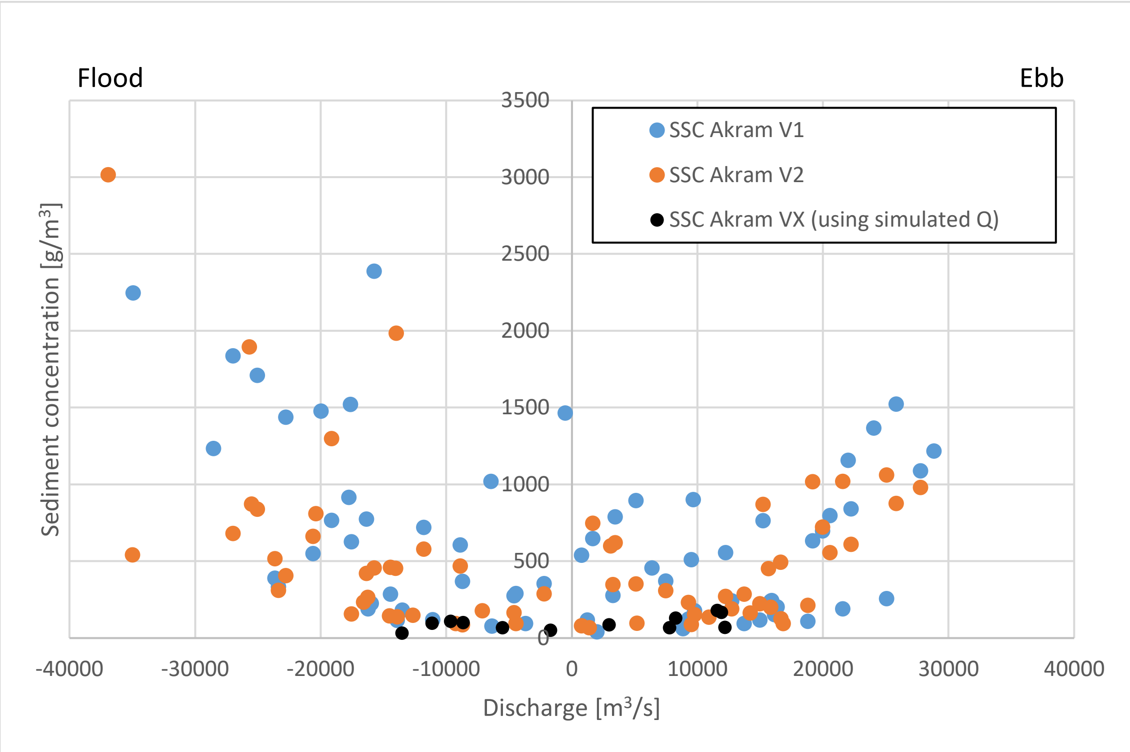

Figure 2-8 Akram Point C(Q) correlation based on observations from 2011 (note that the horizontal scale is different from Figure 2-7). Observations were available with indications of verticals V1 and V2, while some of the observations were not labelled with a vertical (labelled VX in the figure). The coordinates for V1 and V2 were not available in the data files.

The observed discharges at Akram Point were deemed reliable and interpolated to the points in time for which suspended sediment concentration observations were available. For a few of the suspended sediment concentration observations no measured discharges were available. For those data points model simulated discharge data were extracted from the SWRM.

The C(Q) correlation for Akram Point is shown in Figure 2-8.

The figure clearly shows that the sediment concentration increases with the discharge. The sediment concentration is distinctly higher for flood flow than for ebb flow suggesting that there is a net flux of sediment from the sea towards land. It is also noticed that there is a stronger correlation between discharge and sediment concentration for ebb flow.

2.5.3 Mongla suspended sediment concentration as a function of discharge

The Mongla C(Q) correlation was processed from the observed suspended sediment concentrations and observed discharges. Simulated discharges were not used, as observed discharges were available for all concentration observations.

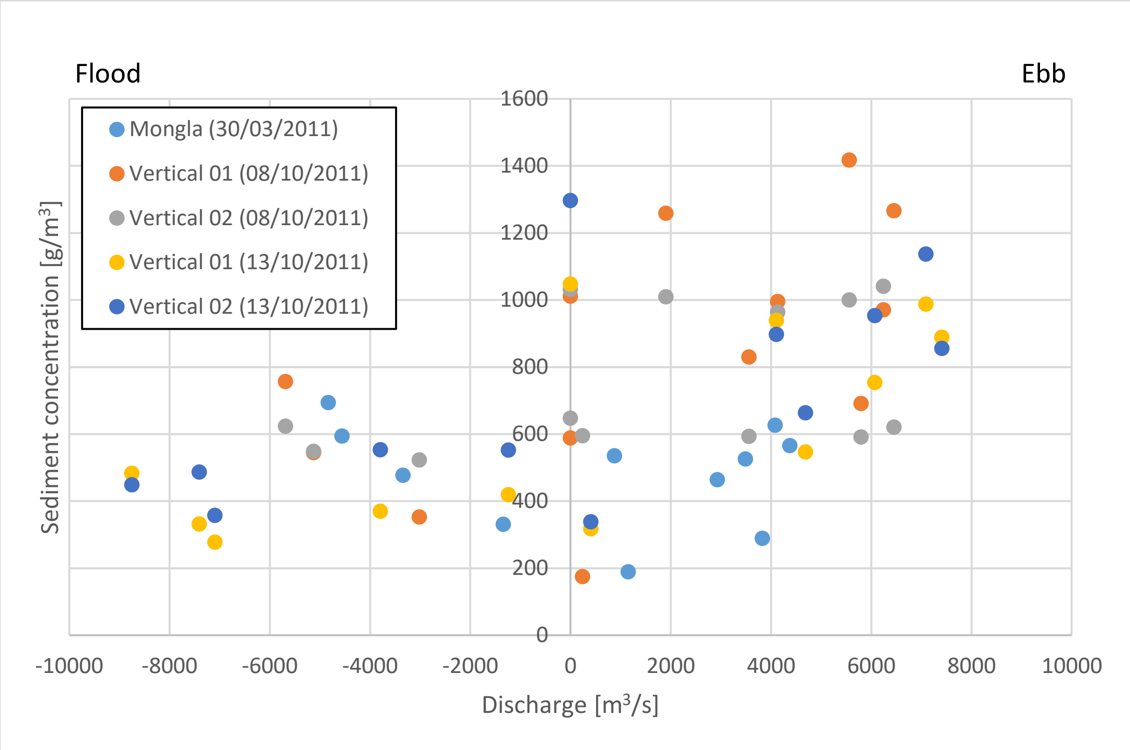

Figure 2-9 Mongla C(Q) correlation based on observed discharges (note that the scale is different from the other figures). The labels refer to three locations at Mongla Port, namely Mongla, Vertical 01 and Vertical 02.

The Mongla C(Q) correlation is shown in Figure 2-9. The Mongla C(Q) is similar to the Rupsha, which is a boundary condition using the estimated silt fraction.

It is observed that Rupsha has similar flood and ebb concentrations, while Mongla has distinctly higher concentrations for ebb flow and Akram Point has distinctly higher concentrations for flood flow. Due to the missing data for the particle size distribution in the suspended sediment, no conclusions can be derived from these observations concerning the associated silt sediment fluxes.

2.6 Historical bank lines from satellite imagery

Historical bank lines were studied based on satellite images. To this end, nine cloud-free scenes of Landsat imagery were acquired for the period of 1988-2019 from the Earth Explorer database of the U.S. Geological Survey. The acquired images cover all the rivers in the coastal zone for which meso-scale modelling is carried out in this project, thus also the Pussur River. All the images are from the dry season from November to February as there were no cloud-free images during other seasons.

Bank lines were digitized from the images from 1988, 1995, 2001, 2011, and 2019 and are shown in Figure 2-10. In this figure, 34 locations with consistent and significantly eroding banks are indicated. It is observed that nearly all the locations with eroding banks are located along outer bends where the water depth adjacent to the bank is large (ebb channels). In addition, some eroding banks (see banks 11 and 21 shown in the figure) can be explained from smaller channels located between the bars and the inner bank (flood channels).

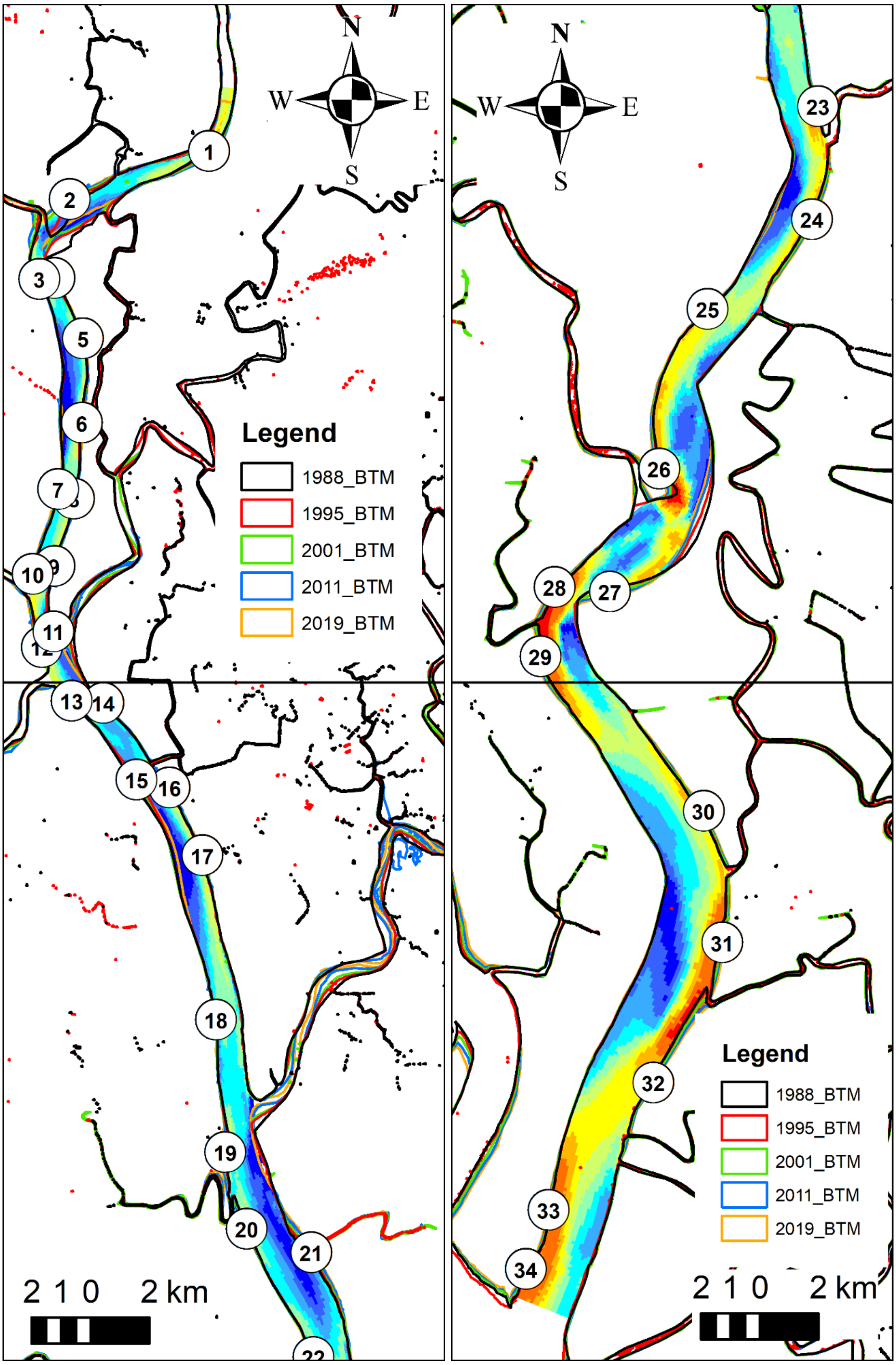

Figure 2-10 Digitized bank lines representing 1988, 1995, 2001, 2011, and 2019 and location of eroding banks. The bathymetry is based on a survey from 2011.

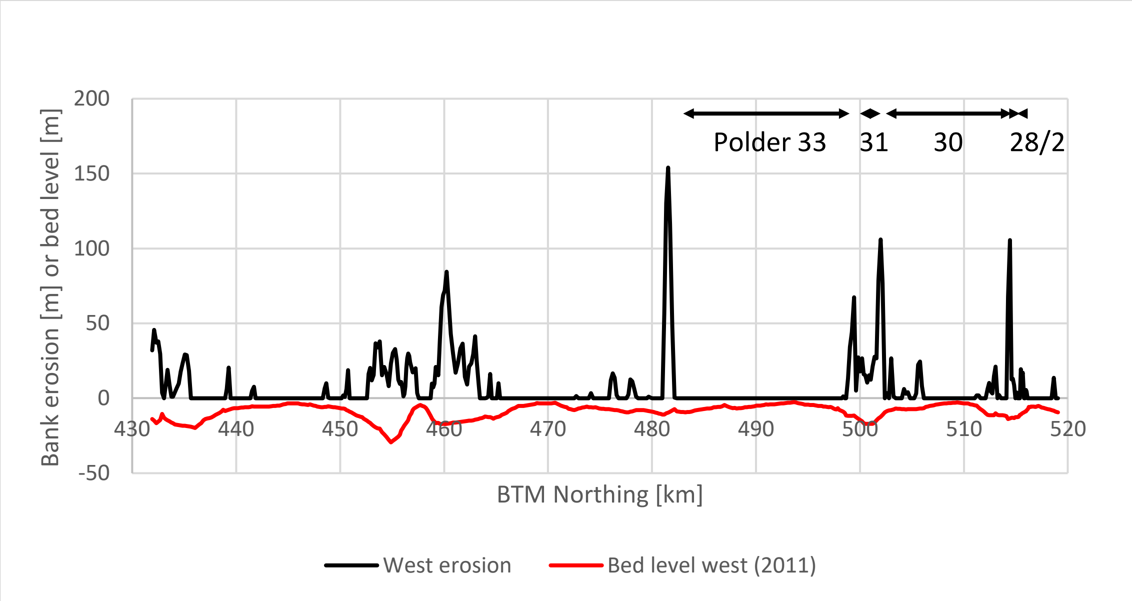

Figure 2-11 Observed west bank erosion 2011-2019 along Pussur River as a function of northing.

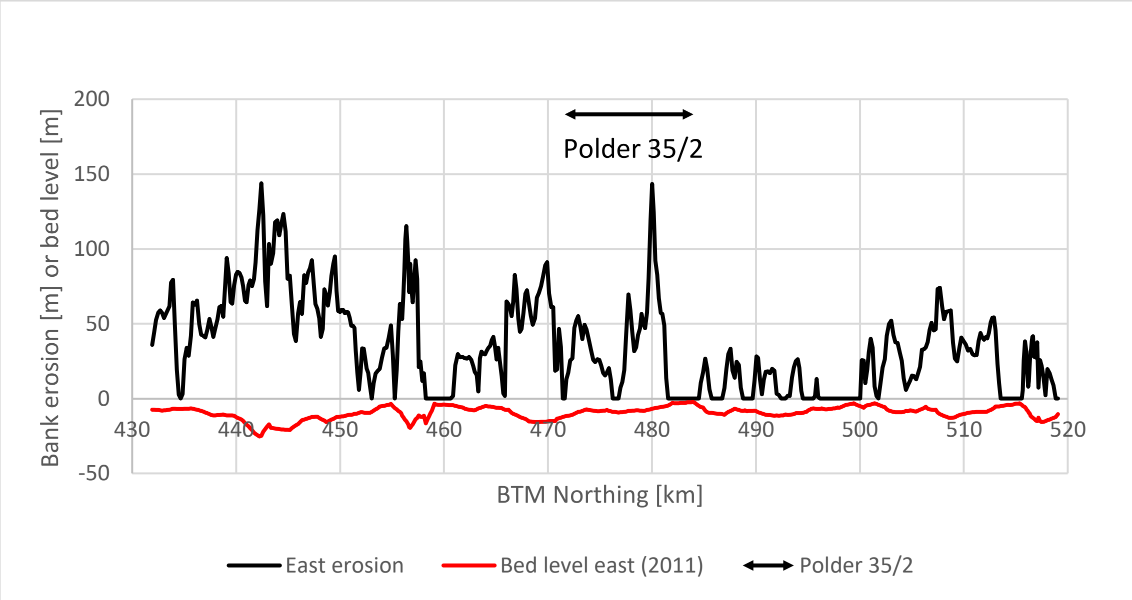

Figure 2-12 Observed east bank erosion 2011-2019 along Pussur River as a function of northing.

The bank erosion for the period 2011 to 2019 was processed from the digitised 2011 and 2019 bank lines by determining the distance from the 2011 to the 2019 bank line along normal vectors based on the 2011 bank lines. The results are shown in Figure 2-11 and Figure 2-12. The horizontal axis in these figures is the BTM northing coordinate since the Pussur River largely runs north to south.

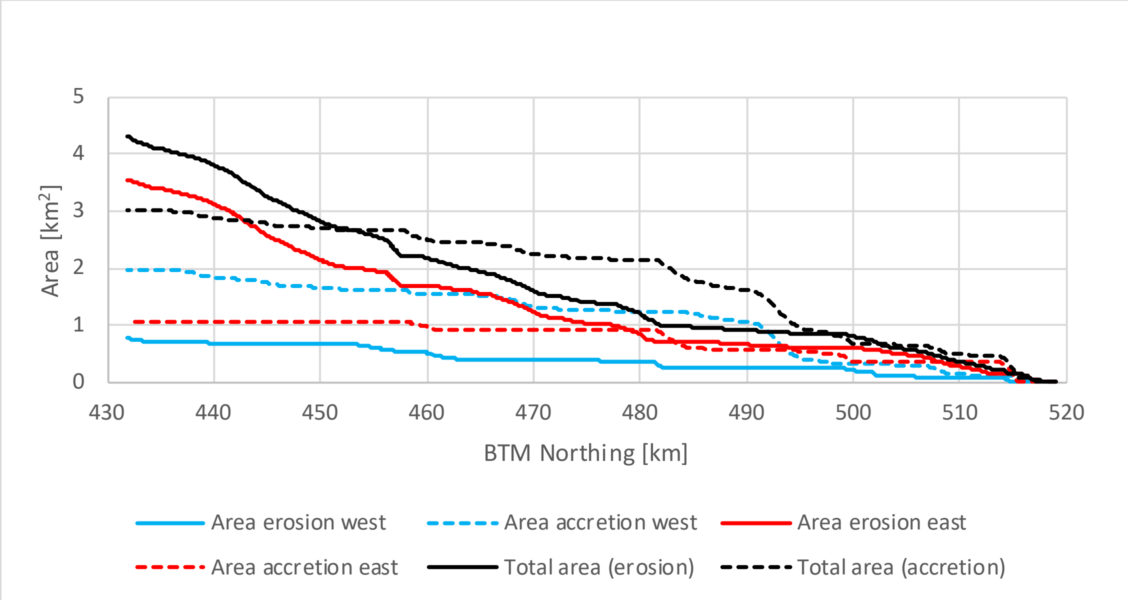

Figure 2-13 Accumulated area curves associated with bank erosion and accretion along each bank and total for the period 2011-2019.

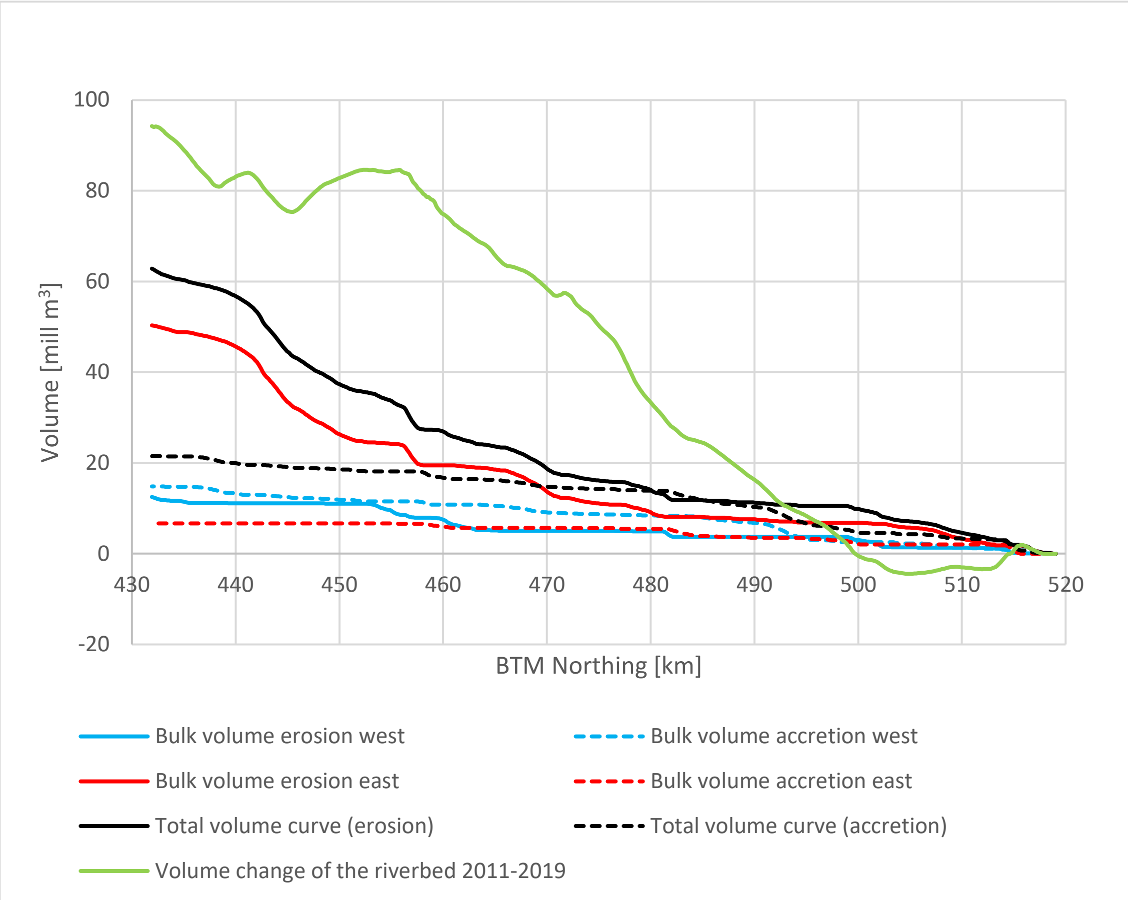

Figure 2-14 Estimated bank erosion accumulated bulk volume curves for Pussur River 2011-2019 compared to the observed accumulated bathymetry changes bulk volume curve for the same period.

The land areas lost to bank erosion along the western and eastern banks have been calculated as the integrated/accumulated erosion (as shown in Figure 2-11 and Figure 2-12) and plotted in Figure 2-13. Here also the total loss of land (sum of east and west bank erosion) as well as the accretion are determined in a similar way. It is interesting to note that the west bank experienced net accretion that exceeds the erosion, while the east bank is dominated by erosion. This implies that overall, the river is moving towards east. A closer analysis suggests that on average the eastern bank has moved about 28 m towards east, the western bank about 13 m towards east and that the river has widened with about 15 m. It should be noticed that these numbers are small compared to the river width and therefore not necessarily significant.

The sediment budget is important for understanding the overall morphology of the river. Therefore, the bank erosion bulk volumes have been estimated and compared to other components of the sediment budget.

The local bulk volume of sediment generated by bank erosion was estimated in the following way:

$$Vol = \mathrm{E}\,(\mathrm{H}_b - \mathrm{z})\Delta s$$

Where H_b is the bank level (estimated 2 mPWD in the Pussur River model), z the local bed level adjacent to the bank, E the erosion [m] and ∆s the local grid spacing [m] in the simulation grid, and the local bed level is extracted from the model representing the 2011 situation. The bulk volume curve is the integration of the eroded volumes along the bank, starting from upstream, i.e. the values are always zero at the upstream end around BTM northing 519 km. Hence the local bulk volume curve represents the eroded volume upstream of the considered location. The resulting bulk volume curves are shown in Figure 2-14. It is seen that the total for bank erosion is 60 mill m^3 for the period 2011-2019, which is comparable to the volume change in the riverbed for the same period, shown as the green line in the figure.

Table 2-5 Observed changes to the Pussur River 2011-2019.

Description	Value
Model area (2011)	132 km^2
Length	90 km
Increase in area 2011-2019	1.31 km^2
Average width (2011)	1468 m
Average increase in width (2011-2019)	14.5 m
Relative width increase 2011-2019	0.99 %
Sedimentation bulk volume (2011-2019)	94 mill m^3
Average sedimentation (2011-2019)	0.71 m
Average depth below 0 mPWD	9.45 m
Relative reduction in depth below 0 mPWD	7.5 %

The bulk volume curves associated with bank accretion show that accretion accounts for smaller volumes than erosion although the area contribution (Figure 2-13) is similar. This is not surprising since banks are generally eroding where the water depth is large, while the opposite is the case for accreting banks.

For simplicity, the same porosity has been used for the bank and bed sediment although the cohesive sediment in the banks is denser than the cohesive sediment in the bed. Publications suggest that the porosity in the bank can be as low as 0.5, while the cohesive sediment in the bed may be 0.7-0.8. If this difference was considered, the curves for volume change of riverbed and banks would be more similar.

Table 2-5 summarizes some overall numbers for the Pussur River. The most interesting features for the period 2011 to 2019 are that the river became wider (+1%) and shallower (depth below 0 mPWD decreased by 7.5%).

2.7 Subsidence

Subsidence was studied as part of the overall project and processed into a raster.

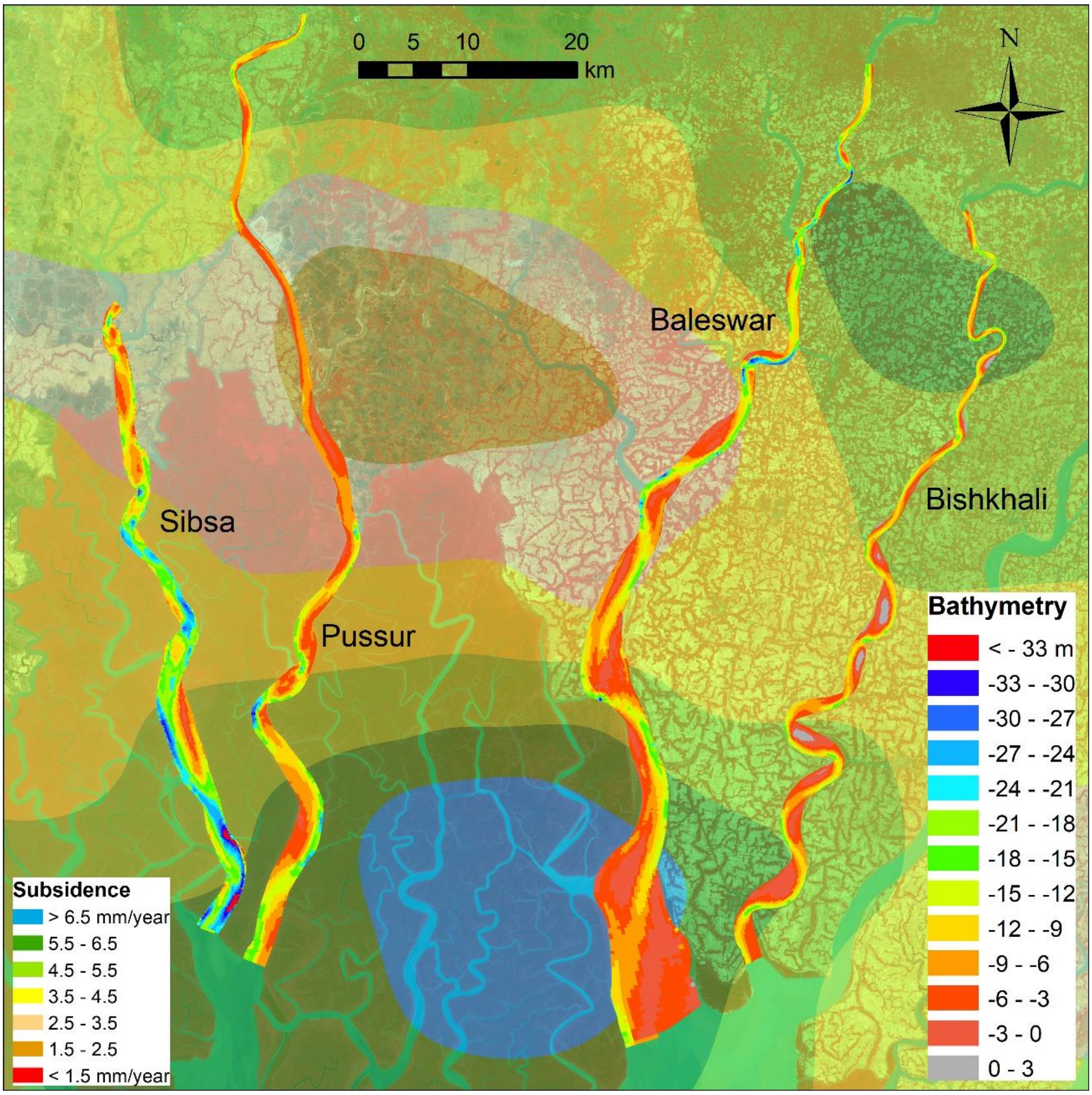

Figure 2-15 Subsidence spatial map in the area where the four models are located.

Figure 2-15 shows the subsidence based on the observations made for the project. The values were contoured to a 100 m raster for use with the MIKE 21C models, and the raster was converted to the individual curvilinear grids.

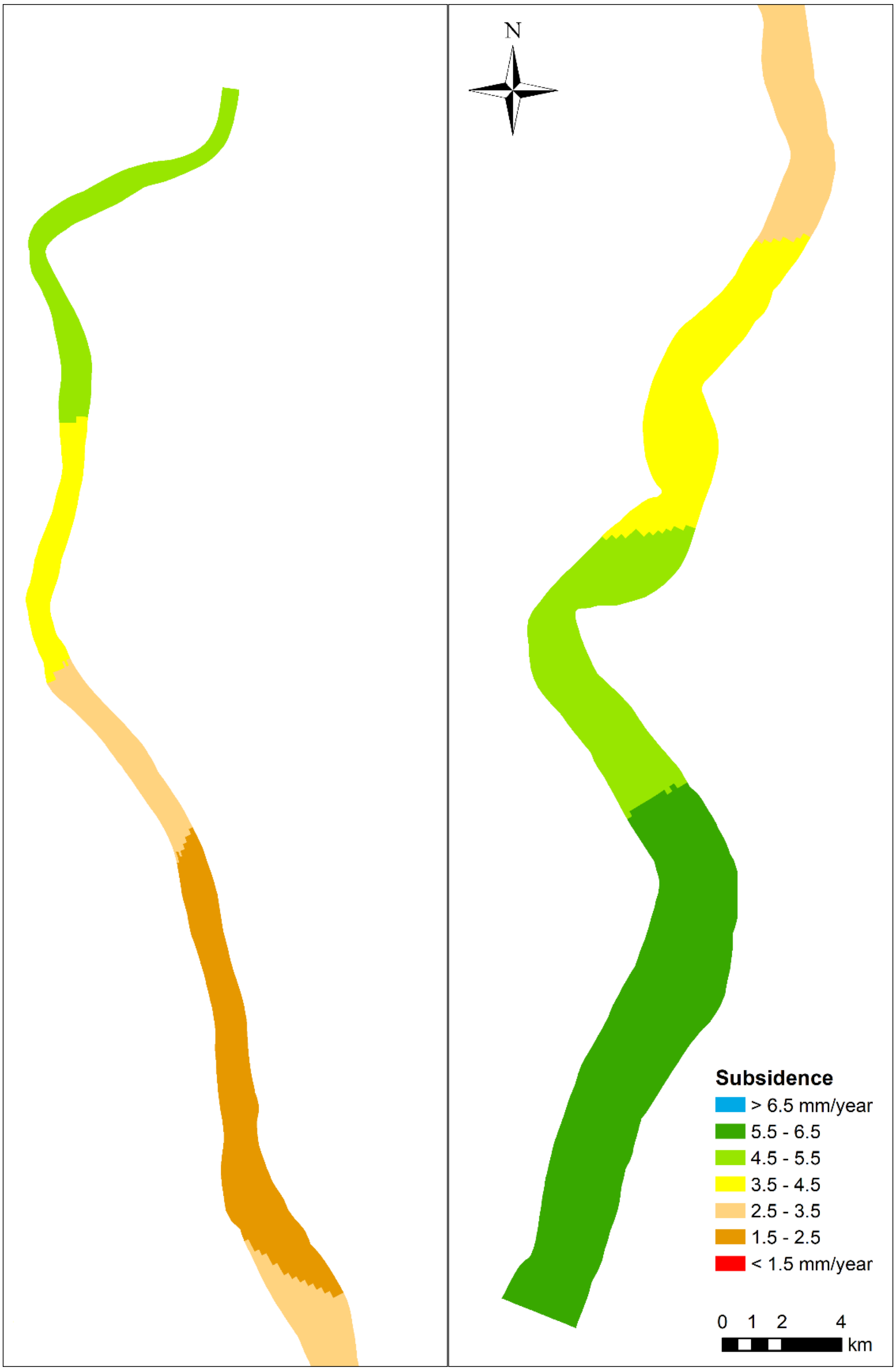

Figure 2-16 Subsidence interpolated to the Pussur 2019 model grid.

Subsidence for the Pussur is shown in Figure 2-16. The rates are generally around 5 mm/year, which means that over 30 years the riverbed will be lowered by 150 mm. The bed level changes associated with subsidence are hence small compared to morphological changes, as the average sedimentation in the period 2011-2019 was 71 cm. Therefore, over 8 years the river can deposit almost five times as much, as subsidence will lower the bed over 30 years.

3 Model development

The model development process involves the following components:

- Curvilinear grid conforming to the bank lines
- Bathymetry contoured to the curvilinear grid
- Boundary conditions (upstream, downstream, side channels)
- Hydrodynamic calibration
- Sediment model formulation
- Sediment boundary conditions
- Sediment model calibration
- Bank erosion model calibration

The components are reported in this chapter.

3.1 Grid and bathymetry

The river system is to a certain degree influenced by floodplain (e.g. mangrove forest and floodplain outside polder areas), which was identified from the available DEM elevations. The MIKE 11 model (SWRM) also shows significant floodplain along Pussur River, which is reflected in the output from the MIKE 11 model.

Initially a full model for 2011 was developed with high resolution (1000x20) in the river channel and with floodplain included. The full 2011 model including floodplain was used for the hydrodynamic calibration.

Originally it was not the intention to run models over several years. However, the available data (2011 and 2019 bathymetries with similar resolution suited for 2D contours) combined with the systematic and slow planform development made it ideal to run simulations hindcasting 8 years (2011-2019) for morphological calibration.

Including the floodplain in the morphological model is not feasible when running simulations covering several years, and the grid resolution in the river channel was very high in the initial model. Several model runs were conducted to explore the impact of floodplain flow, and it was concluded that although the floodplain adds tidal prism, the impact is relatively small. It is also important to optimise the grid in the river channel to avoid excessive simulation times for the long-term morphological simulations. The model was subjected to stepwise coarsening until it was deemed that further coarsening would impact the result. In this way the coarsest grid that would ensure a grid-independent result was achieved.

The morphological model runs were conducted on a 500x10 curvilinear grid.

3.1.1 2011 model grid and bathymetry

The 2011 model grid and bathymetry were used for morphological model calibration and validation. Figure 3-1 shows the 500x10 curvilinear grid conforming to the 2011 bank lines, while the 2011 curvilinear bathymetry is shown in Figure 3-2.

The longitudinal cell size (Δs) varied in the range 70-350 m (average of 200 m), while the transverse cell size (Δn) varied in the range 40-330 m (average 130 m). For the cell area the range was 3,200-116,000 m^2 (average 27,000 m^2).

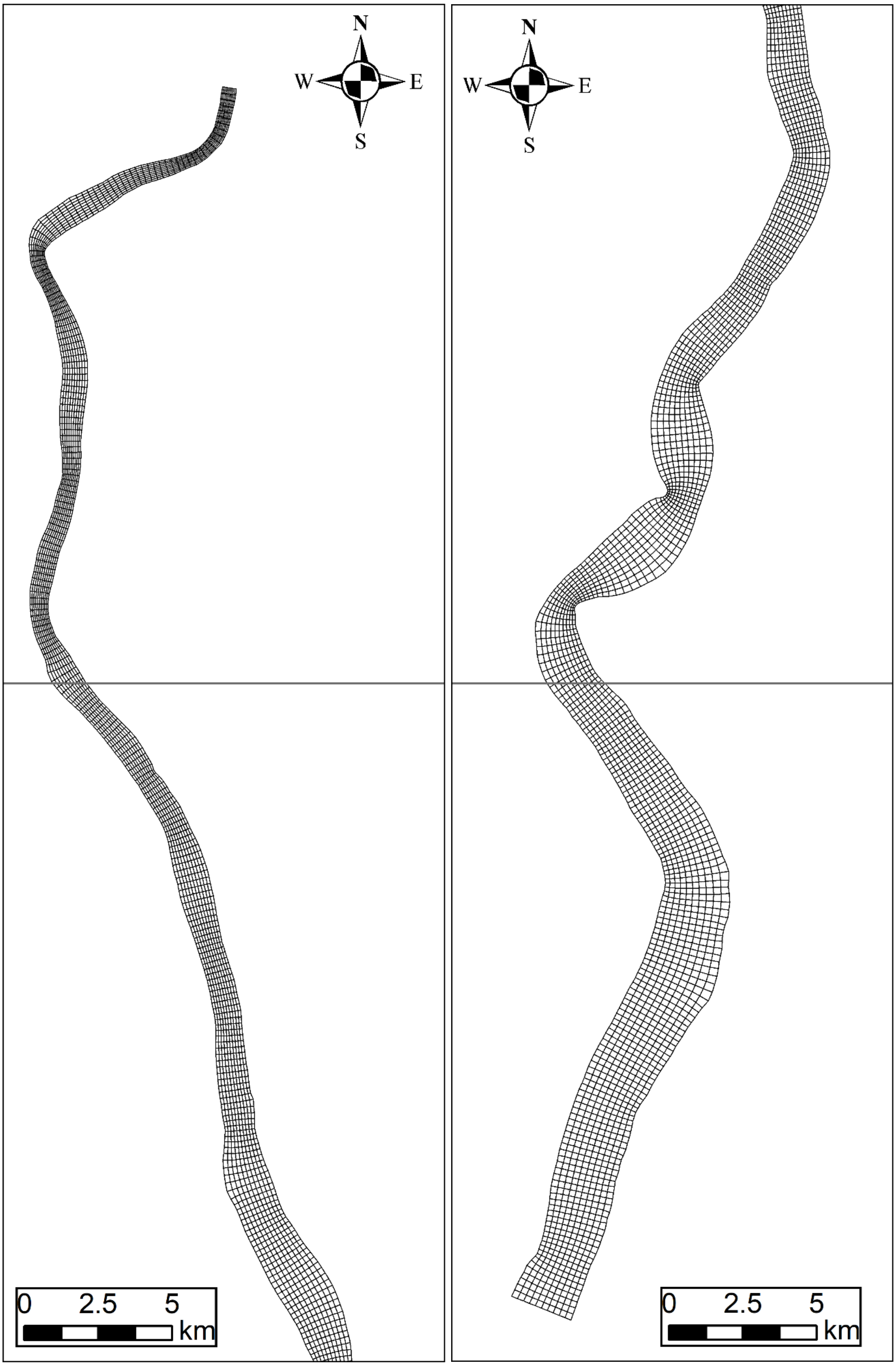

Figure 3-1 2011 grid for the Pussur River model, grid dimensions 500x10.

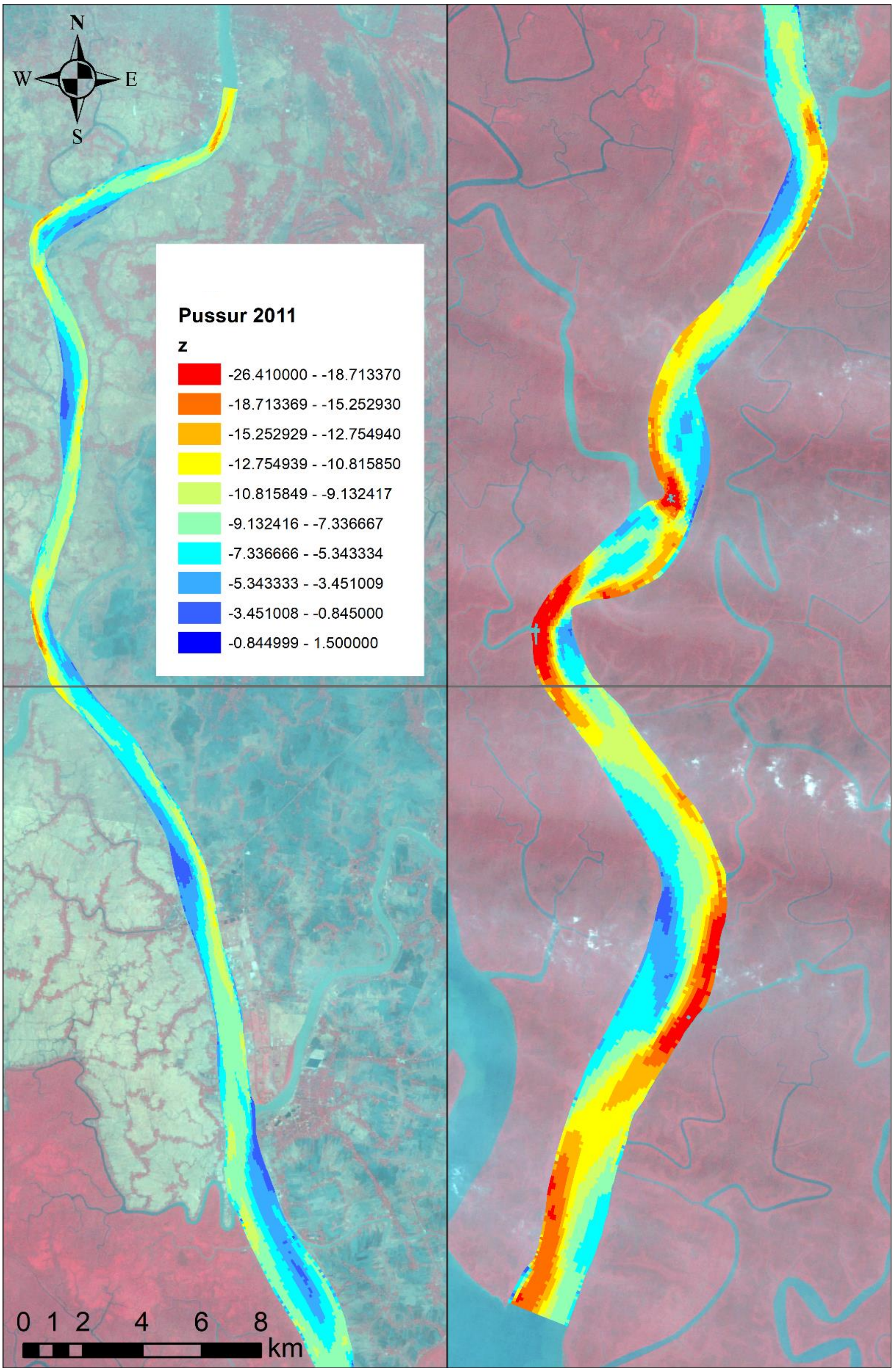

Figure 3-2 2011 bathymetry shown on the 2011 curvilinear grid (and 2011 Landsat image).

3.1.2 2019 model grid and bathymetry

The 2019 model was developed from the 2019 bathymetry collected for the project and the 2019 bank lines digitized from the 2019 Landsat image.

It is not possible to tell the difference between the 2011 and 2019 grids without zooming in on local areas. Figure 3-3 shows a comparison of the 2011 and 2019 grids in a local area located approximately 21 km from the downstream boundary.

The 2019 model will be used for scenario simulations, e.g. bank erosion forecasting. The 2019 model bathymetry is shown in Figure 3-4.

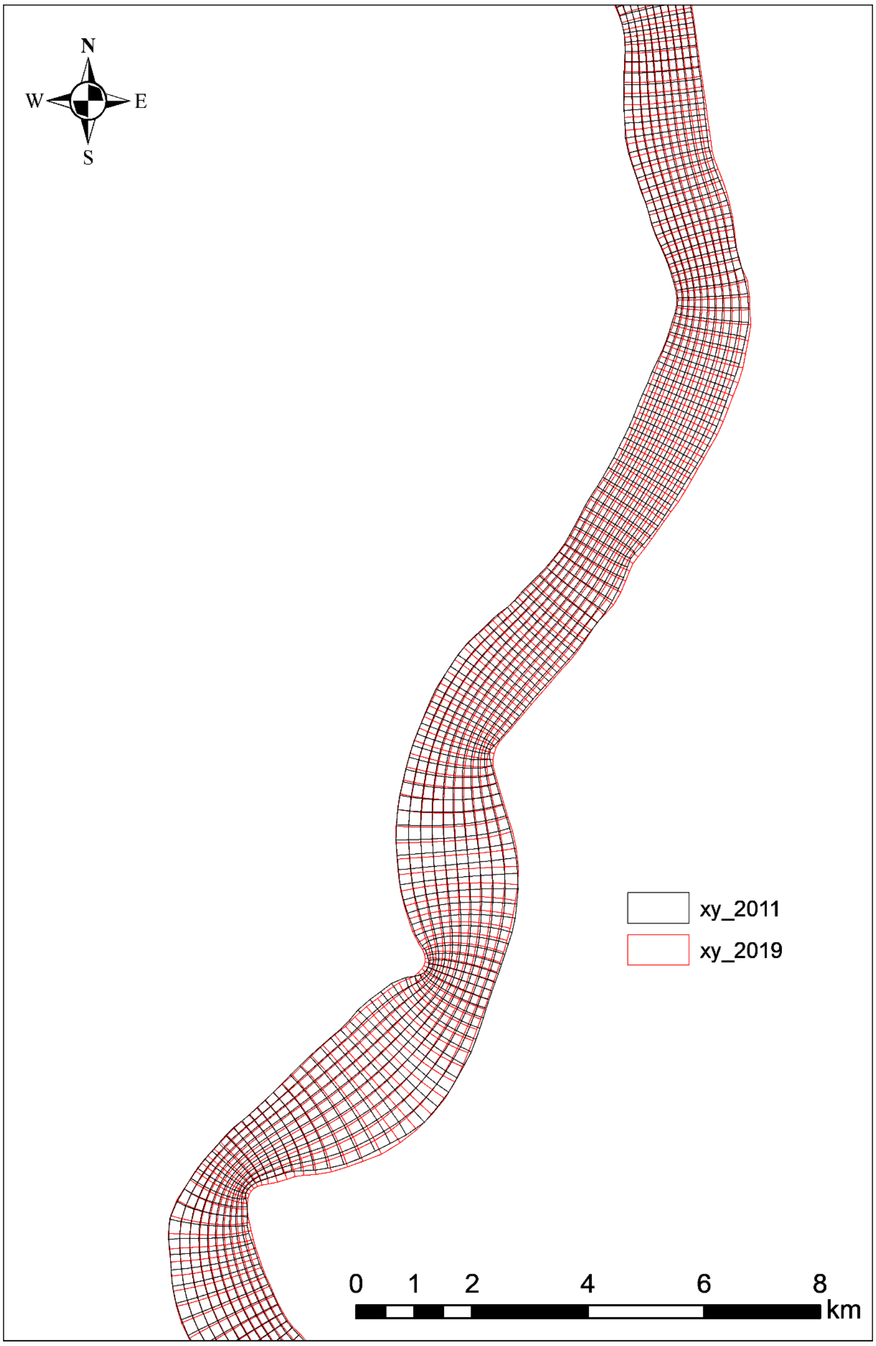

Figure 3-3 Grids for 2011 and 2019, here shown locally to better illustrate the differences between the grids. Both grids conform to the respective (2011 and 2019) bank lines, and both grids have the same number of grid points (500x10).

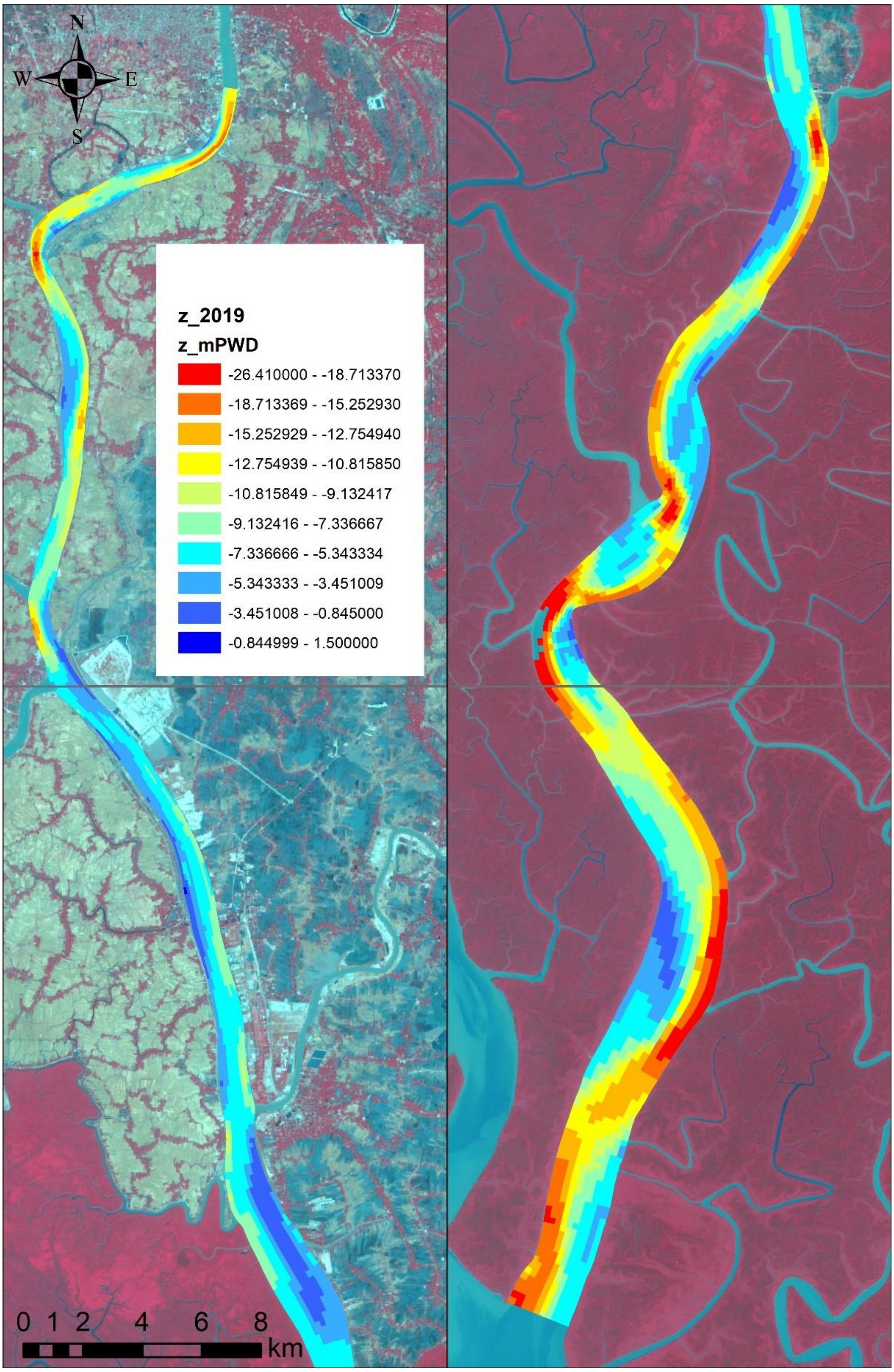

Figure 3-4 2019 bathymetry shown on the 2019 grid (and 2019 Landsat image).

3.2 Hydrodynamic boundary conditions

The Pussur River model uses the following boundary conditions:

- Discharge at the upstream/northern boundary
- Water level at the downstream/southern boundary
- Discharges to and from side channels

Figure 3-5 shows the locations of all boundaries and sources (side channels) in the model.

The upstream boundary condition at Rupsha is a time-series of simulated discharges extracted from the calibrated and validated South West Regional Model (SWRM). The downstream boundary condition is a time-series of water levels extracted from the SWRM.

The side channels discharges were added as source/sink points (adding and removing water to reflect the interaction with the side channels) in the model. It is essential to include the exchange of flow with the side channels in the hydrodynamic model, as the flow exchanges with these side channels are quite significant. All the side channel discharges were extracted from the South West Regional Model.

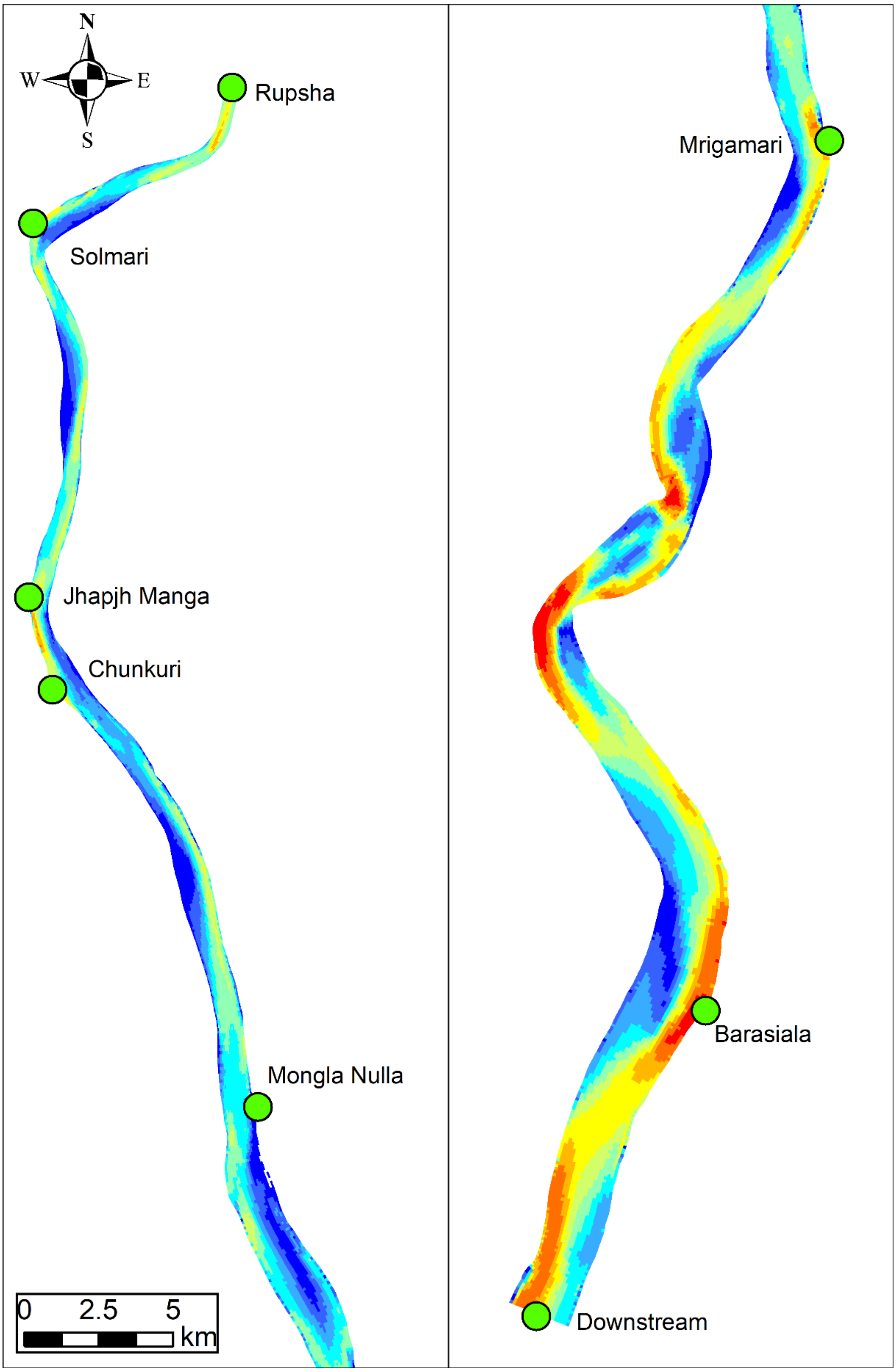

Figure 3-5 Boundaries (Rupsha and downstream, Akram Point) and sources (along the river) locations in the Pussur River model; the location “Jhapjh Manga” is called Badurgacha in the SWRM.

For the morphological model runs, IWM provided a continuous time-series for the period 2011-2018 from the SWRM models available for each year. The SWRM is recalibrated each year, hence the time-series for 2011-2019 were merged from 8 individual model runs.

Table 3-1 SWRM 2011-2018 locations.

BTM X [m]	BTM Y [m]	SWRM station (chainage in m)	Q/H
457718	519182	RUPSA (6000 m)	Q
451026	514600	L-SOLMARI (1000 m)	Q
450888	502002	JHAPJH-MANGA (885 m)	Q
451677	498880	CHUNKURI (875 m)	Q
458593	484821	MONGLA_NULLA (13463 m)	Q
462838	471389	MRIGAMARI (530 m)	Q
458677	442065	BARASIALA_G (1240 m)	Q
452971	431764	PUSSUR (80210 m)	H

The boundary conditions and their locations are listed in Table 3-1.

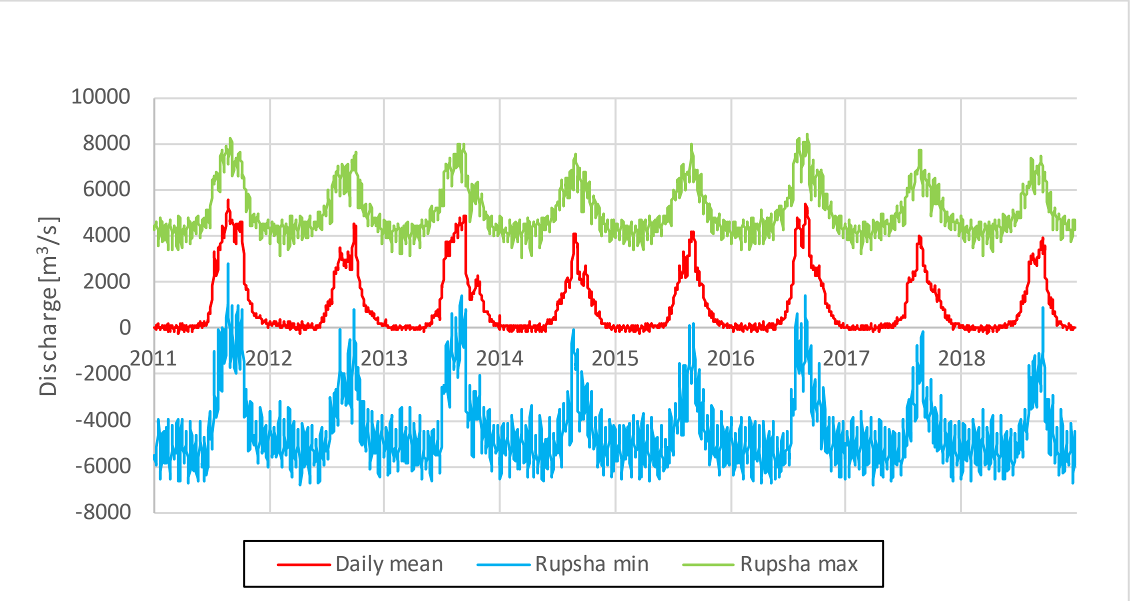

Figure 3-6 Daily minimum, maximum and mean flows 2011-2019 upstream boundary (Rupsha) in the Pussur River model.

Figure 3-6 shows the daily mean flow (flow averaged over two tidal cycles of 24 hour and 50 minutes) at Rupsha along with the corresponding minimum and maximum values. The daily mean flow has a clear seasonal signal with no mean flow in the dry season (i.e. purely tidal flow) and a clear and sizeable mean flow during the monsoon. The various years 2011-2019 even have similar signals, but there are differences between the monsoons.

3.3 Hydrodynamic boundary conditions for scenario simulations

The SWRM was used for generating boundary conditions for the MIKE 21C models with the inclusion of subsidence in the SWRM cross-sections and sea level rise in the Bay of Bengal tidal water level conditions, both calculated for the year 2050. A gradual calculation of annual variations from 2019 to 2050 is cumbersome because it would require preparation of new cross-sections every year due to subsidence, so instead only the 2019 and 2050 years were used in the MIKE 21C models. Both years were simulated using the 2019 SWRM without (baseline) and with subsidence and climate change.

IWM ran the SWRM for the period:

- 2 November 2018 00:00
- 29 October 2019 16:30

Results were extracted for the Pussur model for the two scenarios:

- Existing conditions (baseline)
- Climate Change and Subsidence (Sub+CC)

Pussur has the following open boundaries:

- Upstream discharge
- Downstream water level

There are also several side channels in the Pussur model for which the same procedure was followed. Refer to Section 3.2 for details about the locations of these boundary conditions.

The full time-series is not meaningful to show due to the detail. Instead, the tidal time-series were post-processed to show the daily mean, minimum and maximum for the discharges upstream and for the water levels downstream.

Figure 3-7 shows the post-processed daily discharges. The results show that the 2019 SWRM has no dry season net flow, and monsoon flows are smaller than the tidal flows. The post-processed data above all suggests that in general the tidal discharges increase with subsidence and climate change, which makes sense considering that all tide levels in the Bay of Bengal are increased and the bathymetry is lowered due to subsidence. The monsoon net discharge does not increase due to climate change and subsidence.

The water levels at the downstream boundary daily post-processed values are shown in Figure 3-8. This figure shows the expected rise in the water level due to climate change. The tidal water level increase is 20 cm on average according to the SWRM post-processed results, which is identical to the sea level rise in 2050.

Future sediment concentration boundary conditions were not altered compared to existing concentrations. It should be kept in mind that the model uses sediment concentrations and not sediment fluxes, so while sediment concentrations are considered unchanged in the future, the sediment fluxes can change.

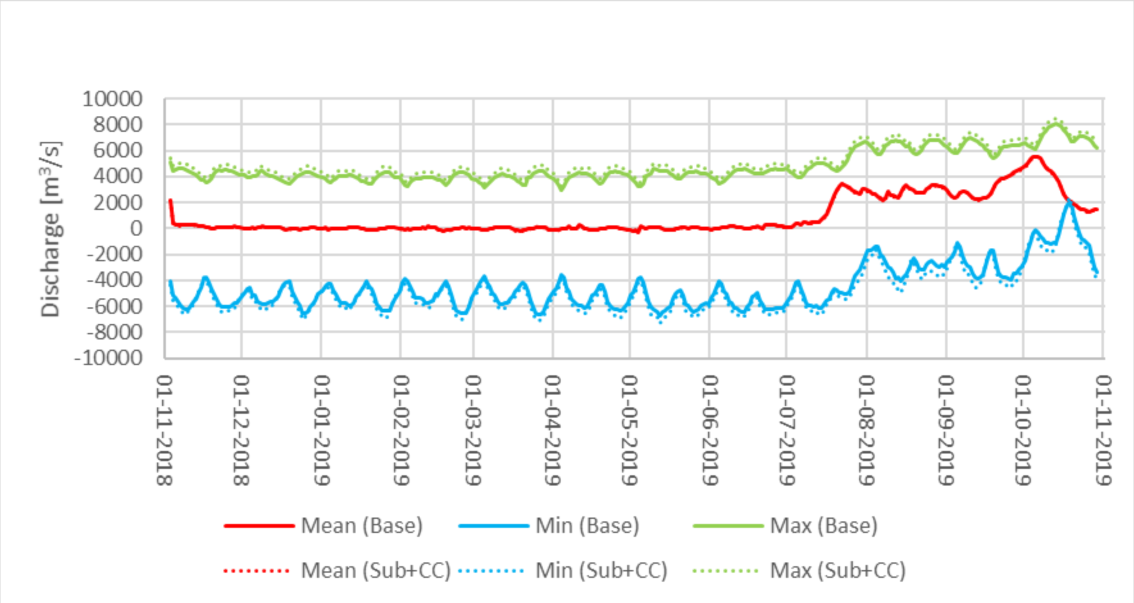

Figure 3-7 Daily minimum, maximum and mean flows 2018-2019 upstream boundary in the Pussur River model for the two cases Base and Sub+CC.

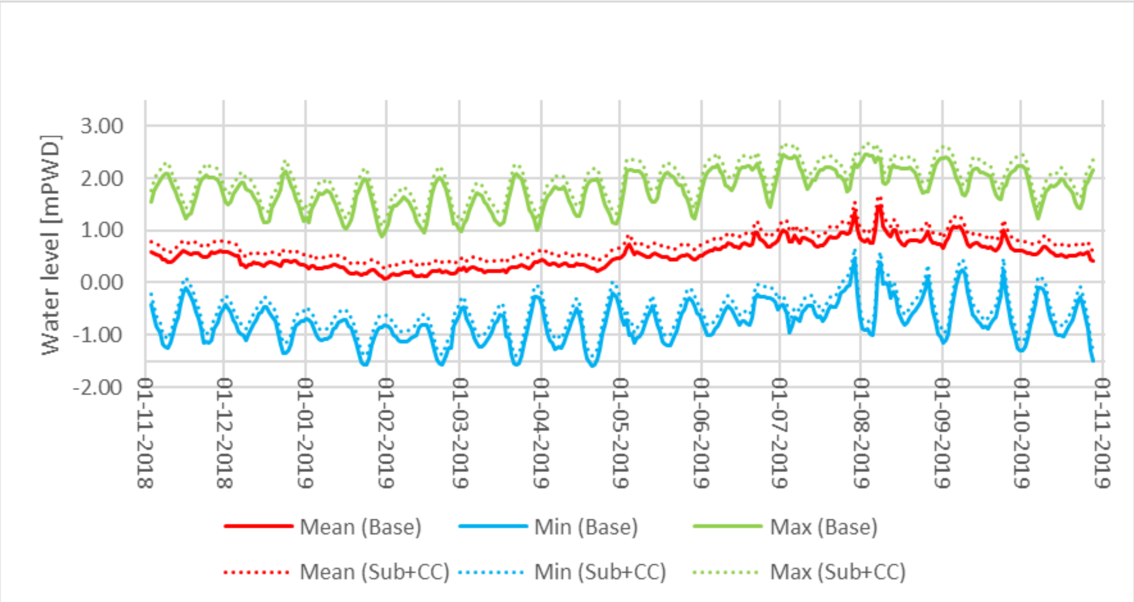

Figure 3-8 Daily minimum, maximum and mean water levels 2018-2019 downstream boundary in the Pussur River model for the two cases Base and Sub+CC.

3.4 Hydrodynamic calibration and validation

The data available for calibration and validation of the model are presented in Section 2.2 of this report. The 2011 data was used for calibration, while validation was conducted for the 2016 data, using the calibration parameters adjusted for the 2011 situation.

The hydrodynamic calibration and validation were conducted in the fine grid model with floodplain included. Subsequently, the calibration parameters were transferred to the grid used in the morphological model.

There are several ways to calibrate the hydrodynamic model. The easiest approach is to use a constant Manning M and adjust the magnitude to match observed water levels and discharges.

However, spatially varying Manning M values can also be adjusted to obtain the same model behaviour in terms of water levels and discharges, but potentially with significantly different velocity distributions. In other words, in the absence of velocity distribution data there is no unique calibration of the hydrodynamic Pussur River, but if only attempting to match discharges and water levels, the various resistance models do not give significant differences.

Options for and relevance of introducing a spatially varying resistance number in the model order to obtain a more realistic flow distribution across bars are discussed in Appendix A.

The only way to fully calibrate the resistance model is to use observed water levels and discharges (as usual) combined with observed velocity distribution, especially in areas with large water depth variations. However, observed velocity distribution was not available for the study.

Alternative resistance models were investigated as part of the calibration process. It is possible to use a spatially varying Manning M with low resistance in the deep channels, representing the cohesive bed, and higher resistance on bars to represent potential dune cover. With such a spatially varying resistance map, water levels and discharges due to the tidal propagation in the deeper channels can still be captured, while obtaining very different velocity profiles in bends with high resistance on bars. The implication is that various resistance models can capture water levels similarly to the constant Manning M, but with very different velocity distributions and hence different sediment transport and morphology.

A constant M=60 $m^{1/3}/s$ was used in the production morphological models, but it must be stressed that the morphological model behaviour is very sensitive to the flow resistance model.

3.4.1 Hydrodynamic model calibration 2011

For calibration of the model continuous observations of water levels have been available at Mongla while discharge observations from one neap and one spring tide during the monsoon period and twice (February and March) during dry season have been available at Akram Point and Mongla (refer to Figure 2-2 for the locations of the stations).

The best overall agreement between model and observations has been achieved using a Manning M = 60 $m^{1/3}/s$. The results of the calibration are discussed below.

The water level calibration plots at Mongla Port are shown in Figure 3-9 and Figure 3-10 for the 2011 monsoon and dry season, respectively. The computed water level is underpredicted, especially in flood tide, but in the ebb tide the water levels match quite well. It is noted that the observed water levels are quite similar during monsoon and dry season suggesting that the water level is controlled by tidal dynamics rather than by net flow and thus bed friction. This is confirmed by model simulations showing that the simulated water level is relatively insensitive to the applied resistance number.

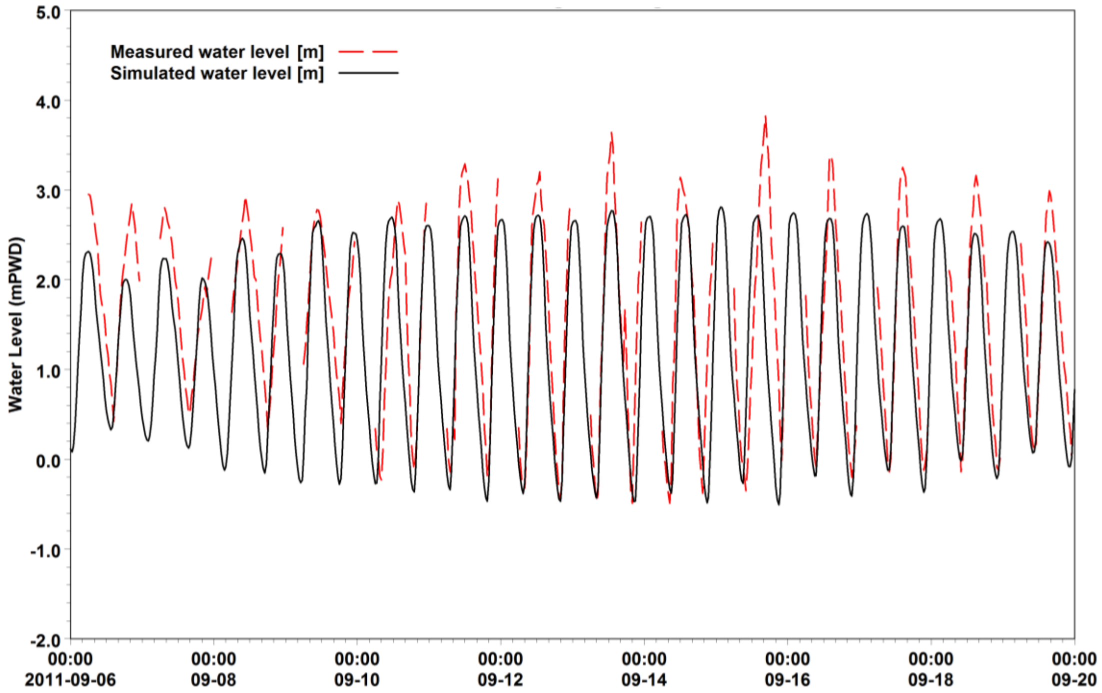

Figure 3-9 Comparison between observed and computed water level at Mongla Port during 2011 monsoon.

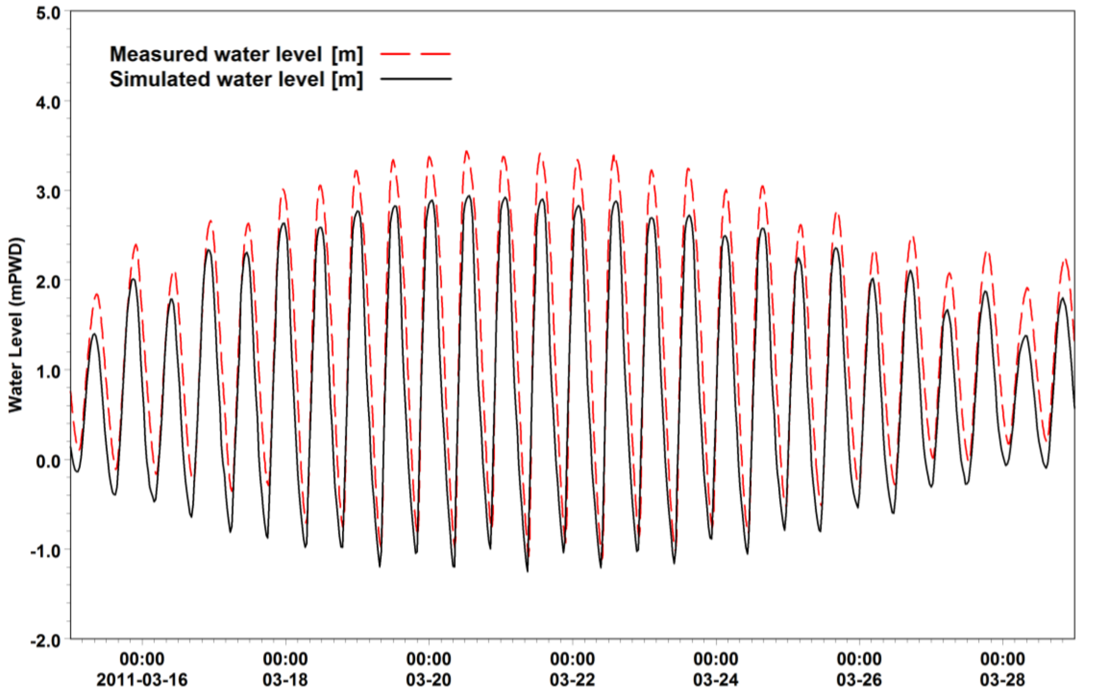

Figure 3-10 Comparison between observed and computed water levels at Mongla Port during 2011 dry season.

Assuming that the Akram Point water levels and discharges match the observations well in the SWRM, the most reasonable explanation for the water level discrepancies at Mongla is too much tidal prism upstream of Mongla (draining the flood flows away from Mongla). The discharges at Rupsha are also satisfactory, which leaves the side channels as the only viable culprits.

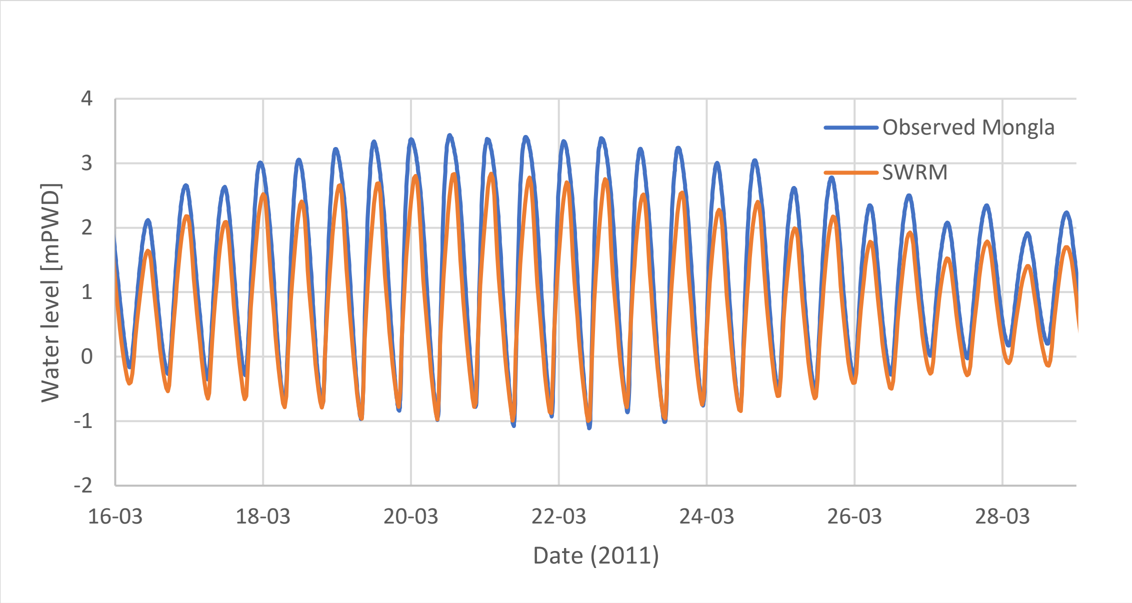

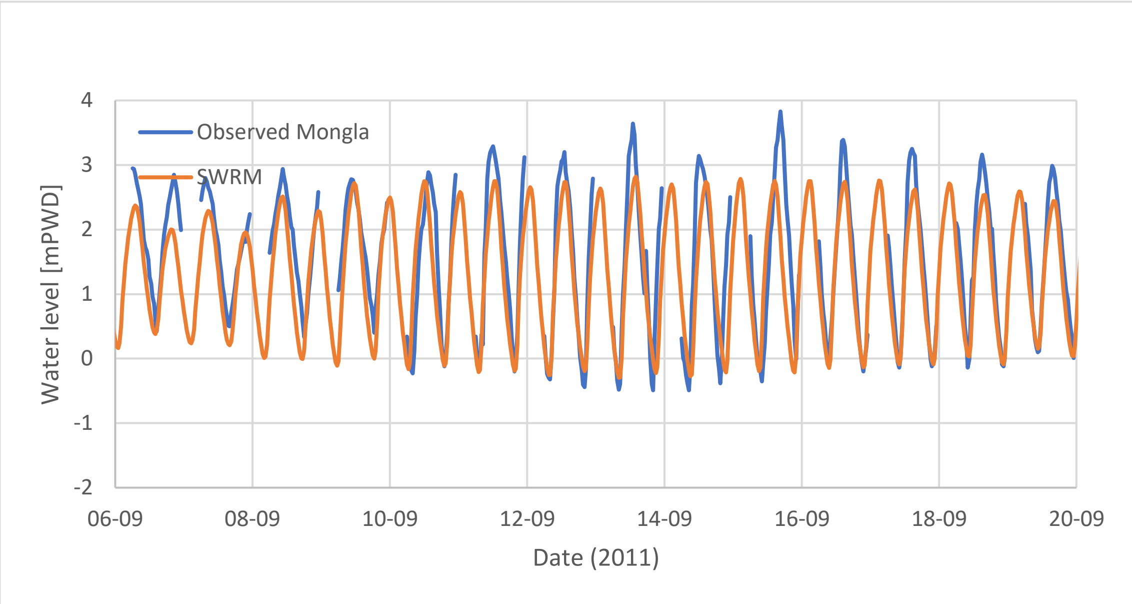

Figure 3-11 Comparison of observed and simulated (SWRM) water levels at Mongla during 2011.

If this analysis is correct, the SWRM should have the same problems at Mongla. The water levels from the SWRM are compared to the Mongla observations in Figure 3-11 showing that the SWRM has the same problem with the Mongla water level. In fact, the SWRM and MIKE 21C water levels are almost identical at Mongla.

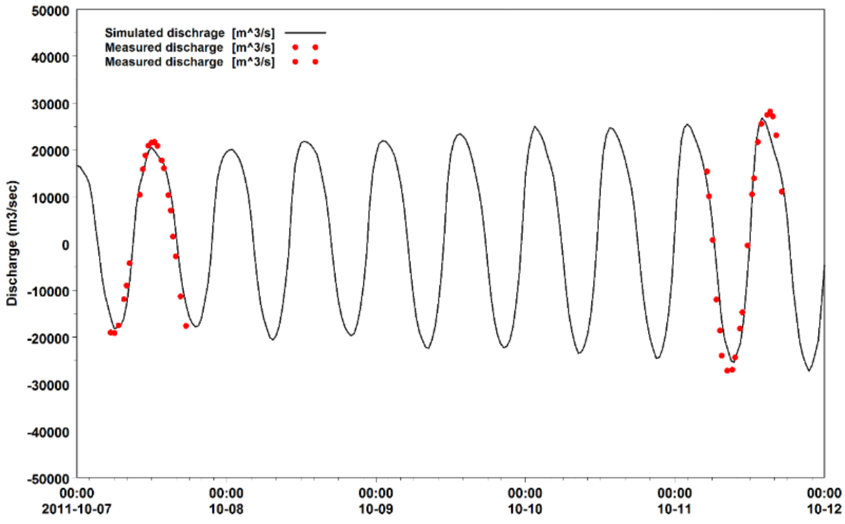

Figure 3-12 Discharge calibration at Akram Point in Pussur River during 2011 monsoon (October).

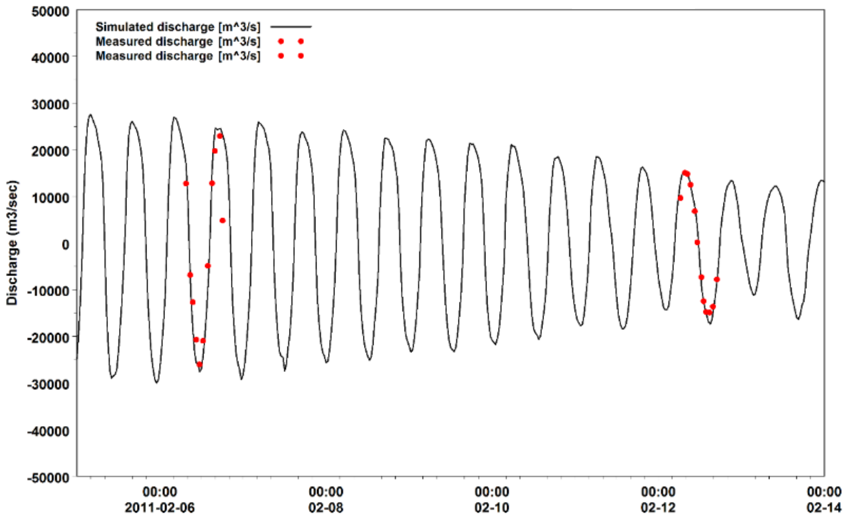

Figure 3-13 Discharge calibration at Akram Point in Pussur River during 2011 dry season (February).

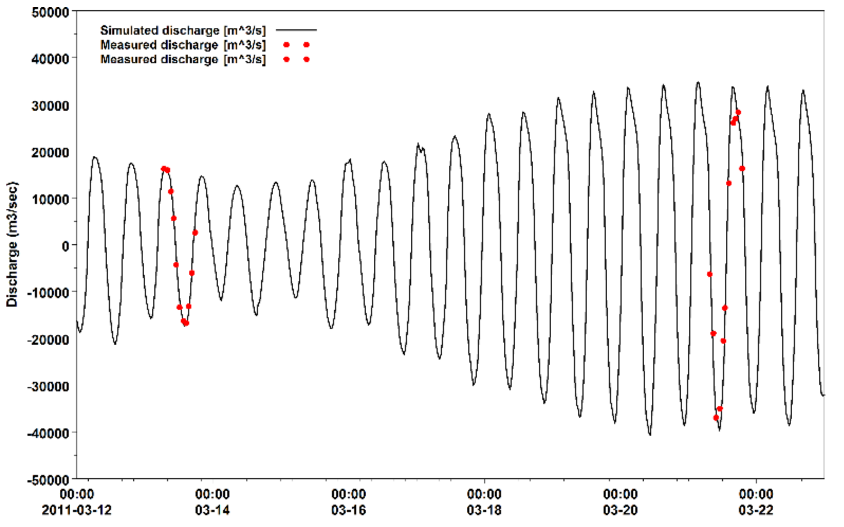

Figure 3-14 Discharge calibration at Akram Point in Pussur River during 2011 dry season (March).

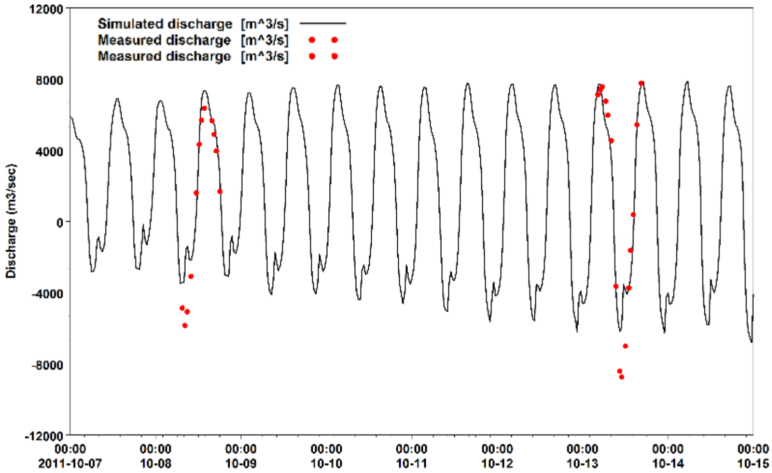

Figure 3-15 Discharge calibration at Mongla Port during the 2011 monsoon (October).

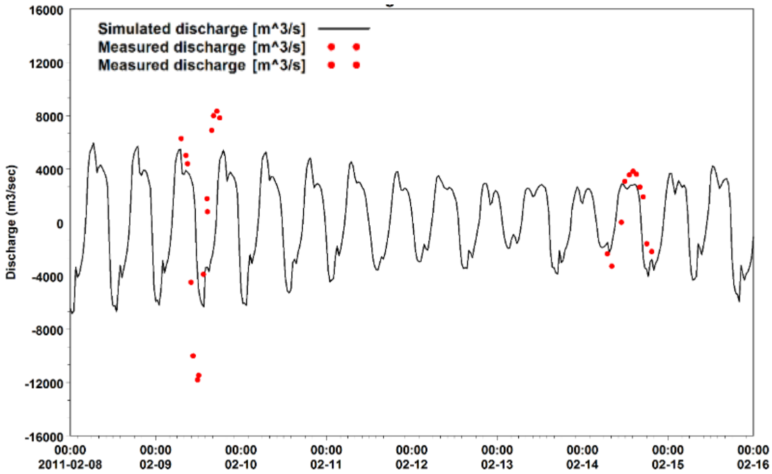

Figure 3-16 Discharge calibration at Mongla Port during 2011 dry season (February).

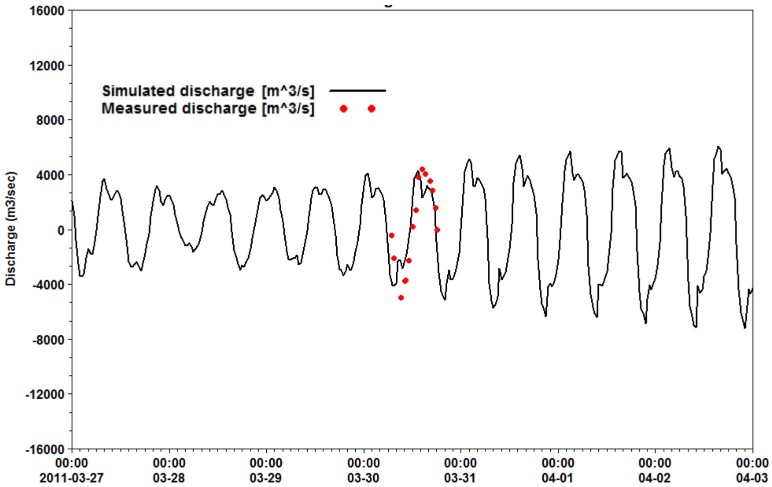

Figure 3-17 Discharge calibration at Mongla Port during 2011 dry season (March).

The observed and simulated discharges at Akram Point are compared in Figure 3-12 to Figure 3-14. The figures show that the dry season discharge at Akram Point is simulated satisfactorily, while the monsoon calibrations show slight underprediction of flood flows of 2-3000 m^3/s (Figure 3-14). Irrespectively of this deviation, the model performance at Akram Point is deemed extremely good, which suggests that the tidal prism upstream of Akram Point is correctly modelled.

The observed and simulated discharges at Mongla are compared in Figure 3-15 to Figure 3-17. At Mongla, the flood flows are also underpredicted with the same magnitude as Akram Point (it is important to note that the vertical scale in the plots for Akram Point is different from the scale used at Mongla). The underprediction of the discharge is consistent with the deviation seen in observed and simulated water level at Mongla (see Figure 3-9 and Figure 3-10). This suggests that the tidal prism upstream of Mongla is not predicted well, especially for spring tide conditions.

The discrepancy between model and observations can thus be attributed to lack of tidal prism in the model upstream Mongla. This prism is implicitly represented in the model through the point inflows representing side channels and the upstream boundaries, all originating from the SWRM. Generally, the simulated discharges correspond better to the observations than the simulated water levels. This is important in a morphological model; hence the overall model calibration is deemed satisfactory.

3.4.2 Hydrodynamic model validation 2016

For verification of the model, discharge observations during a neap and spring tide in the dry season at Rupsha and Mongla have been available.

The validation result is discussed below.

Figure 3-18 shows simulated and observed discharge at Rupsha. Rupsha is the upstream model boundary; hence this plot confirms that the tidal prism upstream Ruphsa in the SWRM is somewhat underpredicted as discussed in the previous sub-section.

The simulated and observed discharge at Mongla is shown in Figure 3-19. The model is good in the phase but underpredicts especially flood flows. The underpredicted discharge at Mongla in 2016 is consistent with the underpredicted water levels in 2011. The difference in magnitude may be explained by different calibrations used in the SWRM that provides boundary conditions for the present model.

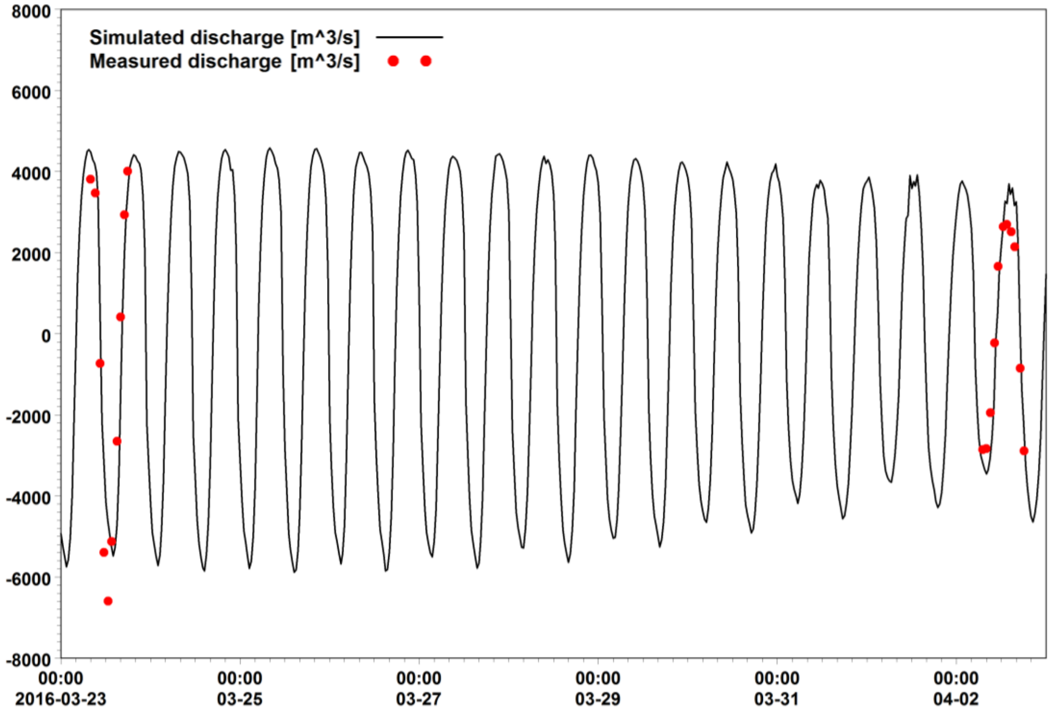

Figure 3-18 Discharge validation at Rupsha in Pussur River during 2016 (March-April).

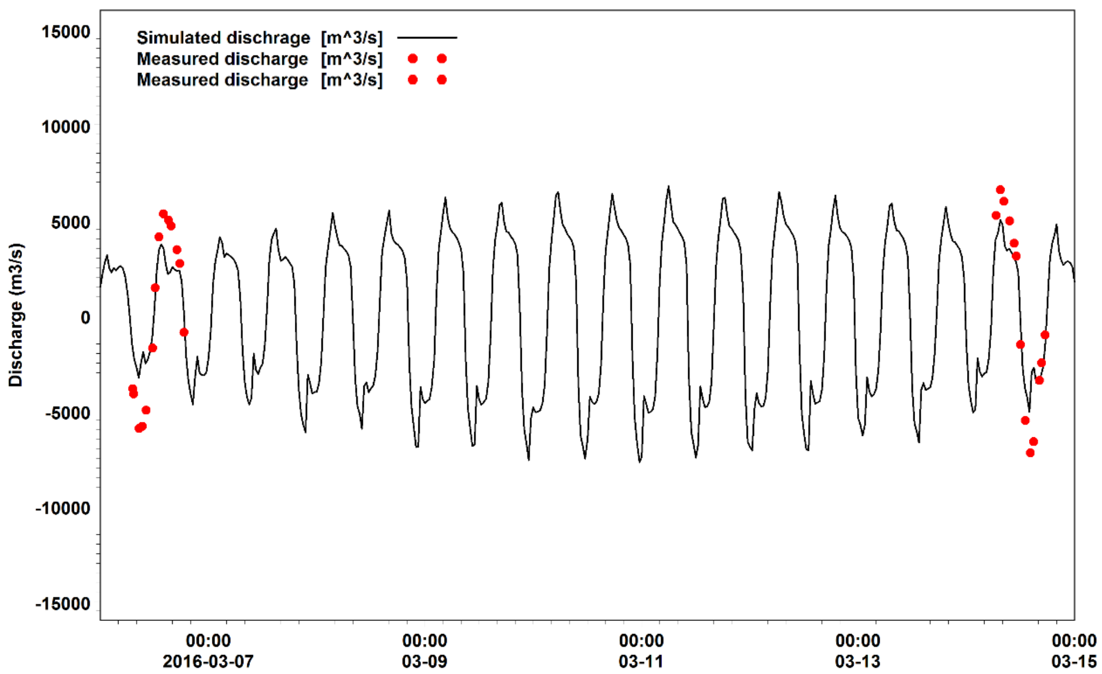

Figure 3-19 Discharge validation at Mongla in Pussur River during 2016 (March).

3.5 Sediment model

The Pussur River model was the first of the models to be developed, and therefore a substantial effort was invested in the calibration of the Pussur River sediment model, since it was expected that the lessons learned could be applied in the calibration of the other models. The work with the calibration is reported in this section.

Almost 200 simulations (each taking 5 hours) were conducted to arrive at what can be considered the best model that can be developed based on the available data.

3.5.1 Particle size distributions

The appropriate sediment regime should be determined based on data. Particle size distribution data should ideally be available for the following:

- Boundary inflows (suspended sediment)
- Bed composition
- Bank composition

There is no particle size distribution data available for the measured sediment concentrations; adjustment of the mud and sand contributions were done indirectly via the bed level changes.

There are many bed samples available for the Pussur River, although not enough for an adequate mapping of the size distribution of the bed surface. The available bed samples suggest that sand is not very frequent in the bed. Sand is found in the outer side slopes of the sand bars, but apart from the fact that sand is not found on the inner bars, it is not known whether sand is consistently found on the whole sand bar surface. The bed samples also suggest that the bed surface is sandier downstream compared to upstream, but the data does not give a sufficiently clear picture.

The particle size distribution of the banks is unknown. Some data from the land surface adjacent to the river show less than 10% sand, but the sand content deeper into the ground could be higher than the surface; the lowest sand content must be expected on the surface. Therefore, it has been assumed that the bank sediment consists of 90% silt and 10% sand (by mass) with porosities of 0.6 and 0.35.

3.5.2 Sediment fractions

The available data from the Pussur River shows that sediment is muddy upstream and with some sand in the downstream end, hence the sediment must be described using at least two sediment fractions in the model.

The Pussur River model was developed using a 2-fraction sediment model with mud and sand:

- Mud: Fall velocity 1 mm/s
- Sand: Grain size 0.125 mm

The sizes selected were based on the bed samples presented in Section 2.3 (Figure 2-3), and the fall velocity for the mud fraction was based on Stokes' Law.

The cohesive sediment is modelled using the traditional cohesive sediment erosion (E) and deposition (D) functions, see Mehta et al. (1989).

The erosion rate [g/m^2/s] was calculated from:

$$E = F_i E_0 \left(\frac{\tau'}{\tau_{ce}} - 1\right)^n, \tau' > \tau_{ce}$$

The deposition rate [g/m^2/s] was calculated from:

$$D = w_s \gamma_0 C \left(1 - \frac{\tau'}{\tau_{cd}}\right), \qquad \tau' < \tau_{cd}$$

Where:

F_i Relative mass of the fraction (i) in the bed surface

E Erosion rate [g/m²/s]

D Deposition rate [g/m²/s]

E_0 Erosion coefficient [g/m²/s]

τ' Skin friction shear stress

τ_{ce} Erosion shear stress threshold [N/m²]

τ_{cd} Deposition shear stress threshold [N/m²]

C Simulated concentration [g/m³]

w_s Fall velocity [m/s]

n Exponent (non-linearity)

γ_0 Ratio between near-bed and depth-integrated concentration (optional)

The calibrated parameters were:

τ_{ce} = 0.2 N/m²

τ_{cd} = 0.1 N/m²

E_0 = 0.02 g/m²/s

w_s = 1 mm/s

n=1

γ_0 = 1

Porosity 0.6

3.5.3 Approach for modelling sediment mixtures

Generally, there are the following options for modelling sediment mixtures:

- Sand-mud model with traditional surface-based separated transport models
- Sand-mud model without interaction (shared erosion functions)
- Sand-mud model with interaction

In the following, based on the experience obtained from preliminary model simulations as well as earlier experience the various options have the following pros and cons:

<u>Sand-mud model with traditional surface-based separated transport models</u>: This traditional approach works well when the bed tends to be either sandy or muddy (ie. patchy) but will cause problems when the sand and mud are mixed as in the Pussur River. When trying to apply this

approach, the sand entrainment rates tend to be very high, which can easily lead to degradation of sand bars in the model of the Pussur River.

Sand-mud model without interaction (shared erosion functions): When the sand and mud are mixed, they tend to entrain together instead of individually. This is often referred to as mass erosion where the bed erodes in mass rather than through selective entrainment. Mass erosion takes place when the mixture exhibits cohesive behaviour, i.e. when the cohesive surface content is above a certain limit. This approach works reasonably well for the model of the Pussur River, except at sand bars in sharp bends, which tend to erode in the model.

Sand-mud model with interaction: Sand-mud interaction also means that the sand and mud erode as mass, but due to the interaction, the erosion resistance of the mixture depends on the mud content. Data shows that the bars often have sediment composition close to be the highest erosion resistance. This offers an explanation for the existence of bars in the model that would otherwise be eroded if other formulations were used. That is the main argument for using a sand-mud model with interaction.

3.5.4 Sand-mud interaction

This section introduces the simple sand-mud interaction model that was applied for the Pussur River. The most important observation from bed samples is that the bars are characterized by mixed sediment, which could be the most erosion-resistant bed composition in the bed surface, while the muddy bed usually seen in the main flow channels is much easier to erode. In other words, the bars have the most erosion-resistant sediment composition when seen through a sand-mud interaction model, while a traditional sand model would suggest that the bars are composed of the most erosional sediment in the Pussur River.

The possibility that the sediment mixture has the same erosion function for all fractions was explored. The argument for the shared erosion function is that the sediment components (fractions) erode as a mass (together) and not individually.

The (traditional) individual treatment of the sand and mud entrainment does not give convincing results. Especially the bars in the sharp bends are clearly subjected to flows that will erode the sand from the bars, which is not consistent with observations. It is noted that this is not necessarily a problem with the sand entrainment, as it is also heavily dependent on the flow resistance model.

Some publications were studied to find a reasonable model approach for the sand-mud interaction in the Pussur River, namely Mitchener & Torfs (1995), Waeles et al. (2007) and van Ledden (2003).

With at least 20% cohesive content in the bed surface, the sediment mixture will exhibit cohesive behaviour according to Mitchener & Torfs (1995), i.e. the sediment mixture will be subjected to mass erosion rather than erosion of the individual sediment fractions. The cohesive content in the Pussur River is usually higher than 20%, except at the bars.

Waeles et al. (2007) give the highest erosion shear stress threshold even for sand/mud in the bed surface for a critical cohesive content of 30%. Waeles et al. used shared erosion functions when the bed surface exhibits cohesive behaviour, while a separate erosion function was used for sandy behaviour.

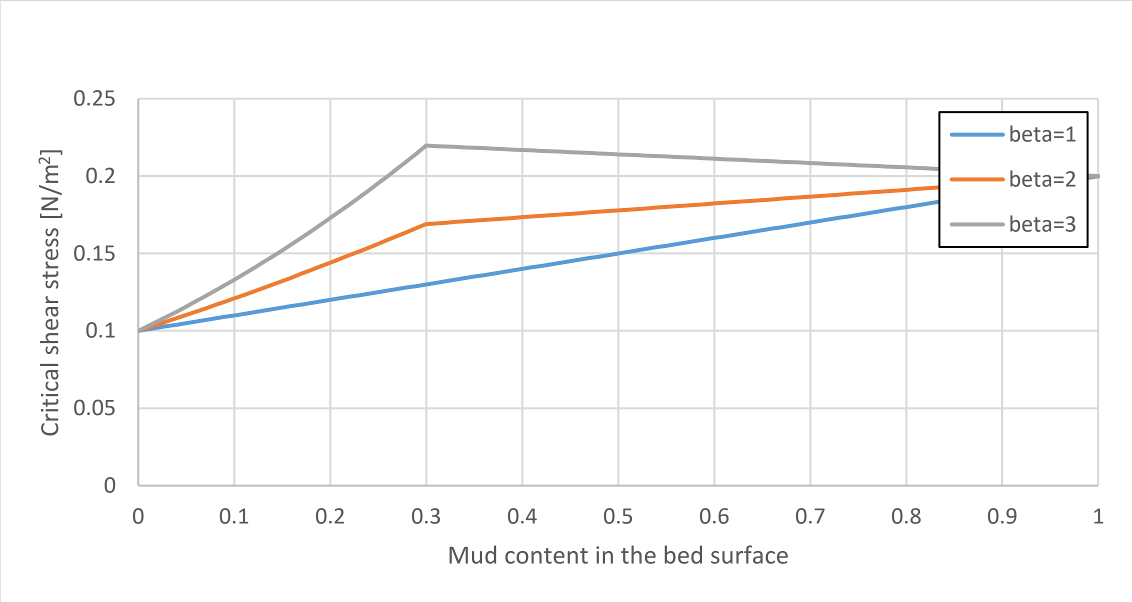

Figure 3-20 van Ledden (2003) curves examples with 0.15 N/m² critical sand shear stress, 0.2 N/m² mud critical shear stress, 0.3 critical mud content, beta=1,2,3.

van Ledden (2003) gives the following for the critical shear stresses for mud and sand as a function of the mud content:

$$\frac{\tau_{e,nc}}{\tau_{cr}} = (1 + p_m)^{\beta}, \qquad p_m < p_{m,cr}$$

$$\tau_{e,c} = \frac{\tau_{cr}\,(1 + p_{m,cr})^{\beta} - \tau_e}{1 - p_{m,cr}}(1 - p_m) + \tau_e\,, \qquad p_m > p_{m,cr}$$

Examples of the critical shear stress curve as a function of mud content in the bed surface are shown in Figure 3-20. van Ledden (2003) found for the non-cohesive regime typically β=1 (based on very limited data).

The most interesting observation is that the bars are the location with the most pronounced mixture of sediment, and the above sand-mud interaction model suggests that the bars will have the highest erosion-resistance.

The model development has shown that including a model for sand-mud interaction provides the best model results and hindcast of the observed morphology:

- A traditional sand model cannot explain the bars; the bars will tend to degrade in the sharp bends
- The bars are characterized by sediment composition close to what would be expected to have the highest erosion resistance
- The bars and bend scours are important for bank erosion

A simple variant of the sand-mud interaction description where the sediment mixture will exhibit cohesive behaviour and therefore share erosion functions has been applied. The erosion shear stress threshold is calculated from the above-mentioned van Ledden model with the same value for sand and mud varying with the mud content.

The sand erosion shear stress threshold is estimated in the following. First, the critical shear stress for the sand (0.125 mm) can be calculated from the Brownlie (1981) representation of the Shields curve:

$$\theta_c = 0.22\, Re^{-0.6} + 0.06 \cdot 10^{-7.7\, Re^{-0.6}}$$

Where Re is the grain Reynolds number:

$$Re = \frac{\sqrt{(s-1)gd}}{\nu}$$

Assuming a viscosity of 10^{-6} m^2/s, the grain Reynolds number becomes Re=5.62, and the critical Shields parameter becomes θ_c=0.078. Hence the critical shear stress for 0.125 mm sand is:

$$\tau_c = \theta_c\, \rho(s-1)gd$$

Yielding:

$\tau_c =$ 0.158 N/m^2

It is noted that this is lower than the value used in the mud erosion models (0.2 N/m^2). No data was available for the critical shear stress of the mud, so the value for the mud was selected and the mud erosion model calibrated accordingly. A critical shear stress of 0.2 N/m^2 is typical for unconsolidated mud, which dominates the riverbed due to the continual erosion and deposition of material (no consolidation).

3.5.5 Development of the bed model

The bed model describes the spatial and vertical distribution of the sediment fractions in the bed.

The bed model was developed through an iterative process. In connection with this, it is critically important to understand that the bed model is associated with a long timescale (meaning that bed composition will change very slowly in the model), and simulation results will therefore be influenced significantly by the initial conditions. Hence, the initial conditions need to be selected carefully.

To explore potential systematic behaviour of the sediment bed composition, the available bed samples were processed as follows:

- Bed levels were extracted from the contoured 2011 bathymetry at each bed sample point. This is not 100% accurate as the bed samples are from different years, but in the present context this is not considered important.
- Each bed sample location was assigned a bed morphology class: Channel, bar, or inner bar (can also be interpreted as flood channel; inner bar means on a bar, but closer to the bank).

In the following, plots of sand contents as a function of longitudinal coordinate along the river and bed level are presented.

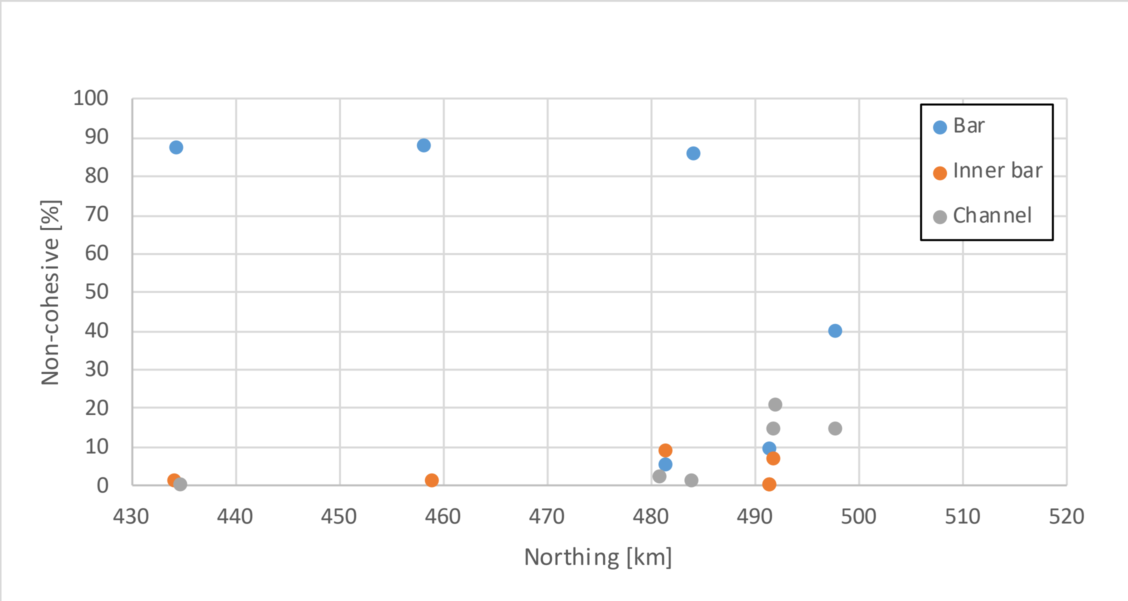

Figure 3-21 Longitudinal (northing) variation in the non-cohesive (=sand) content in the three morphological classes: Channel, bar, inner bar.

The bed samples show the following longitudinal pattern illustrated in Figure 3-21:

- Generally, sand content is much higher in bars than in the channel and at inner bars
- Inner bars are muddy
- Sand content in bars increases in the downstream direction
- The channel bed sand content increases in the upstream direction

The observations show that only the parts of the bars located away from the banks are sandy, while the inner bars are always muddy.

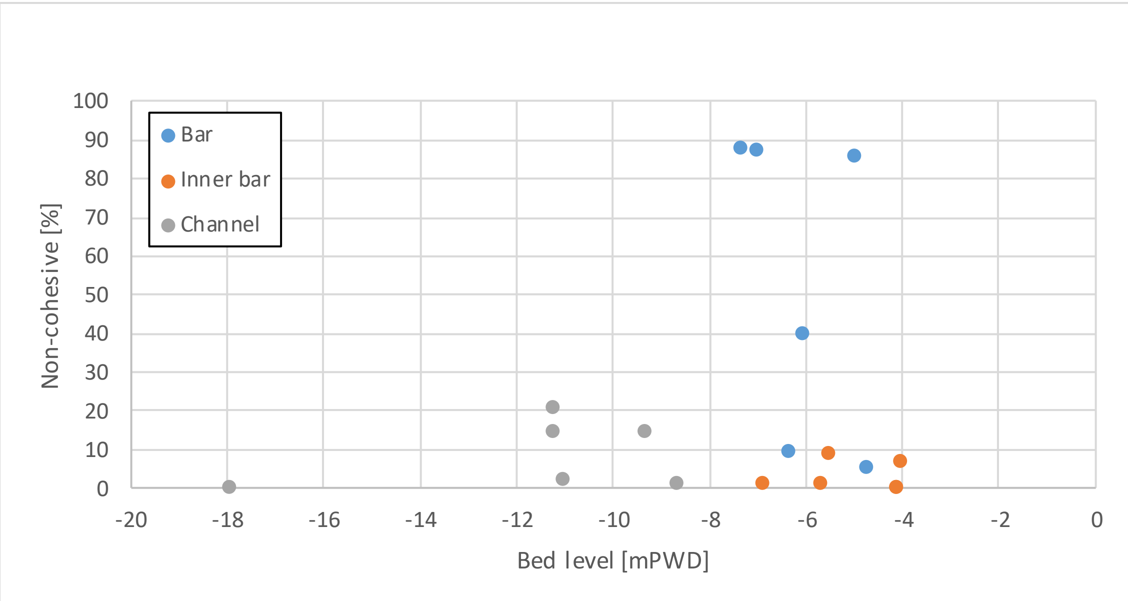

Figure 3-22 Correlation with bed level for the three bed classes.

The percentage of non-cohesive sediment versus bed level is illustrated in Figure 3-22. It is first observed that in general, the sand content increases with elevation, and there is generally no sand in the deep channels. For bars it is observed that the bar and inner bar have similar elevations, but also a big difference in sand content. Bars can have varying degrees of sand content (due to the longitudinal correlation), while inner bars are never muddy according to the available samples.

The bed model was based on these general correlations. A relatively simple model was applied with bars being sandy and the sand content varying longitudinally.

3.5.6 Water temperature and fall velocity

The water viscosity is influenced by the temperature of the water and is important for the fall velocity.

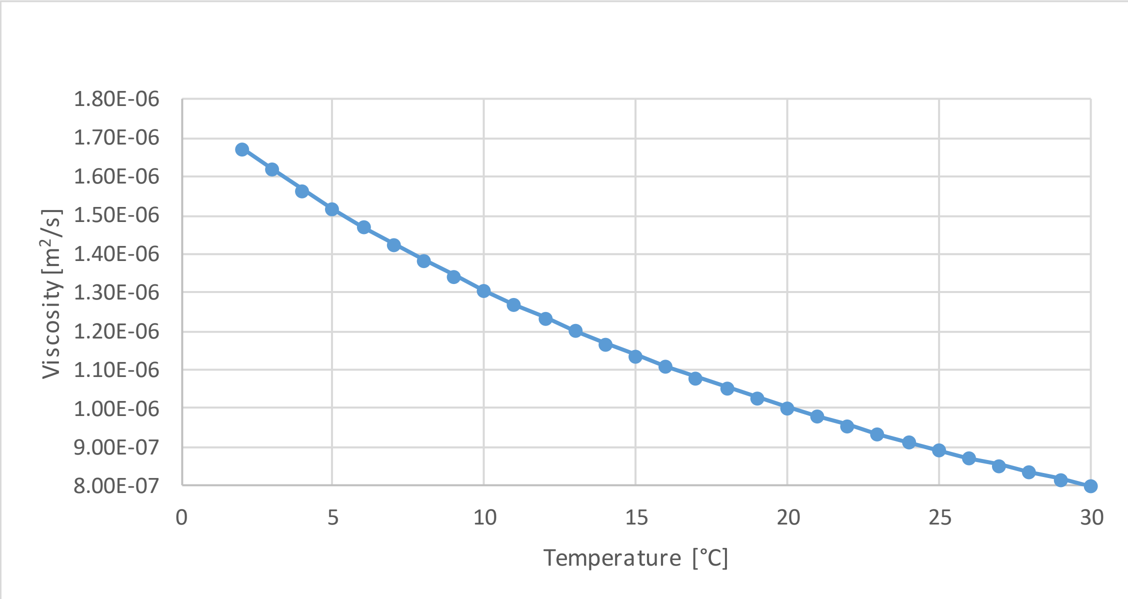

Figure 3-23 Water viscosity as a function of temperature

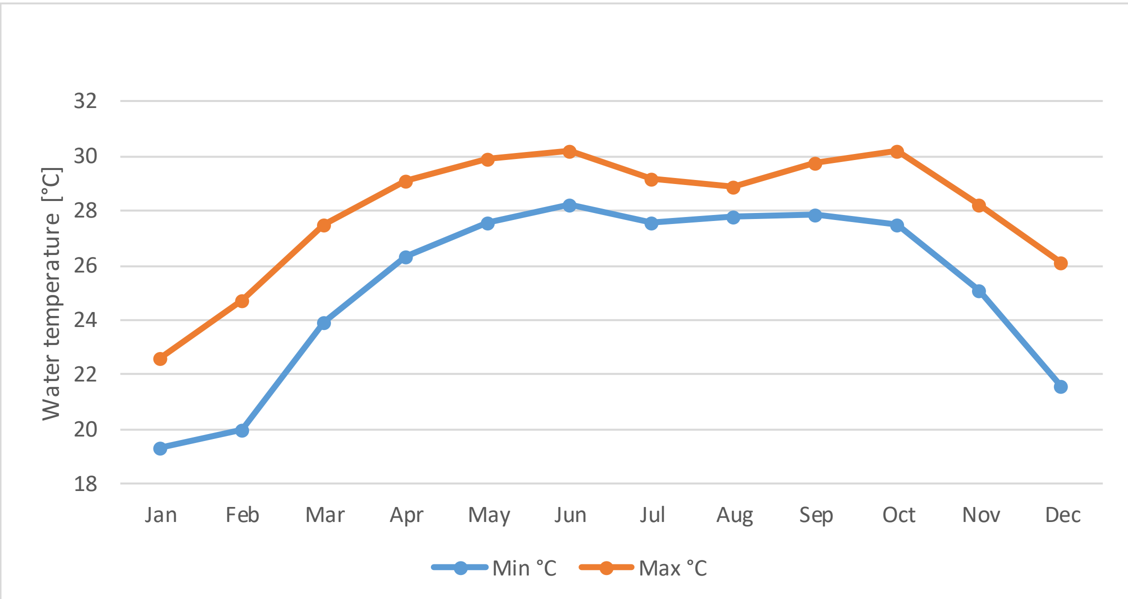

Figure 3-24 Water temperatures at Chittagong (www.seatemperature.org/asia/bangladesh/chittagong.htm)

The fall velocity in MIKE 21C is calculated from Rubey (1933), except for cohesive sediment fractions for which the fall velocities are set by the user. The Rubey formula reads:

$$w_s = \sqrt{(s-1)gd}\left(\sqrt{\frac{2}{3}+\frac{36\upsilon^2}{(s-1)gd^3}}-\sqrt{\frac{36\upsilon^2}{(s-1)gd^3}}\right)$$

With the specific gravity s=2.65.

The median grain size for the sand is 0.125 mm, hence the fall velocity is:

- 20 degrees: 0.0124 m/s
- 25 degrees: 0.0135 m/s
- 27 degrees: 0.0141 m/s
- 28 degrees: 0.0143 m/s
- 30 degrees: 0.0147 m/s

The fall velocity during the monsoon is more important, so a representative water temperature of 28 degrees (viscosity 0.836×10^{-6} m^2/s) was applied, i.e. fall velocity 0.0143 m/s.

The fall velocity for the mud was set to 1 mm/s, which was used in all MIKE 21C models. The value was estimated from Stokes' Law using 0.03 mm (typical median silt size, although it varies from river to river) and a viscosity of 0.836×10^{-6} m^2/s.

3.6 Sediment transport boundary conditions

The model requires sediment boundary conditions at all boundaries where inflow occurs. These are:

- Rupsha
- Akram Point
- Side channels

The boundary conditions for these are reported in the following sub-sections.

3.6.1 Upstream sediment concentration boundary condition at Rupsha

Data of observed sediment concentration and discharge are available at Rupsha, see Section 0. There is no data available on the size distribution of the observed sediment concentration, i.e. the data does not provide any information concerning the relative contents of clay, silt and sand in the suspended sediment.

A sediment rating curve was generated using all ebb flow observations at Rupsha. The resulting curve was shown in Figure 2-7, where a simple expression was manually adjusted (automatic curve fitting does not work well due to the influence from small discharges and concentrations):

$C(Q) = C_0 * (Q/Q_0)^2$

Where C_0=1200 g/m^3 and Q_0=8000 m^3/s.

Subsequently, the proportion of silt in the sediment rating curve was determined using the model by trial and error. This resulted in an estimated 20% silt in the Rupsha suspended rating curve, i.e. 80% of the sediment is assumed to be finer fractions (clay) not interacting with the morphology.

It was assumed that the sand content in the sediment rating curve was negligible.

3.6.2 Downstream sediment concentration boundary condition at Akram Point

The Akram Point data shows good correlation between the discharge and suspended sediment concentration. For simplicity, constant concentrations were adopted instead of varying with the concentration. The simplicity is both in terms of making it easier, but also that the discharge at Akram Point is not known prior to running a model simulation (water level boundary condition), so the C(Q) relation cannot be directly imposed via a concentration time-series. The downstream suspended sediment concentration is not very important in the sand-mud interaction formulation because tidal pumping is relatively weak when the dominating sediment is mud.

The Akram Point sediment concentration boundary conditions were set as 100 g/m^3 for mud and 0 g/m^3 for sand.

3.6.3 Side channels sediment concentrations

There are no sediment concentration observations available for the side channels in the Pussur River. The discharges into the side channels are small compared to the discharge in the Pussur River itself, and hence the applied boundary sediment concentration at the side channels will not significantly impact the overall sediment dynamics in the model. For convenience, side channel concentrations have been assumed zero, both for inflows and outflows to the side channels. In other words, the side channels are neutral in terms of sediment fluxes, while they exchange water.

The side channels/peripheral rivers adjacent to the Pussur River are reported to diminish through sedimentation, thus presumably there is a net export of sediment from the Pussur River to the side channels. This, however, is deemed to be negligible compared to the vast quantity of sediment transported in the river itself.

3.7 Calibration against observed bed level changes 2011-2019

The best way to calibrate a morphological model is always to hindcast the observed morphological development. In the present project bathymetries for 2011 and 2019 are available. Both datasets have been collected by IWM using similar resolution and survey methodology. The time span between these two datasets and their quality offers an excellent basis for determining the morphological changes accurately and thereby the opportunity to calibrate the morphological model.

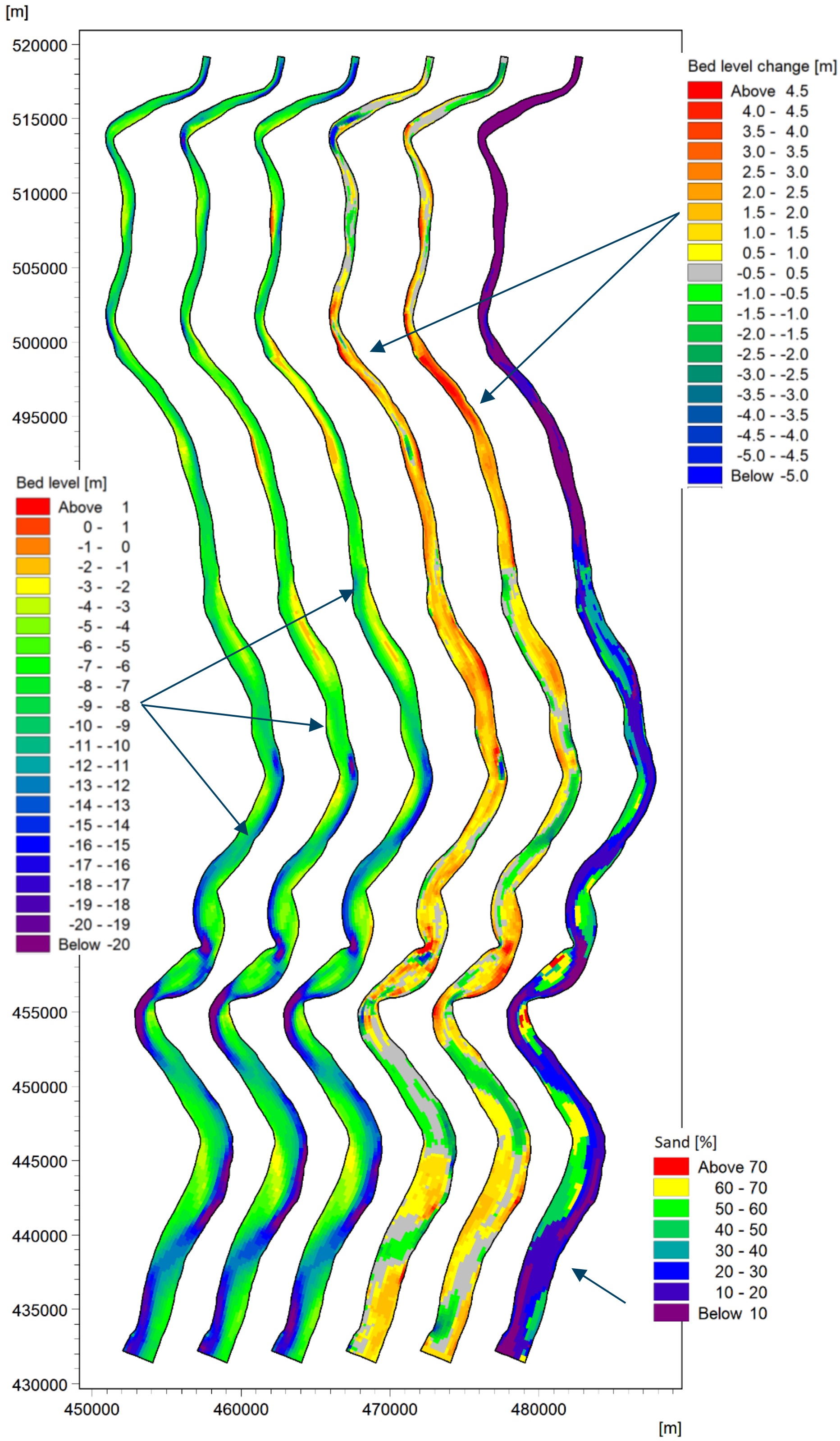

Figure 3-25 Comparison of observations and hindcast 2011-2019. From left: 1) observed 2011 bathymetry, 2) observed 2019 bathymetry, 3) simulated 2019 bathymetry, 4) observed bed level changes 2011-2019, 5) simulated bed level changes 2011-2019, 6) simulated 2019 surface sand mass (%).

The hindcast is compared to observations in Figure 3-25.

The model is calibrated to the bulk volume curve (see e.g. Figure 2-14) and the general pattern shown here. The model results, especially the locations of bars and channels, are very sensitive to model parameters, hence the good agreement between model and observations suggest that the model parameters are well estimated.

Even with the good comparison, there are still shortcomings that are almost impossible to do anything about, especially the cases where the transverse slope in the model is clearly higher than in the observations.

The relative sand mass in the bed surface is somewhat influenced by the initial conditions. The understanding is that the time scale during which the sand mass adjusts is very long.

3.8 Longitudinal validations

The comparison of simulation and observed results presented in Figure 3-25 is primarily valuable for qualitative comparison. In the following, the simulated width-integrated bed level changes are compared to observations, as well as the associated integrated bulk volume curves.

The purpose of this section is to demonstrate that the longitudinal distribution of erosion and deposition is remarkably well represented in the model. The Pussur River generally flows north to south, and therefore the BTM northing is used as independent coordinate.

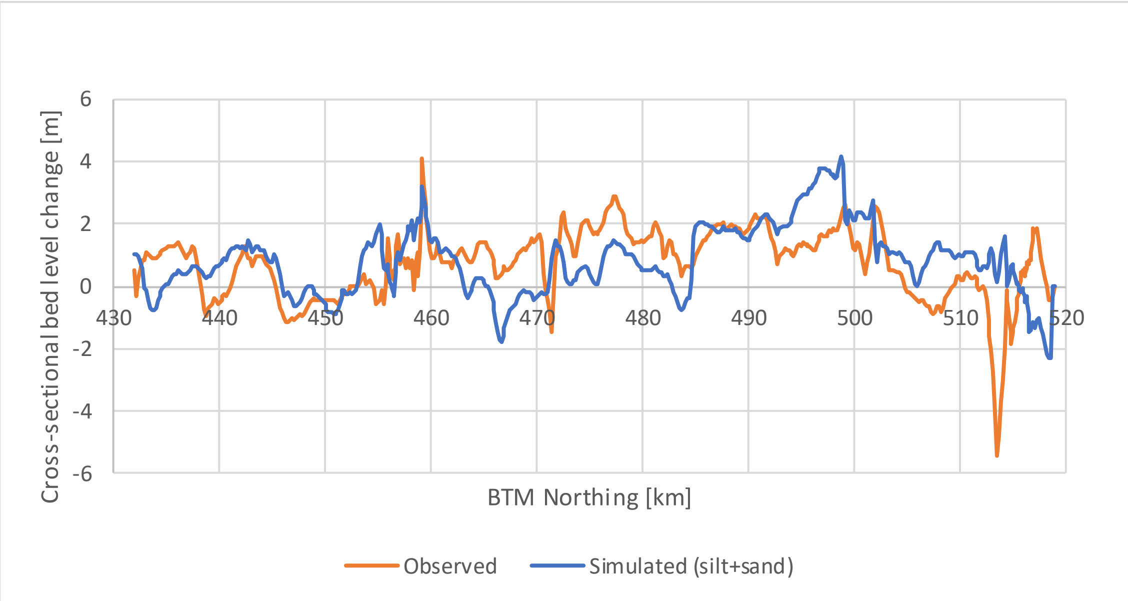

Figure 3-26 Comparison of observed and simulated cross-section average bed level changes 2011-2019 (from downstream to upstream).

The observed and simulated width-integrated (mean) bed level changes along the river are shown in Figure 3-26. It is seen that the general pattern of (primarily) deposition and erosion along the river is very well represented in the model. Further improvement would either require the use of a spatial varying erosion coefficient or introduction of a different particle size distribution map. Neither of these changes, however, can be justified by the available data.

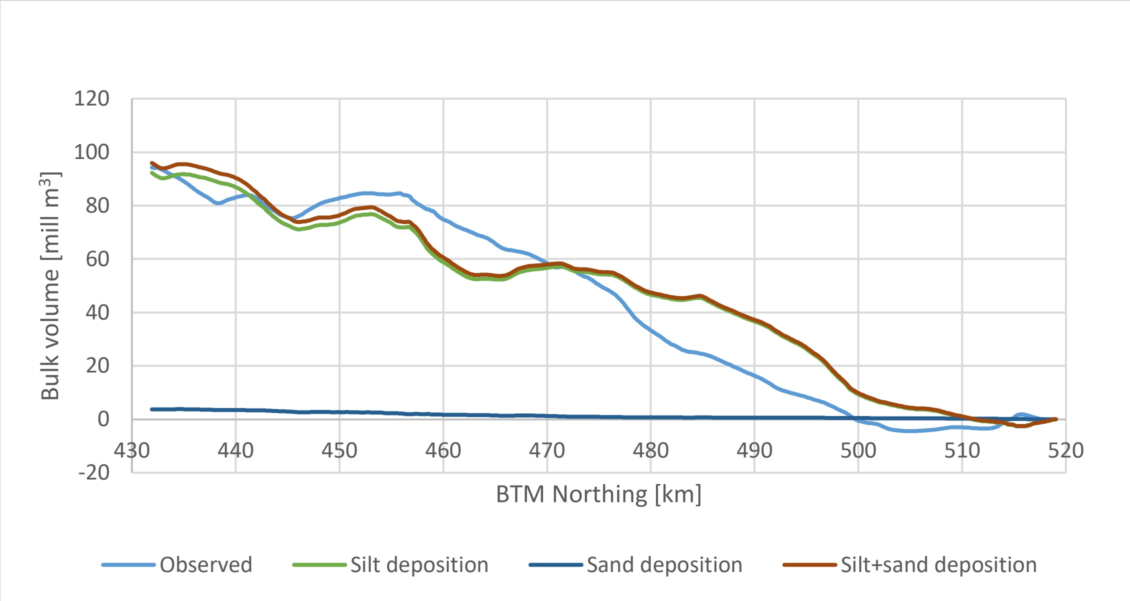

Figure 3-27 Observed and simulated bulk volume curves 2011-2019. The bulk volume curves were integrated for both sediment fractions (silt and sand) and added together.

Bulk bed volume curves have been obtained by integrating the bed elevation changes. The bulk volume curve is shown in Figure 3-27.

The budget was the key calibration target, which can also be seen in the curves. The total deposition in the estuary is about 100 mill m^3, which is very well matched by the model. Assuming a length and width of the river of approx. 100 km and 2 km, respectively, this corresponds to an average deposition of 0.5 m.

It is also observed that the sand contribution is very small, which is not necessarily correct, but the data does not suggest significant sand masses in the bed surface.

It must be kept in mind that bank erosion contributes significantly to this volume curve and exceeds (or corresponds to) the net import of sediment across the boundaries.

3.9 Bank erosion model

Several bank erosion formulas were tested during the developments of the models. A formula based on Hasegawa (1989) was selected as the most optimal formula:

$$E = E_h \, |V| \left(1 - \left(\frac{h_c}{h}\right)^{2/3}\right)$$

Where E is the erosion rate [m/s], E_h a non-dimensional calibration parameter, V is the near-bank flow velocity [m/s], h the near-bank water depth [m], and h_c the critical water depth [m] below which no erosion takes place. Calibration simulations resulted in the following parameters in the derived Hasegawa (1989) bank erosion formula:

$E_h = 10^{-6}$

$h_c = 8$ m

The calibration result is presented and discussed in the following.

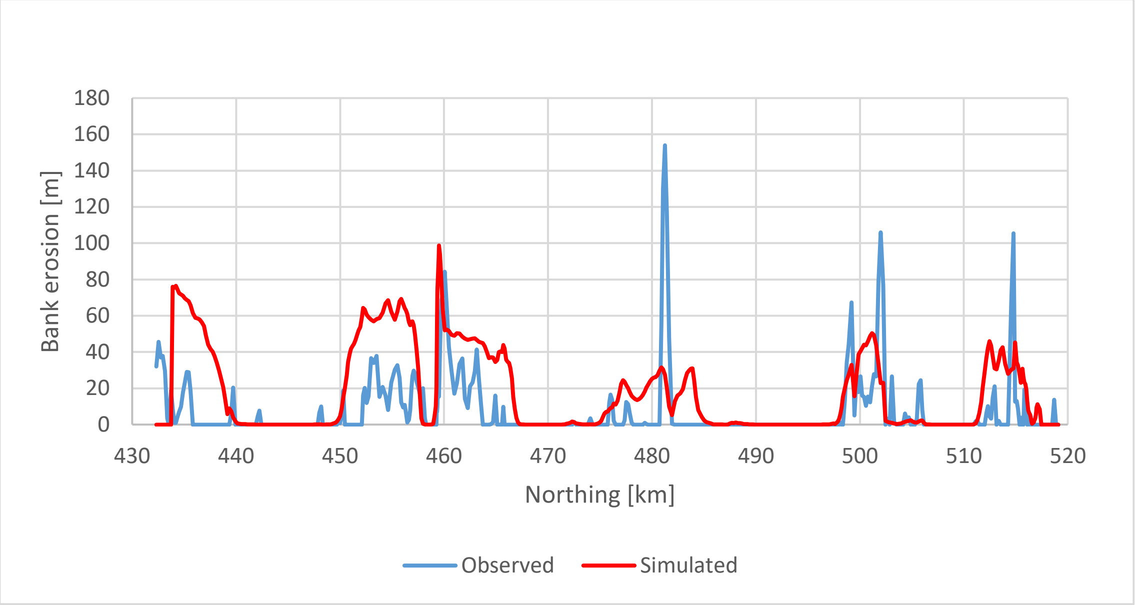

Figure 3-28 Observed and simulated west bank erosion for the Pussur River model 2011-2019.

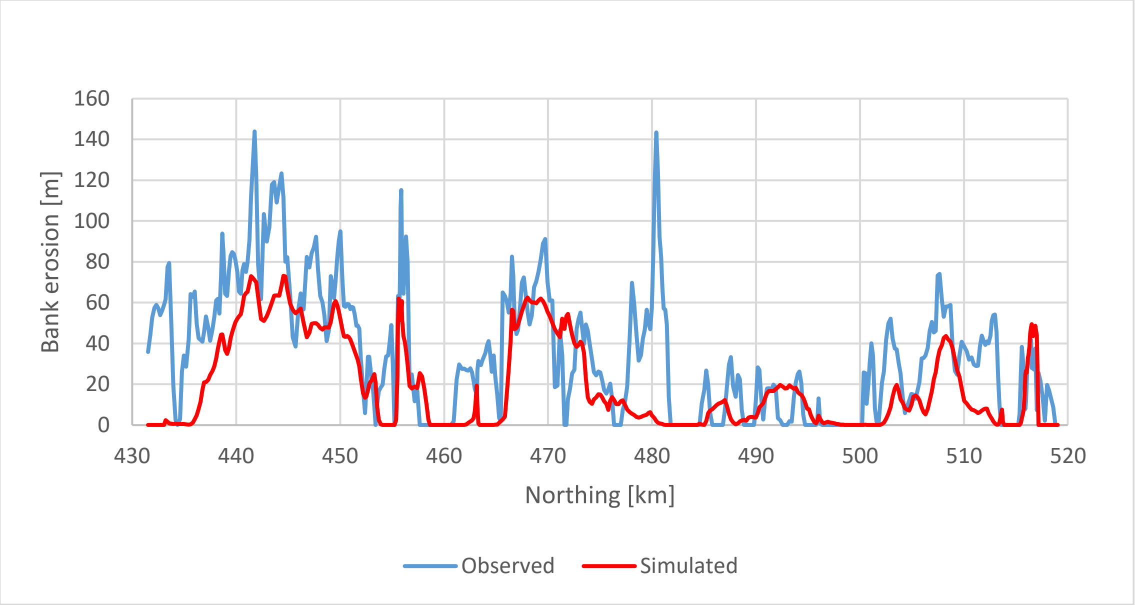

Figure 3-29 Observed and simulated east bank erosion for the Pussur River model 2011-2019.

Figure 3-28 and Figure 3-29 show the observed and simulated erosion of the east and west bank, respectively, for the period 2011-2019.

The model correctly reproduces the magnitude of the erosion of the banks and also predicts the correct locations of erosion.

Bank erosion along the western bank is somewhat overpredicted, while erosion along the eastern bank is somewhat underpredicted. There is no justification for using different parameters along the banks, as both banks are in the Sundarbans (at least with the Sundarbans on both sides of the river, while the upstream end is not in the Sundarbans) presumably with the same sediment and vegetation characteristics.

It should be kept in mind that the observed bank erosion is subjected to the uncertainty associated with a 30 m grid cell size in the Landsat images. The observed erosion along the western bank is often smaller than 30 m, so these observations should be interpreted with some caution.

Considering the erosion along the eastern bank (Figure 3-29) in the downstream end, it is noticed that the model correctly reproduces the location of the erosion, but the simulated erosion is less erratic than the observed and probably somewhat underestimated. This is not necessarily an issue with the bank erosion formula, as the comparison between observed and simulated bed level changes shows that the model tends to be depositional along the eastern bank, while the observations show a more neutral behaviour. If the model predicts too high bed levels along this bank, predicted bank erosion will tend to be too low. There is an additional feedback mechanism in the shape of the sediment eroded locally increasing the sediment transport, which will tend to increase the local bed elevation. This is a good example of how the various processes influence each other. The impact of bank erosion on the local bathymetry depends on the particle size distribution in the riverbank, i.e. fine sediment will have less impact, hence the model performance could here be improved by assuming a finer bank material, but no data is available to substantiate that.

Despite the shortcomings in the bank erosion prediction, the overall conclusion is that the bank erosion model for the Pussur River works extremely well.

3.10 Comparison of observed and simulated bank lines 2011-2019

The bank erosion hindcast simulation was conducted without updating the bank lines. This is easier for calibration purposes because updating of the bank lines will change the grid, leading to many complications when post-processing the results. The error associated with not updating the bank lines is small for cases where the bank erosion is much smaller than the width, which is the case for 2011-2019. However, for longer model runs, the feedback between planform and bathymetry must be accounted for. Considering that the application model should run much longer timescales compared to 2011-2019, the application model was prepared for using dynamic grid updating.

Bank line changes are small compared to the width of the river. It is therefore necessary to zoom in to specific reaches of the river to detect the detailed developments. In the following, the simulated and observed bank lines changes at selected reaches are presented.

Observed and simulated bank lines are shown in Figure 3-30 to Figure 3-32. The three reaches were selected because they have high bank erosion rates during the 2011-2019 period and because the model predictions are quite good in these reaches. The model does not simulate explicitly accretion of the riverbank, but the model will simulate this implicitly through deposition of the riverbed and thus diminish the depth adjacent to the accreting banks.

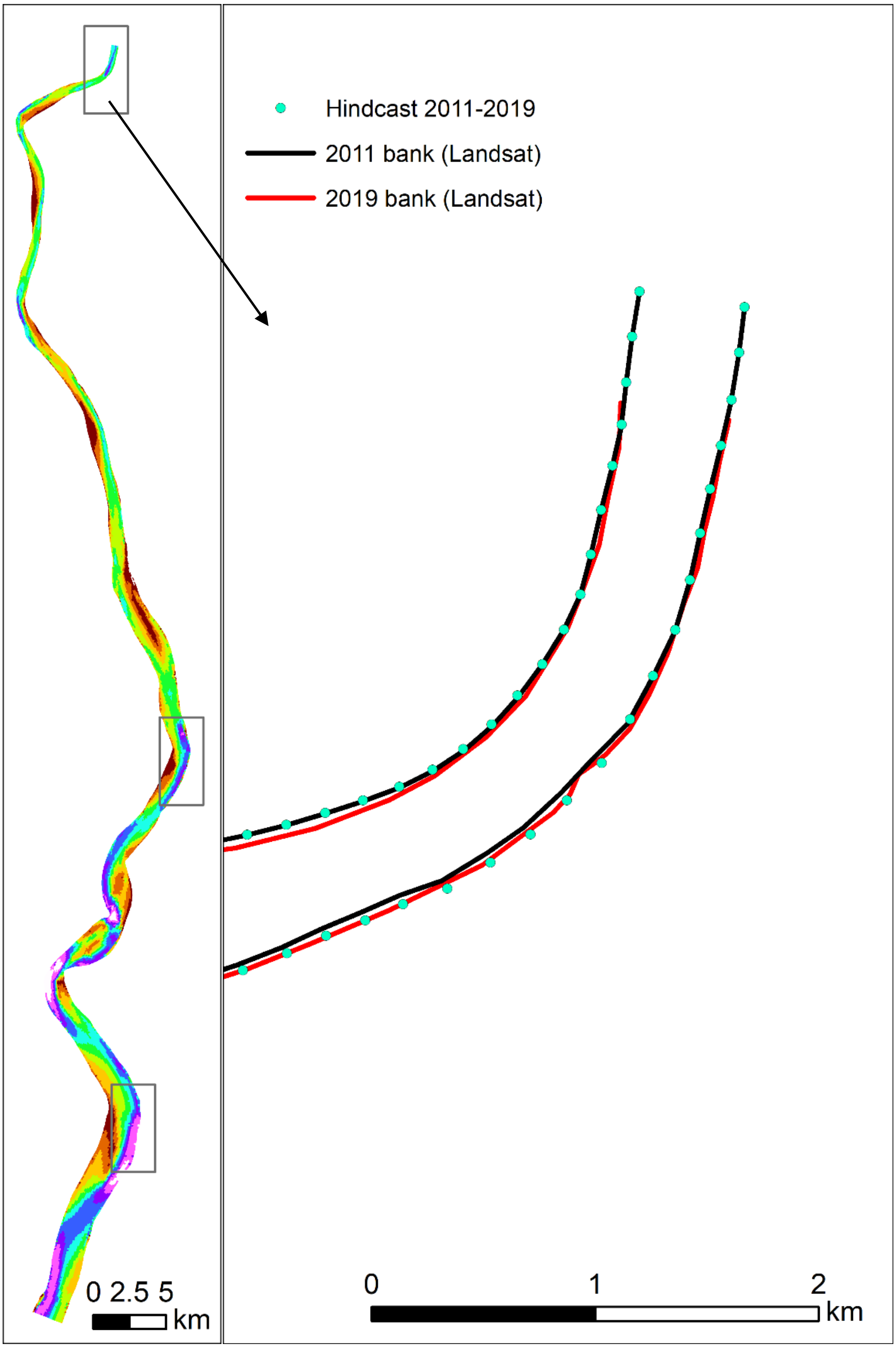

Figure 3-30 Comparison of observed and simulated bank lines 2011-2019 in a bend located upstream, where erosion in the outer bend and accretion in the inner bend are noted.

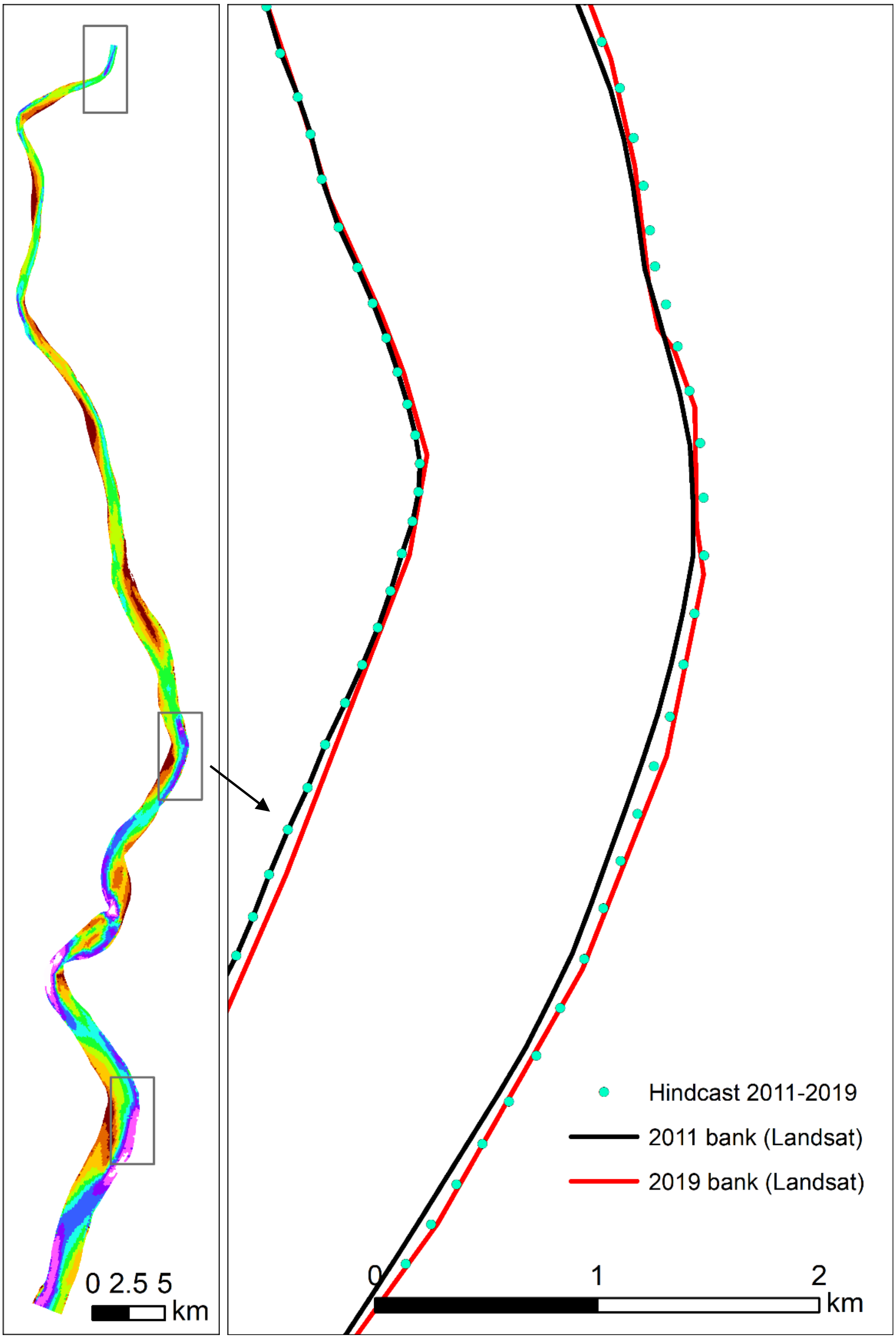

Figure 3-31 Comparison of observed and simulated bank lines 2011-2019, middle bend with high bank erosion along east bank and accretion west according to the data.

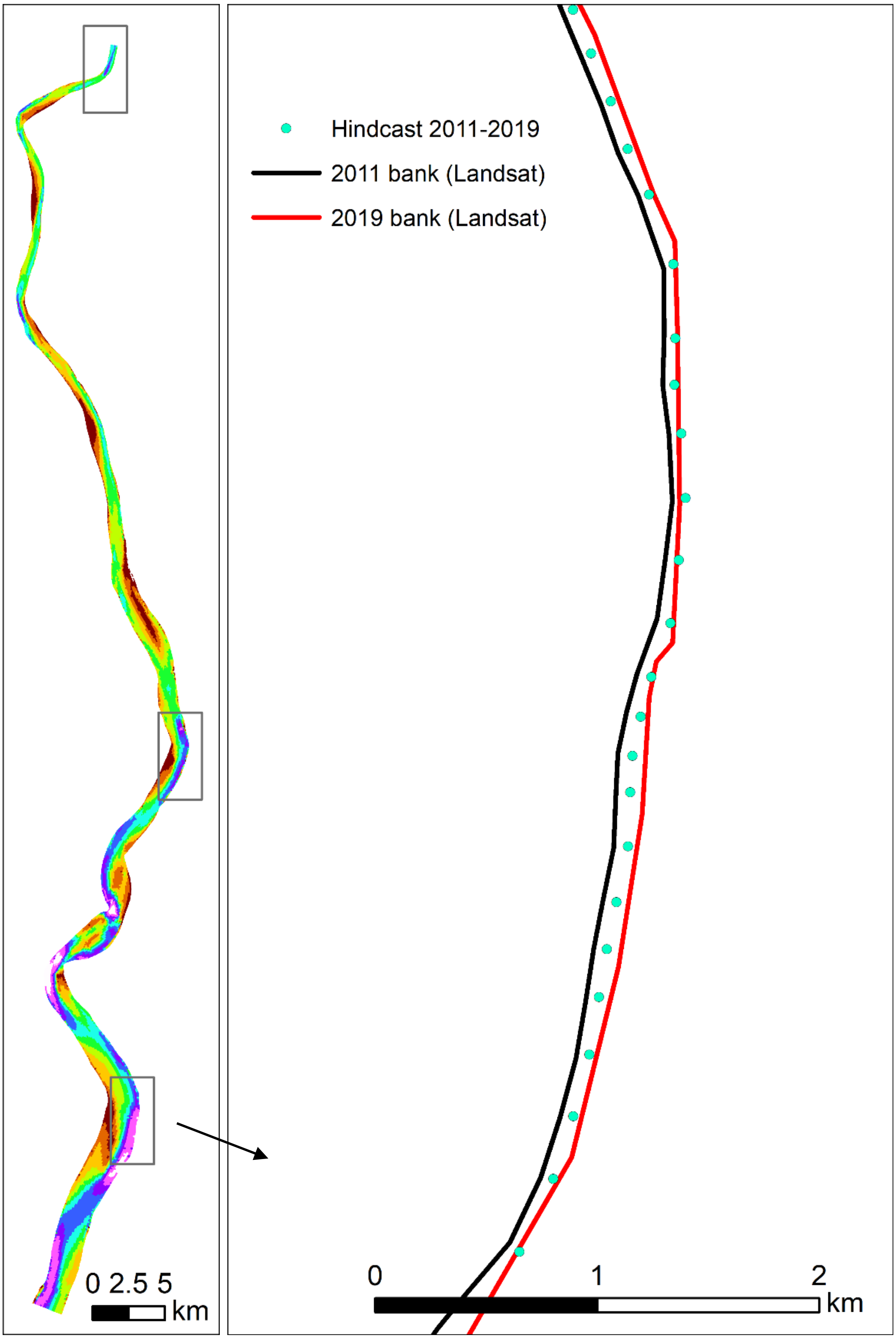

Figure 3-32 Comparison of observed and simulated bank lines 2011-2019 in the downstream end.

4 Model applications

The model applications are reported in this section.

4.1 Bank erosion forecast 30 years into the future

The existing and 30 years into the future boundary conditions were applied in conjunction to represent a reasonable time-series representing the next 30 years. Ideally, a continuous time-series should be available for the whole period to reflect the gradual increase in sea level and gradual lowering of the bathymetry due to subsidence. However, this is very cumbersome to do in the SWRM that provides boundary conditions for the Pussur model. Instead, the 30 years are covered by two simulations. The first simulation covers 15 years starting from the 2019 conditions (grid and bathymetry) using the existing 2019 boundary conditions generated by the SWRM. When this simulation is done, the results are processed into conditions representing 15 years into the future with subsidence representing 30 years into the future subtracted from the bathymetry. The second simulation uses that bathymetry and the associated grid as initial condition and runs 15 years using the future boundary conditions from the SWRM.

This is hence a stepwise approach in which the first 15 years represent existing conditions and the next 15 years represent conditions 30 years into the future.

The bathymetries are qualitatively similar, i.e. the locations of bars and channels are similar, which implies that the bank erosion pattern will not change over the considered time-scale of 30 years. However, it can also be seen that the bed levels generally increase, especially in the middle section of the Pussur where Mongla Port is located. This implies that Mongla Port will continue experiencing sedimentation in the future.

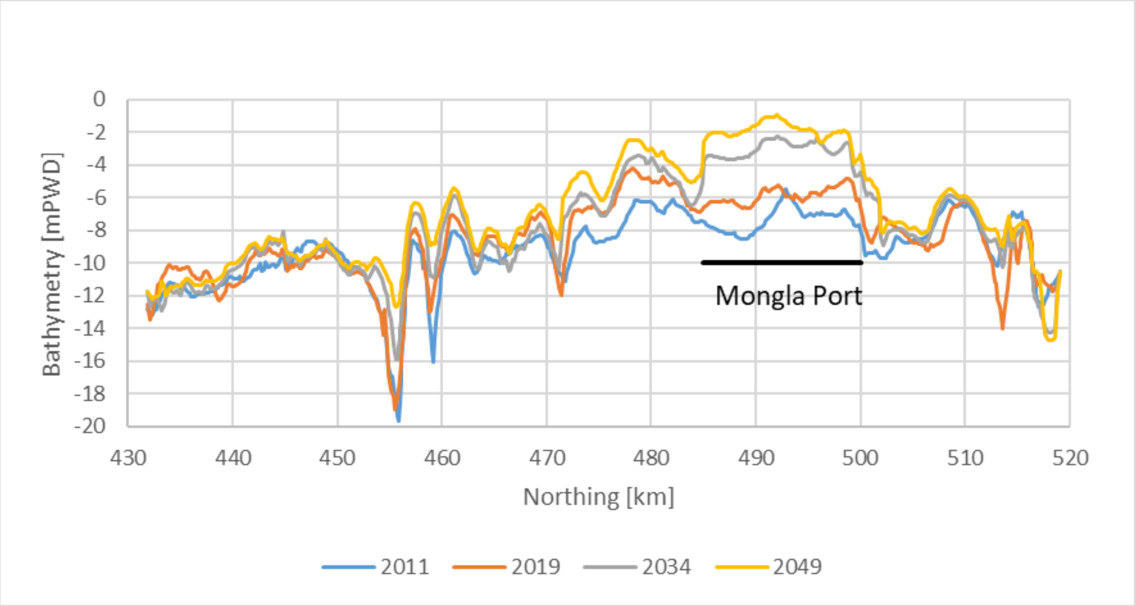

Figure 4-1 Width-integrated bed levels as a function of northing in the Pussur River for 2011 (observed), 2019 (observed), 2034 (simulated) and 2049 (simulated). The location of Mongla Port is shown to illustrate that the port is located where Pussur River has the highest deposition rate in the simulations.

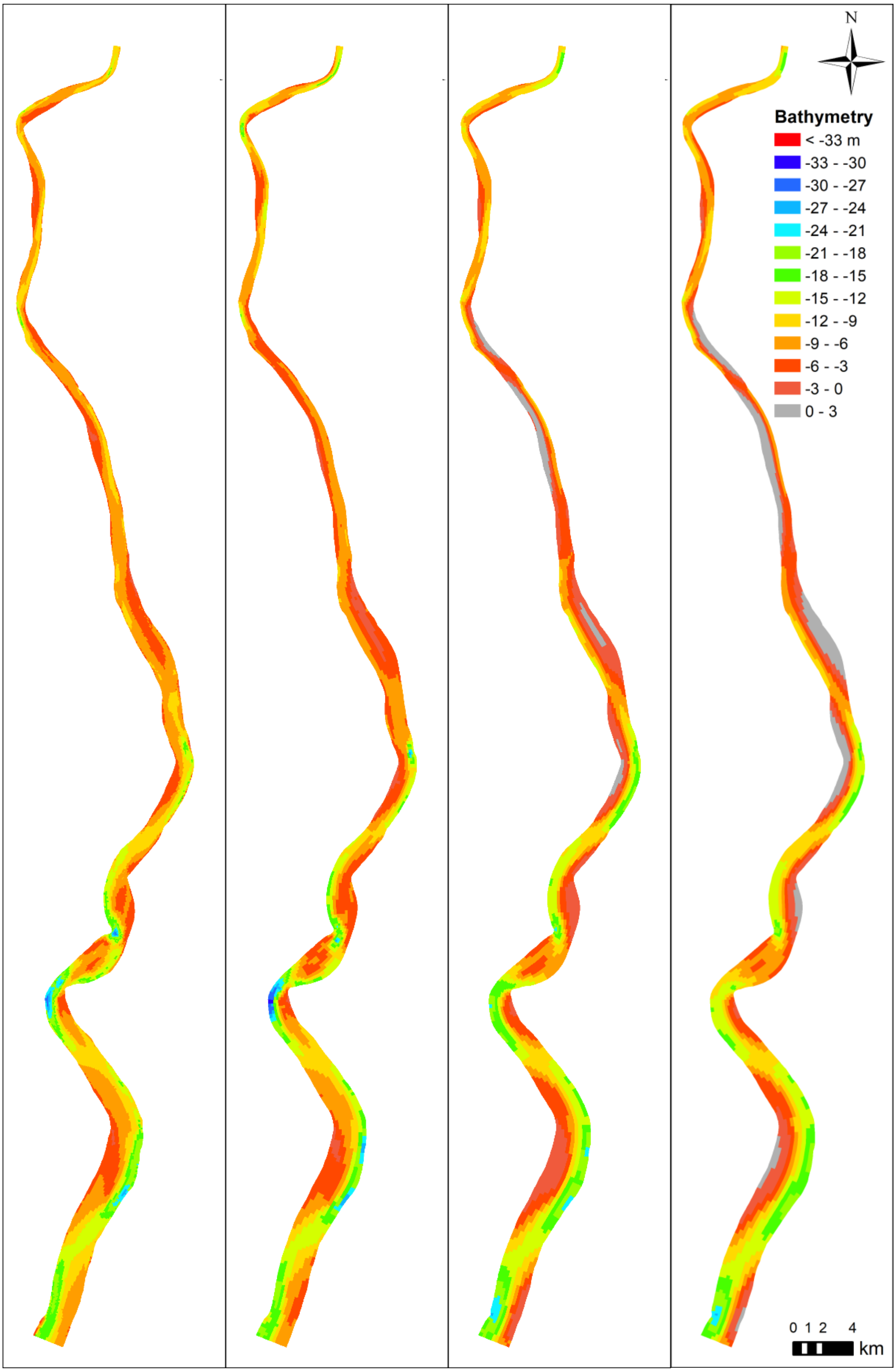

Figure 4-2 Bathymetries from various years. From left: 2011 (observed), 2019 (observed), 2034 (simulated), 2049 (simulated).

Figure 4-2 shows observed bathymetries from 2011 and 2019 along with simulated future bathymetries from 2034 and 2049.

The width-integrated bed levels over time are shown in Figure 4-1. The profiles confirm that the Pussur River is relatively neutral at Rupsha (upstream) and Akram Point (downstream), while the central part exhibits sedimentation in both observations and simulations. It should be kept in mind that the model was calibrated by hindcasting the period 2011-2019, but without including dredging at Mongla Port. The results could be interpreted as an average sedimentation rate around 2 m over 15 years based on 2019-2034, but the results show that the bed levels at Mongla approach to the tidal levels, so Mongla will converge towards an equilibrium, leading to less sedimentation over time. Hence, it is likely that the model underestimates the sedimentation rates at Mongla Port.

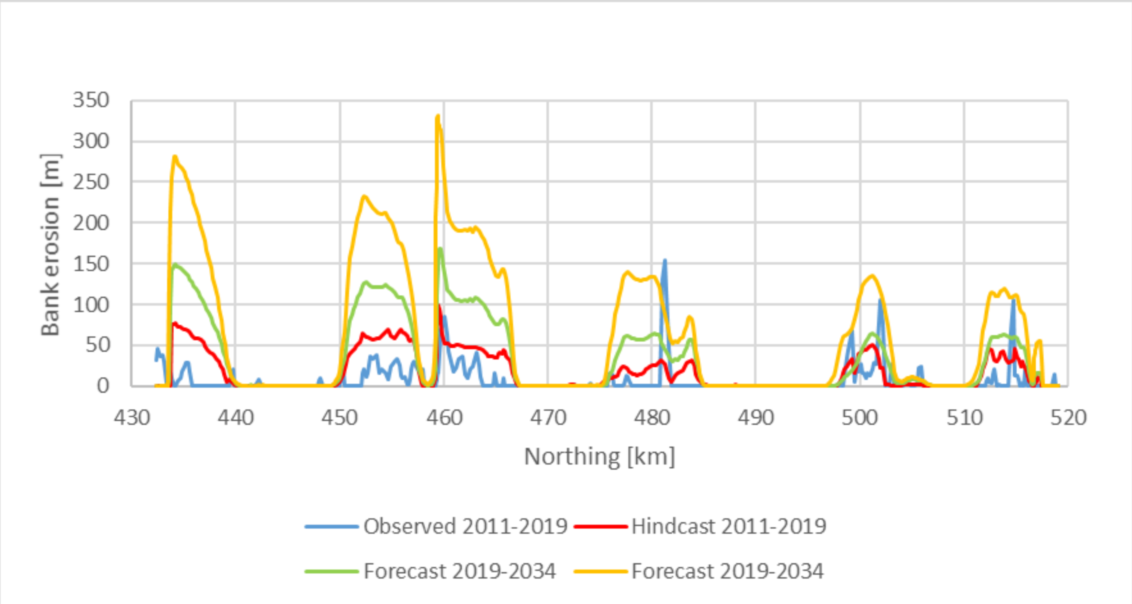

Figure 4-3 Bank erosion along the Pussur River west bank for 2011-2019, 2019-2034 and 2019-2049.

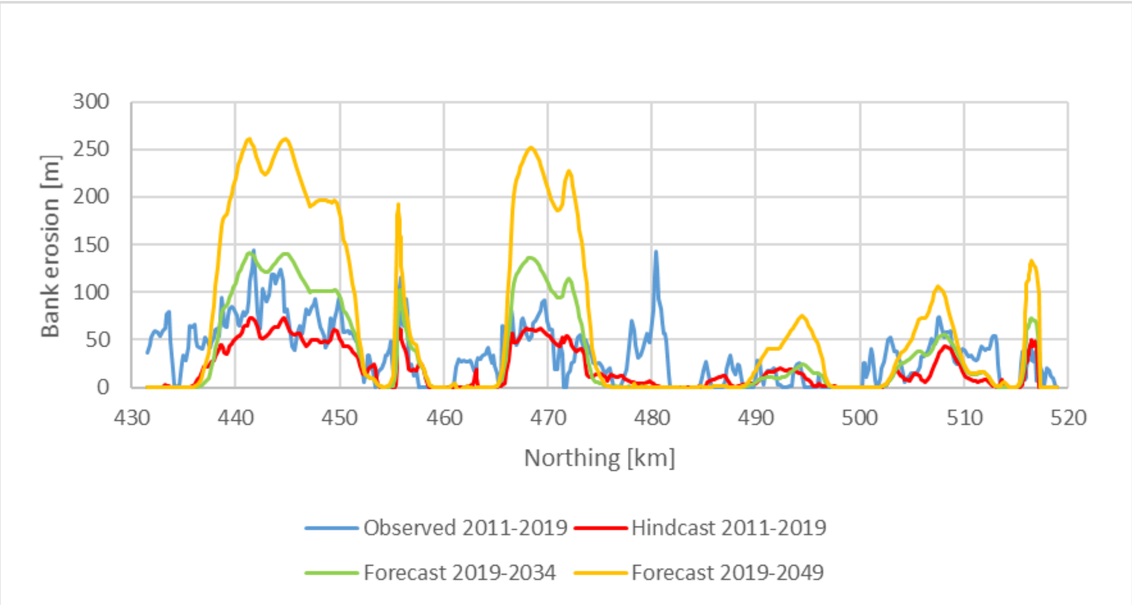

Figure 4-4 Bank erosion along the Pussur River east bank for 2011-2019, 2019-2034 and 2019-2049.

Figure 4-3 and Figure 4-4 show the simulated bank erosion as a function of the northing coordinate, for reference compared to the 2011-2019 simulations and observations. It is seen that the same banks will erode in the future, but there are also some quantitative changes, especially at Mongla. Overall, it is safe to say that the model does not project significant changes to the erosion rates, and the curves should be inspected with the fact in mind that bank erosion is essentially shown for periods of 8 years, 15 years and 30 years.

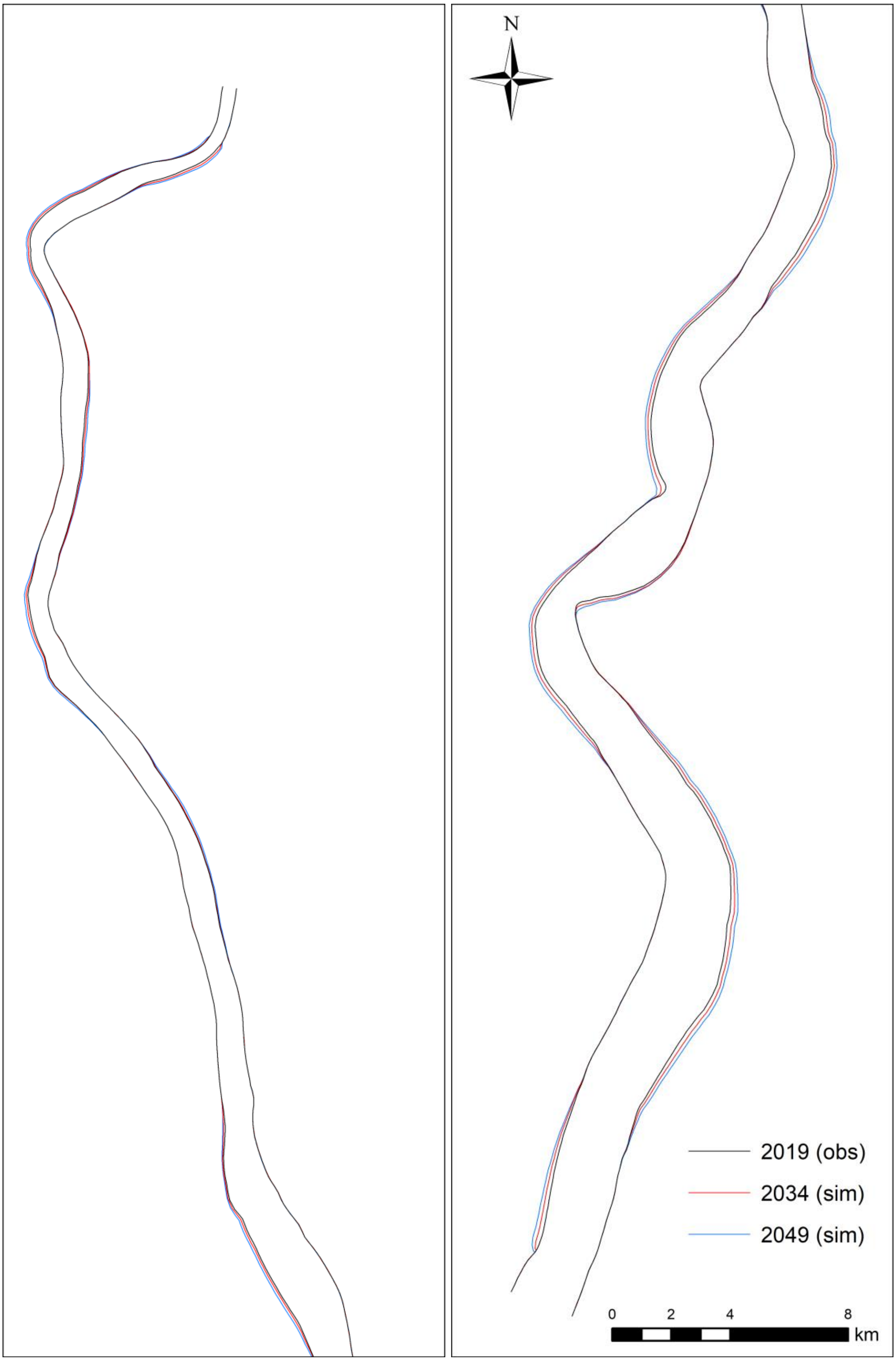

Figure 4-5 Bank lines 2019 (observed), 2034 (simulated), 2049 (simulated).

4.2 Impact of climate change on future bank erosion

The impact of climate change was quantified by running the model for 2019-2049 with and without climate change. To make post-processing easier, the simulations were conducted without updating the grids, while the bank eroded material was still added to the local concentration. Subsidence was included in both simulations.

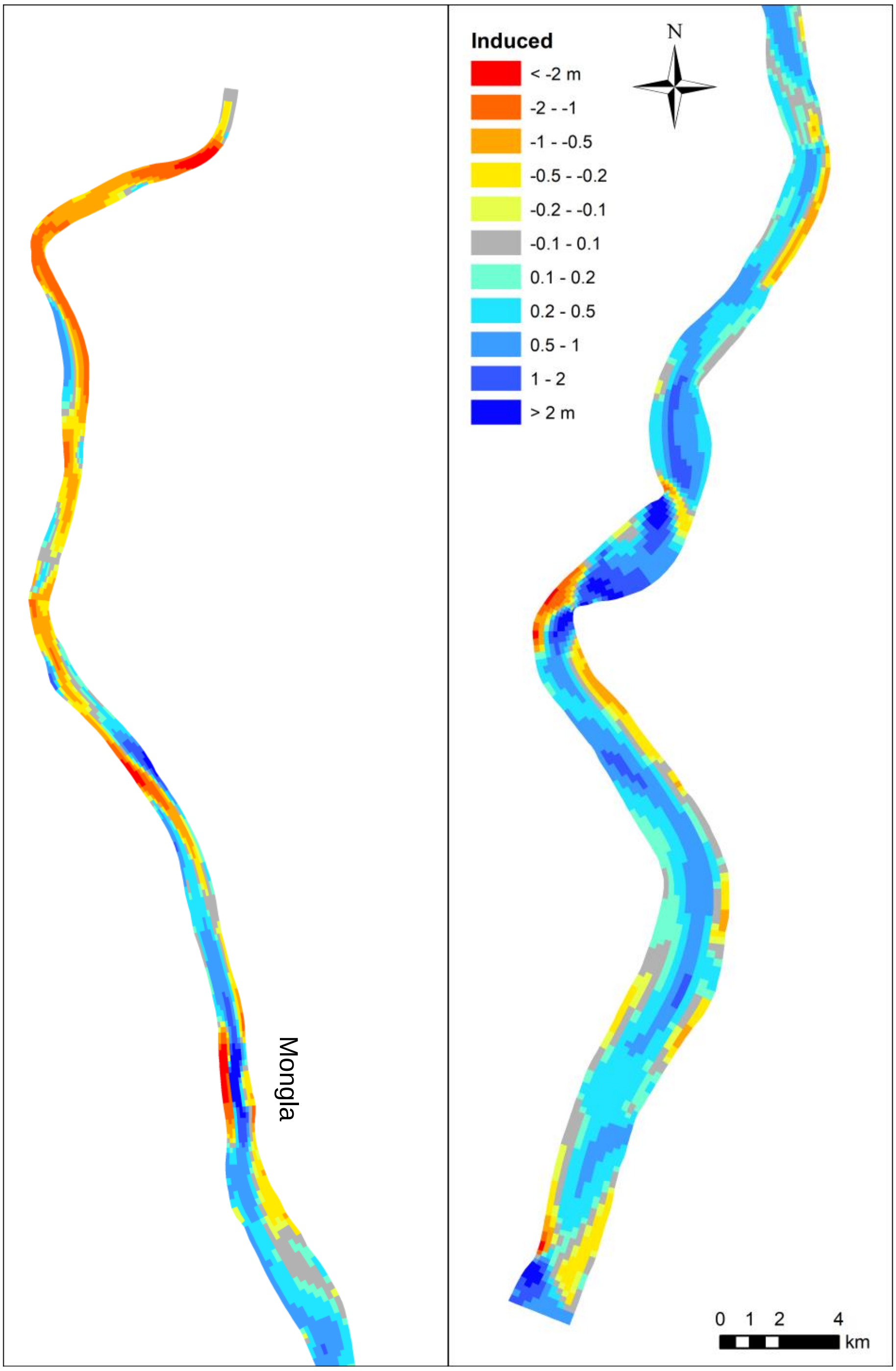

Figure 4-6 Simulated bed level differences in 2049 due to climate change. These were calculated as the differences between the simulated bathymetry for existing conditions (no climate change) and with climate change.

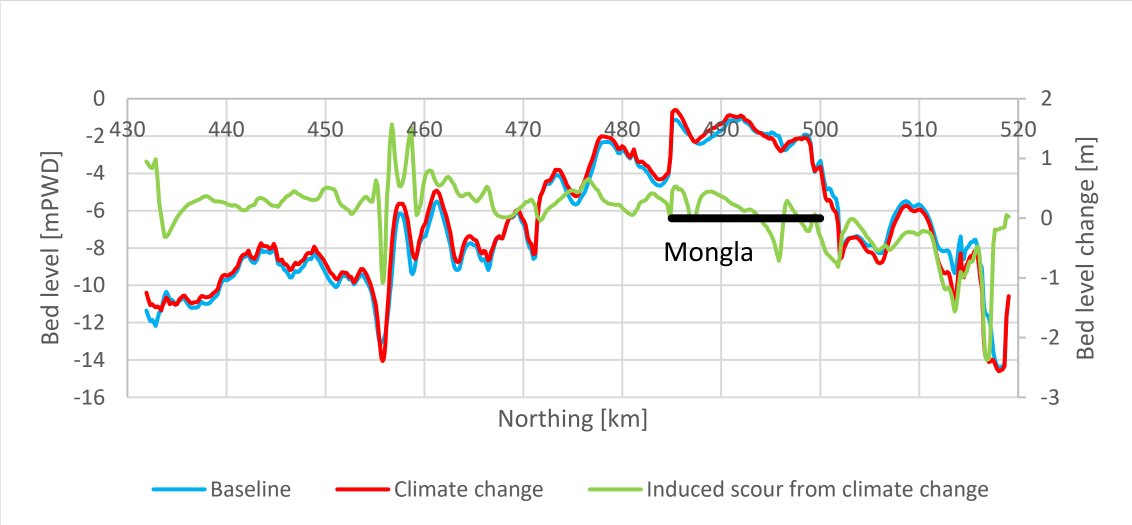

Figure 4-7 Simulated width-integrated bed levels and associated induced changes, i.e. the impact on bed levels from climate change.

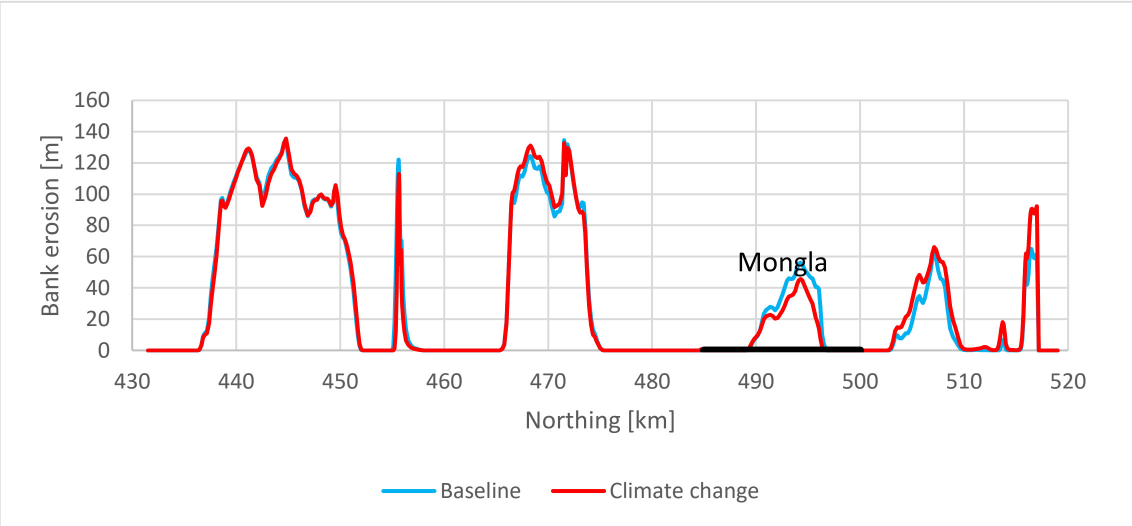

Figure 4-8 Simulated bank erosion along the east bank 2019-2049 with and without climate change.

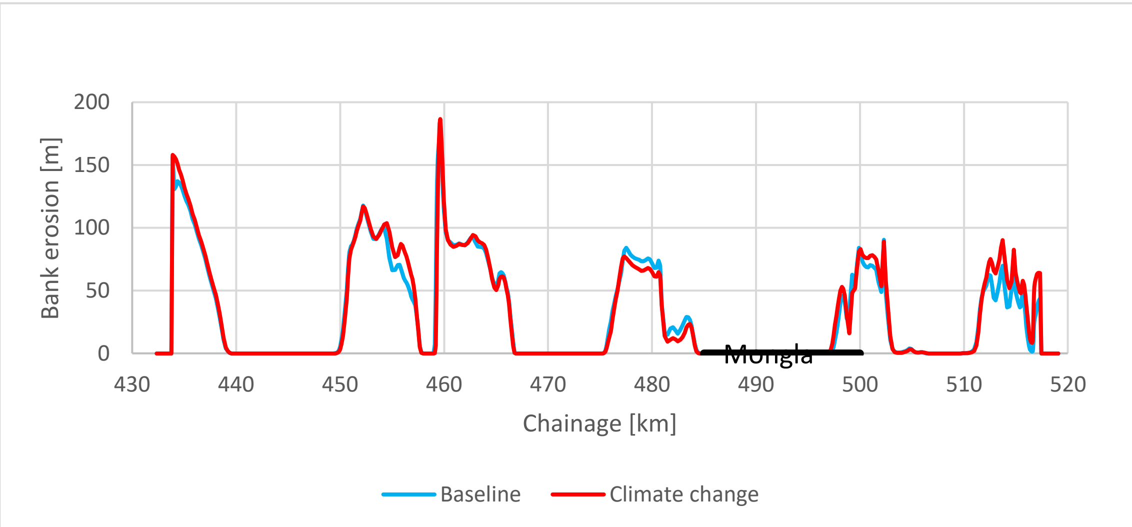

Figure 4-9 Simulated bank erosion along the west bank 2019-2049 with and without climate change.

Figure 4-6 shows the simulated bed level differences in 2049, i.e. the simulated bathymetry with climate change minus the bathymetry with existing climate. The equivalent width-integrated bed levels and induced differences are shown in Figure 4-7. Overall, it is seen that climate change induces scour upstream of Mongla and sedimentation from Mongla and downstream.

The results suggest that climate change will worsen sedimentation at Mongla Port. Comparing to Figure 4-1 it is noticed that the climate change induced changes are smaller than the autonomous development, i.e. the impact of climate change is relatively small.

The impact on bank erosion is illustrated in Figure 4-8 and Figure 4-9. The general picture is that bank erosion increases upstream of Mongla Port and is reduced at Mongla Port, while downstream of Mongla Port the changes are small, although there is a slight increase. Increased erosion upstream is caused by the increased flows upstream, which are not controlled by Pussur, but by Sibsa (flow capture). At Mongla Port the reduced erosion is probably caused by a combination of increased bed levels and the associated reduced tidal exchange from downstream.

4.3 Impact of bank protection

It is known from the observations of sedimentation and bank erosion that bank erosion is important for the sedimentation in Pussur River, i.e. that bank erosion caused bed aggradation. This was extensively discussed in Chapter 2.

An analysis of the impact of bank protection was conducted for the extreme case where all banks are protected in Pussur by excluding bank erosion in the model simulation. This case will thus show the potential for causing bed degradation through bank protection.

The simulation results for 2019-2034 with existing boundary conditions were applied in the analysis with static grids.

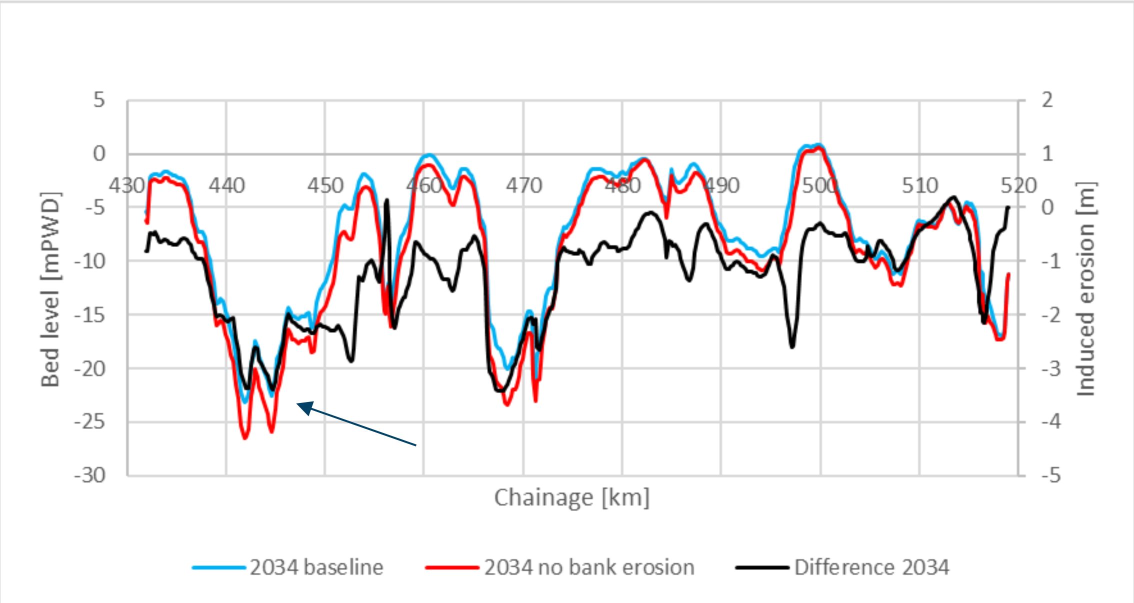

Figure 4-10 Simulated bed levels along the east bank and the induced reduction in bed levels caused by protecting all banks from erosion along the Pussur River. Arrow: The bed level will be reduced by 3 m along the large outer bend in the downstream end if all banks are protected.

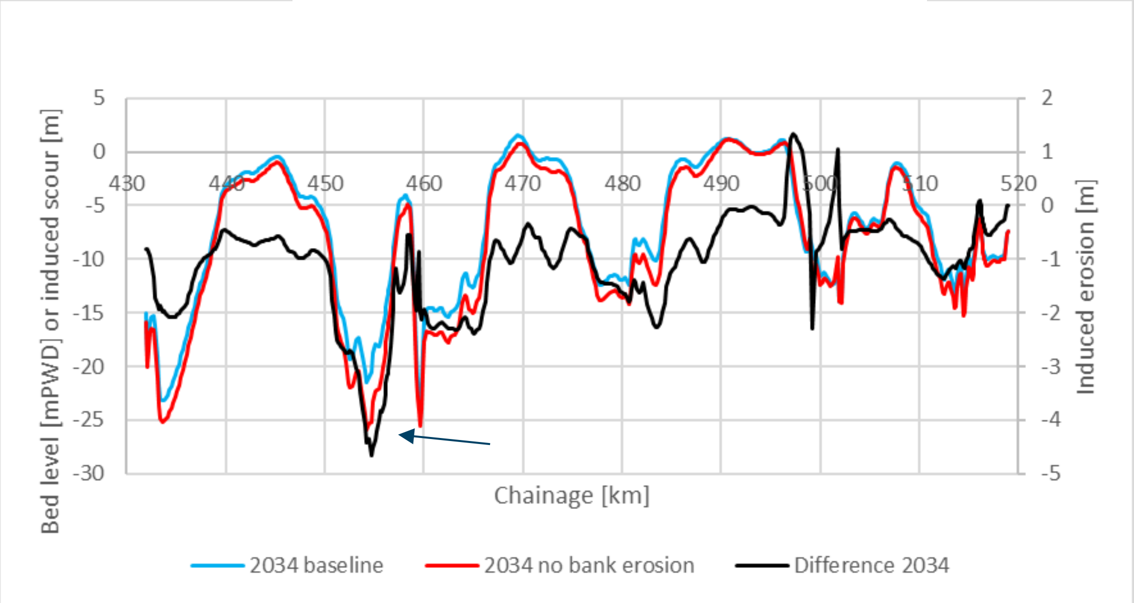

Figure 4-11 Simulated bed levels along the west bank and the induced reduction in bed levels caused by protecting all banks from erosion along the Pussur River. Arrow: The black line shows that this deep outer bend will exhibit 4-5 m lower bed levels if all banks are protected.

The results are shown in Figure 4-10 and Figure 4-11. The results show that in general, the induced erosion increases in the downstream direction and that deeper outer bends will exhibit larger reductions in bed levels; the reductions in bed levels correlate quite well with the bed levels.

The induced scour in the deep outer bends ranges from 2 m in the upstream end to 4-5 m in the downstream end. Although the scenario is extreme, it shows how much the eroded bank material influences the Pussur River sediment budget.

4.4 Mongla Port scenarios

The model has been used to study the development of the sedimentation in the Pussur at Mongla Port as well as possible mitigating measures. The following scenarios were simulated with the Pussur model with emphasis on Mongla Port:

A Existing conditions (baseline)

B Ganges Barrage

C No bank erosion

D Close upstream connections to Sibsa

E Regulate upstream connections to Sibsa

F Install groynes at Mongla Port

G Apply TRM for Polder 33

H Add tidal basins to Sibsa River (not tested)

All simulations were conducted for a period of 10 years from 2019 to 2029 with the 2019 conditions repeating; thus climate change was not considered. Subsidence was disregarded. All interventions were implemented in the 2019 SWRM, which was used for generating boundary conditions for the MIKE 21C model.

Most scenarios started from the 2019 bathymetry. The curvilinear grid was not updated in any of the simulations, as this would introduce complications when comparing results on different grids. This approach is acceptable on shorter timescales.

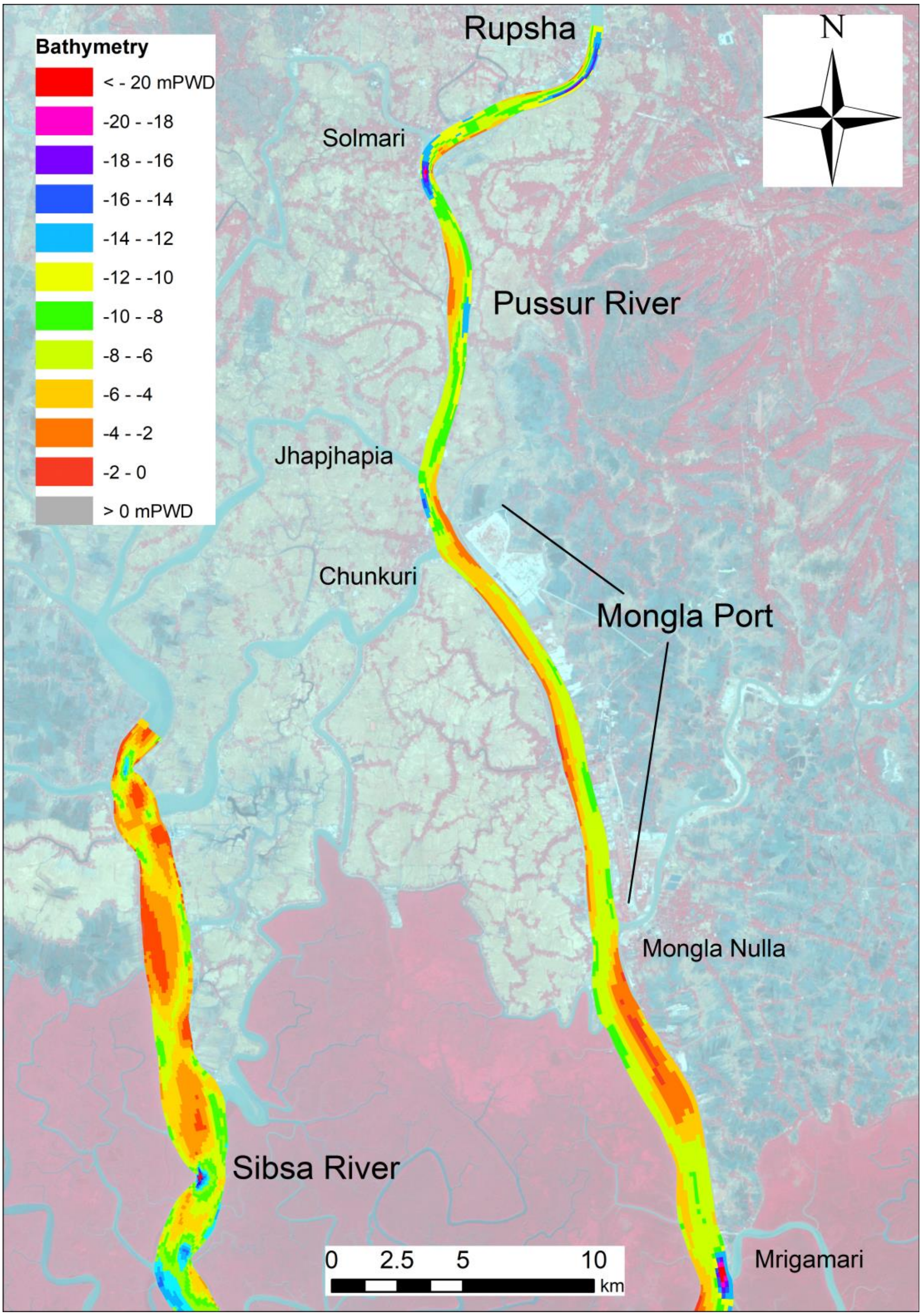

Figure 4-12 Overview of Mongla Port, Pussur-Sibsa and the associated side channels on the Pussur River (2019 Landsat shown as background).

The Pussur MIKE 21C model was mainly calibrated to the general behaviour of the Pussur River in the period 2011-2019.

There are several reports calculating backfilling at Mongla Port, but it is understood in this report that none of them operated with a morphological model running over longer timescales. Traditionally, backfilling calculations are performed over relatively short timescales and without morphological updating, and backfilling rates can be obtainedwithout morphological updating.

The model was adjusted reasonably well to the overall observed bed level and bank line development in the Pussur river from 2011 to 2019, but there was never particular emphasis on the local conditions at Mongla Port. The model behavour at Mongla Port is not as convincing as the overall behavior, possibly because the extensive dredging at Mongla Port was not included. Due to this, the Pussur model must be used with caution when concerning local conditions at Mongla.

4.4.1 Scenario A: Existing conditions

The baseline simulation (A) covers 2019-2029 using existing boundary conditions without updating the curvilinear grid and is used in the following for comparison with all other scenarios.

4.4.2 Scenario B: Ganges Barrage

Ganges Barrage was tested in the model by using boundary conditions from the SWRM for the Ganges Barrage scenario, which was provided by IWM.

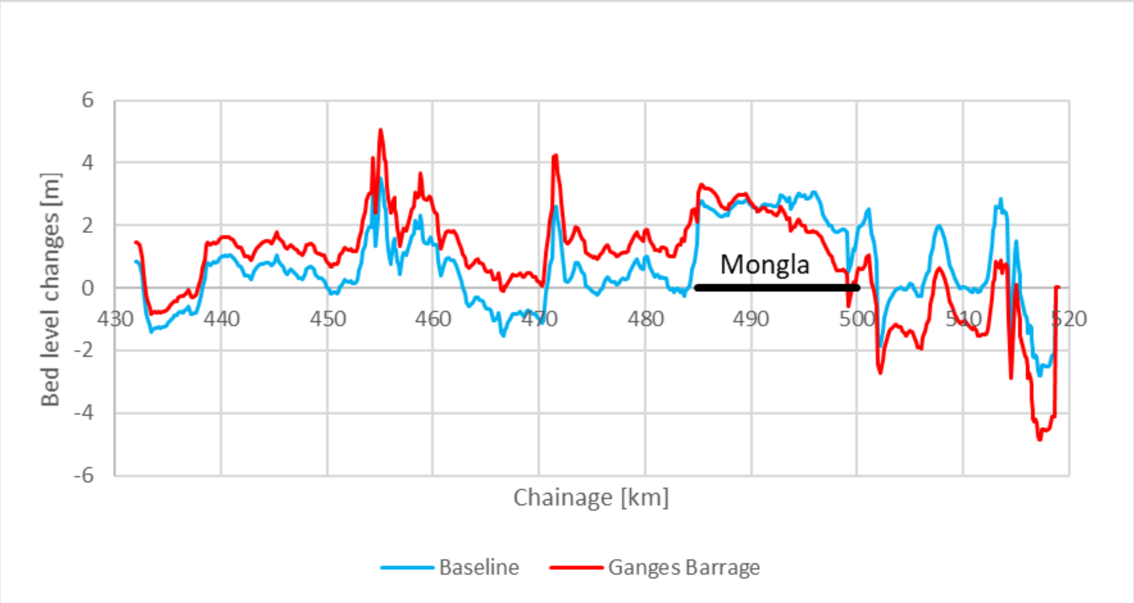

Figure 4-13 Simulated bed level changes 2019-2029 for existing conditions and with Ganges Barrage.

The Ganges Barrage scenario increases the freshwater discharge and sediment transport upstream of Mongla Port, leading to increased sedimentation at the port. The simulated bed level changes show scour upstream of Mongla Port and deposition from Mongla Port and downstream. Ganges Barrage is clearly not helping the situation at Mongla Port.

It could be speculated that the development at Mongla Port is transient and that the model results really show the increased fresh water flow pushing the sediment downstream in the Pussur River. This was tested in the model, and turned out that after some years, the difference between the simulations does not develop over time. Hence, the impact of Ganges Barrage reaches an equilibrium characterized by erosion upstream of Mongla Port and deposition downstream.

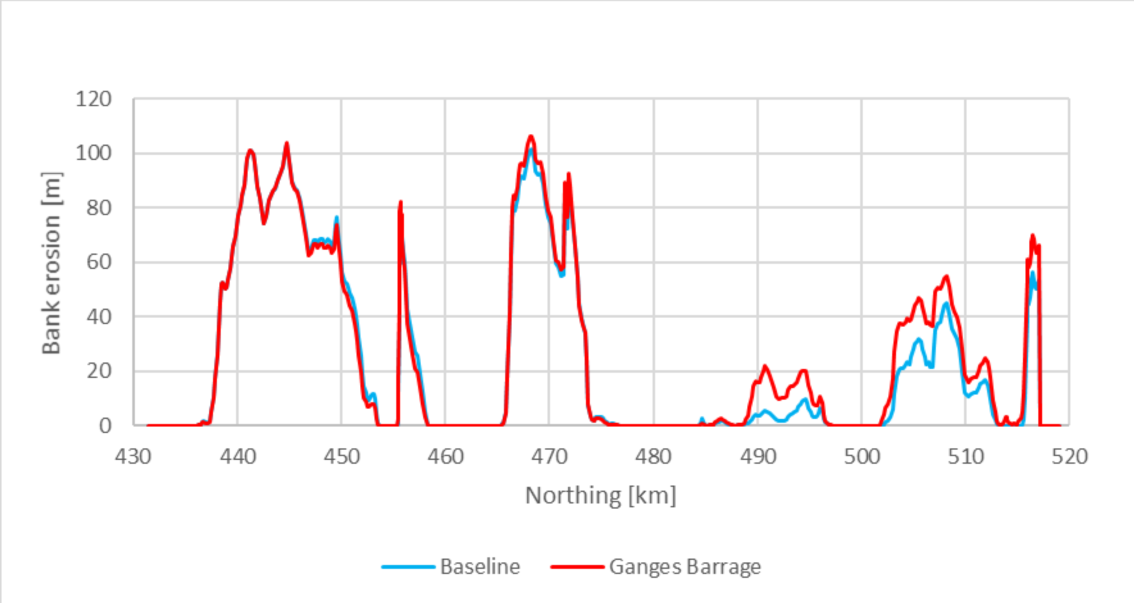

Figure 4-14 Simulated east bank erosion 2019-2029 for existing conditions and with Ganges Barrage.

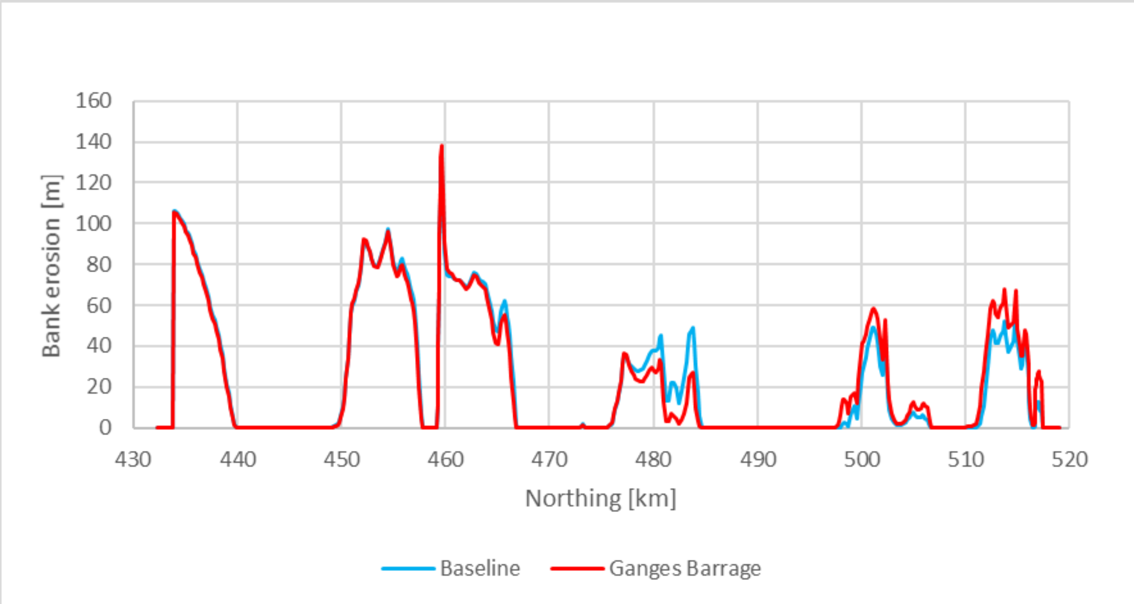

Figure 4-15 Simulated west bank erosion 2019-2029 for existing conditions and with Ganges Barrage.

Simulated bank erosion for existing conditions and with Ganges Barrage are shown in Figure 4-14 and Figure 4-15. The figures show increased bank erosion upstream of Mongla, and very small changes downstream of Mongla. The increased erosion upstream of Mongla is caused by the increased discharge, but this clearly does not make it downstream of Mongla due to the tidal divide (a lot of the ebb flow is diverted to Sibsa).

Conclusion: Ganges Barrage will increase the sedimentation rate at Mongla Port.

4.4.3 Scenario C: No bank erosion

It was established during the model development that bank erosion contributes significantly to the bed sedimentation volumes in Pussur River. A very simple simulation was carried out in which bank erosion was completely removed in order to quantify the impact on the Mongla Port sedimentation rate.

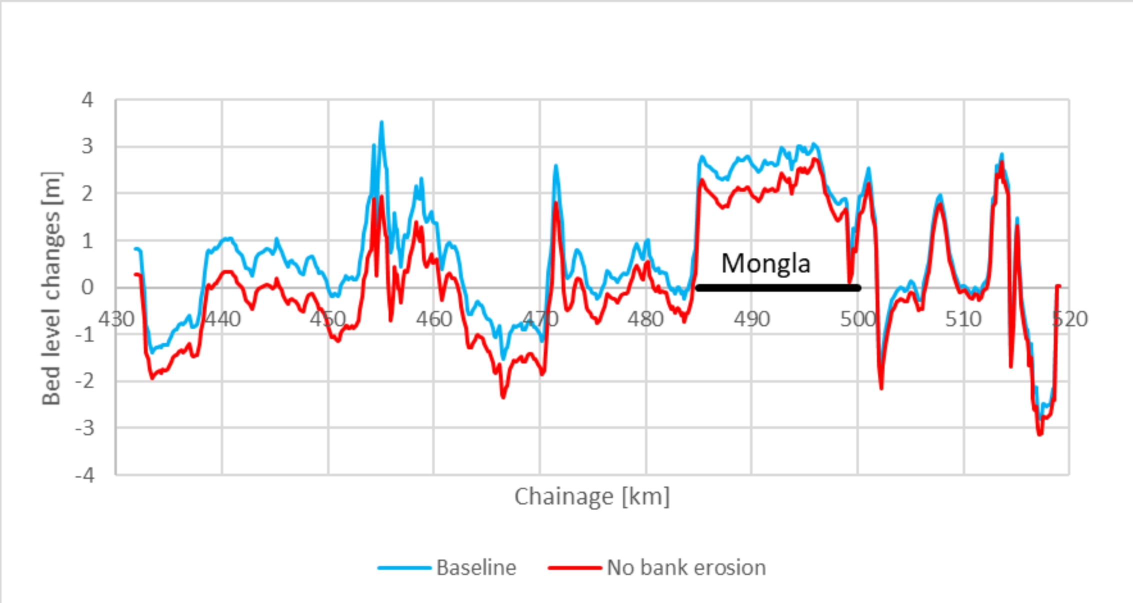

Figure 4-16 Simulated bed level changes 2019-2029 for existing condition and with bank erosion removed.

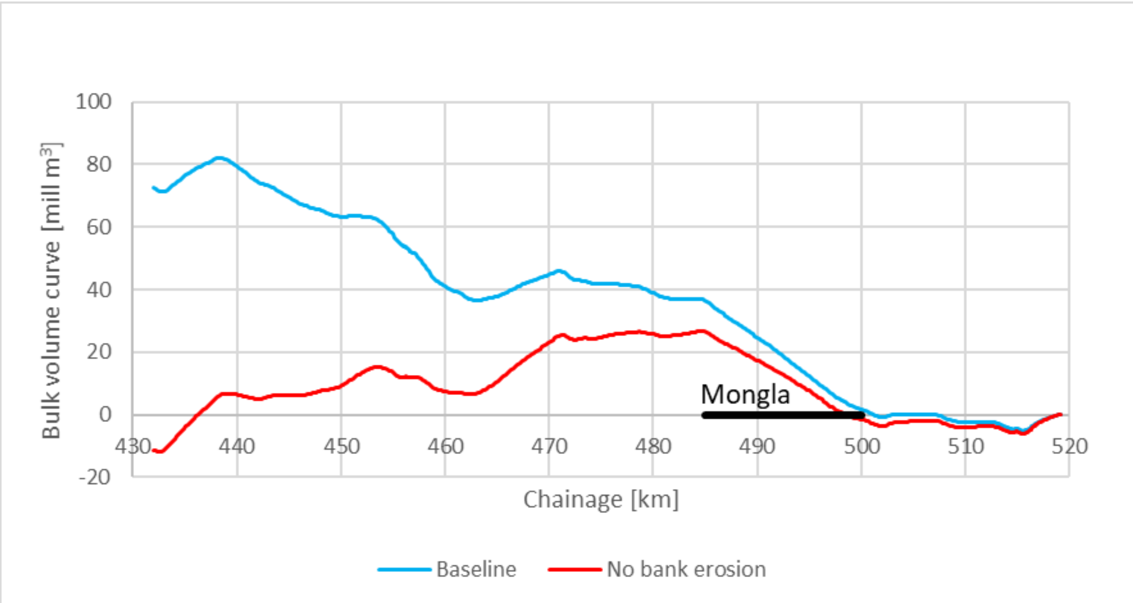

Figure 4-17 Simulated accumulated bulk volume curves (local value equals deposited volume upstream of the location) for existing conditions and with bank erosion removed.

The simulated bed level changes with and without bank erosion are shown in Figure 4-16, while the corresponding bulk volume curves representing simulated sedimentation 2019-2029 are shown in Figure 4-17.

The results show that the bed levels are significantly reduced when all banks are protected from erosion, and the effect is strongest downstream of Mongla, while upstream of Mongla the impact is small. The bulk volume curves show that the sedimentation rate at Mongla is reduced by 1/3, and the curves show that the total sedimentation in Pussur River vanishes when all banks are protected from erosion. This does not mean that bank protection eliminates the need for dredging, which can be seen clearly from the bulk volume curve at Mongla.

The scenario is not realistic, but shown for illustration purposes. Most of the banks in Pussur run along the Sundarbans without polders, and considering the cost of bank protection works, protection of banks downstream of Mongla would not be practical. However, bank protection upstream of Mongla is clearly beneficial to the Mongla sedimentation rate.

Conclusion: Eroded bank material plays a significant role in the bed sedimentation of the Pussur River. The hypothetic scenario in which bank erosion is eliminated in Pussur River would lead to a somewhat (1/3) reduced sedimentation rate at Mongla Port, but sedimentation would not be halted. Considering how expensive bank protection is, and how much of Pussur River runs through the Sundarbans without polders to protect, the scenario is not viable.

4.4.4 Scenario D: Closing the upstream connections to Sibsa River

The three channels upstream of Mongla (Solmari, Jhapjhapia, Chunkuri) all connect the Pussur River to Sibsa River and carry net discharge from Sibsa to Pussur during flood conditions and flow out through Sibsa during ebb. In other words, these three rivers allow the Sibsa River to utilize the tidal prism north of Mongla.

This problem has been identified many times as critically important for understanding why Mongla Port exhibits sedimentation. In essence there is a tidal divide just north of Mongla, where the Sibsa flood tides flow into and take over the tidal prism north of Mongla Port. Hence, Mongla Port is located at a tidal meeting point where the tidal wave running through the lower Pussur meets the tidal wave running through the Sibsa and interconnecting channels upstream of Mongla, causing high sedimentation rates.

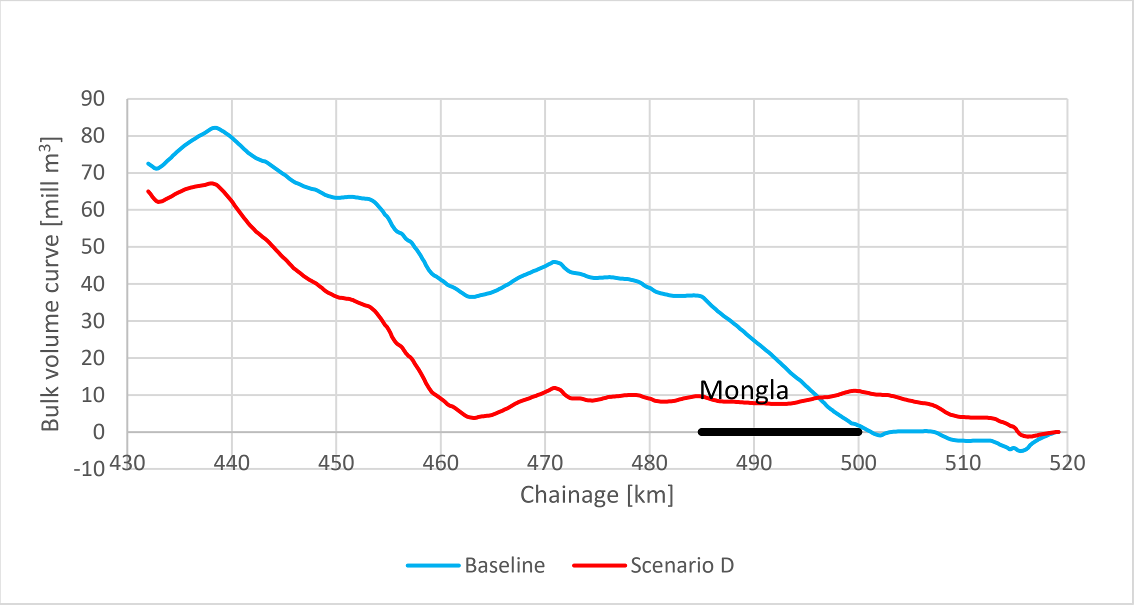

Figure 4-18 Simulated bulk volume curves 2019-2029 for existing conditions and with 3 side channels closed.

The bulk volume curves relative to 2019 are useful as well for understanding the results, see Figure 4-18. The bulk volume curves show that the Pussur overall experiences the same sedimentation volume, but the sedimentation is pushed downstream to much deeper water where it is of no concern. The bulk volume curves also show that closing the side channels will stop further sedimentation at Mongla but on the other hand does not improve the current situation.

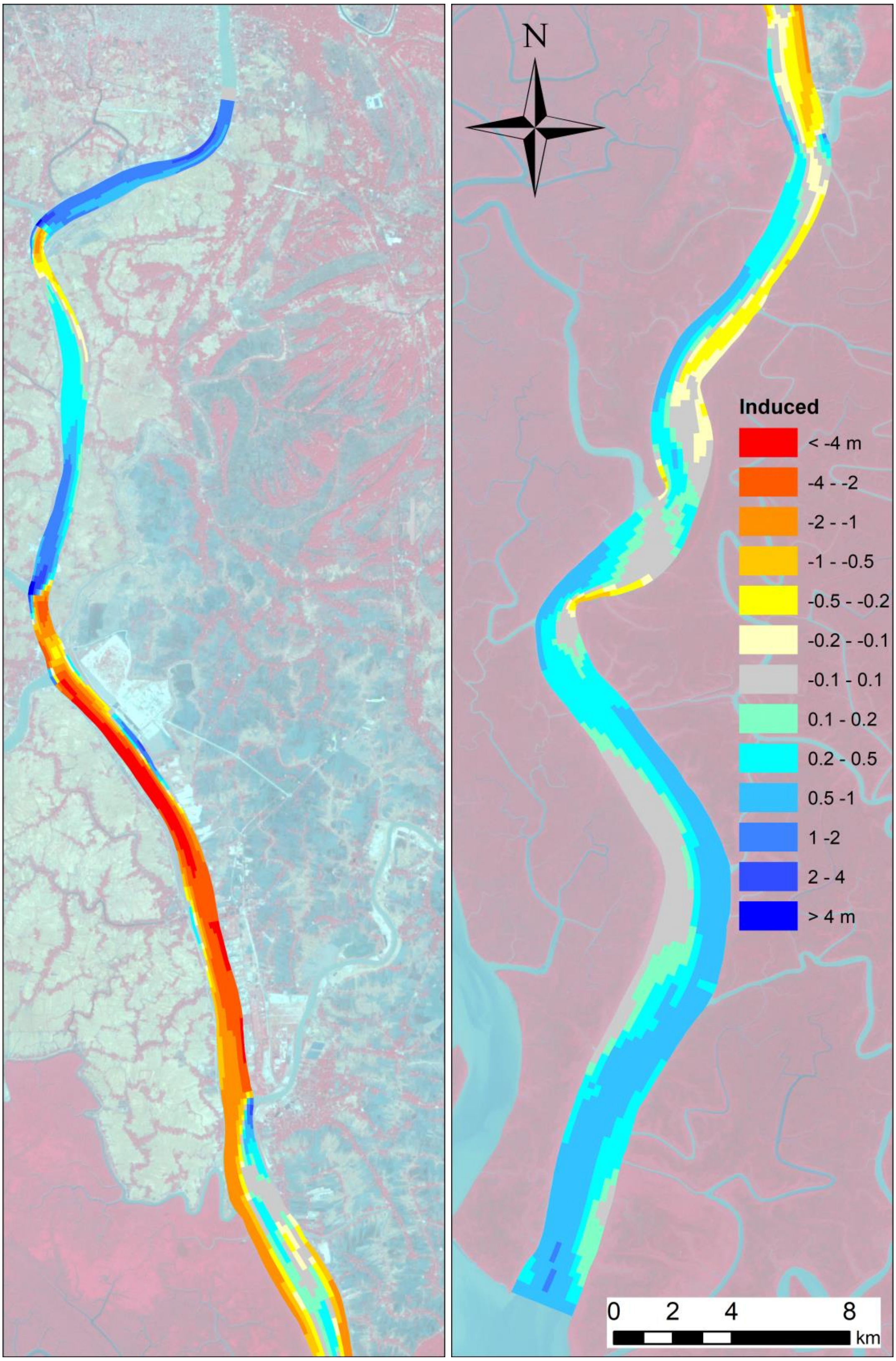

Figure 4-19 Simulated induced bed level changes 2019-2020 caused by closing the three upstream side channels connecting Pussur and Sibsa.

Figure 4-19 shows the impact of closing the side channels illustrated by the induced bed level changes 2019-2029, i.e. the difference to the baseline. The induced bed level changes show sedimentation upstream of Mongla, scouring along Mongla Port and sedimentation further downstream in Pussur River. This pattern appears very attractive due to the induced scour at Mongla Port, while sedimentation further downstream is not a problem because the bed levels downstream are quite low already.

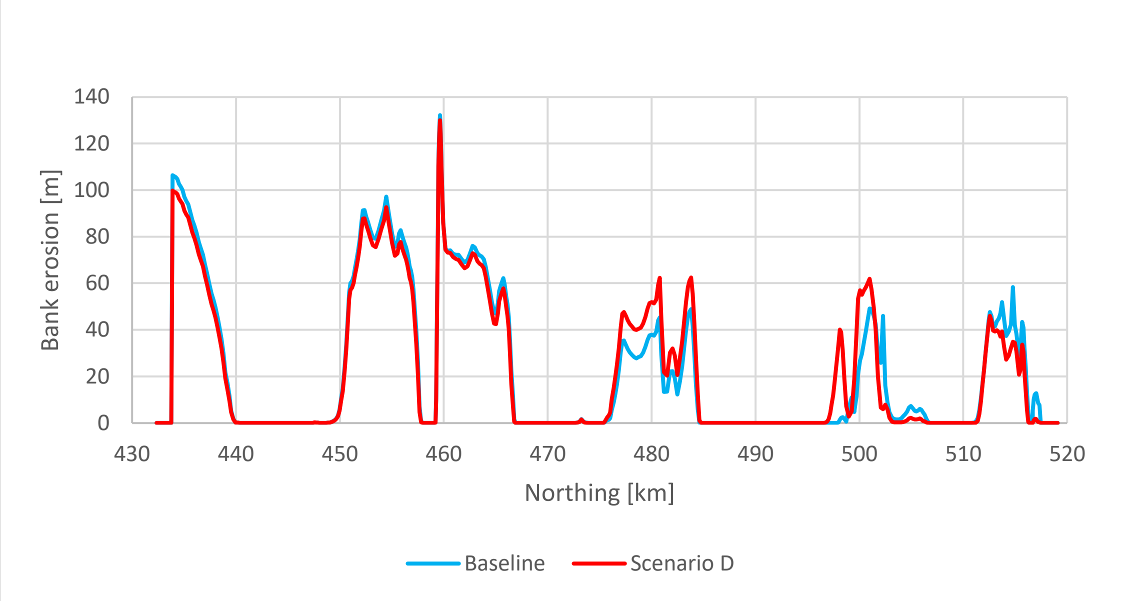

Figure 4-20 Simulated east bank erosion 2019-2029 for existing conditions and with 3 side channels closed.

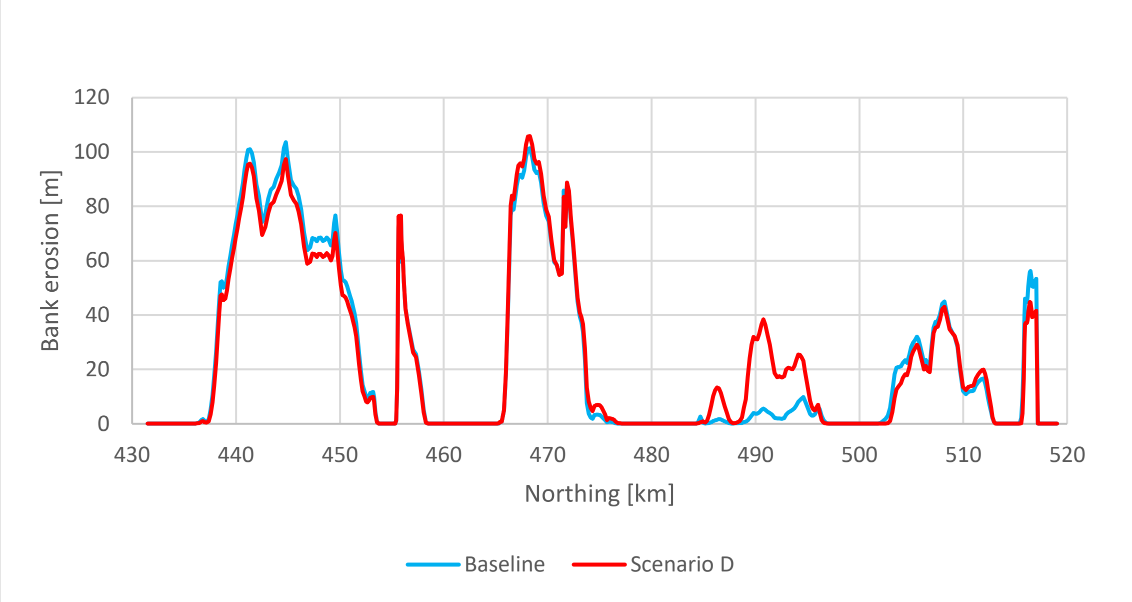

Figure 4-21 Simulated west bank erosion 2019-2029 for existing conditions and with 3 side channels closed.

The impact on bank erosion is illustrated in Figure 4-20 and Figure 4-21. It is observed that bank erosion increases along Mongla Port, while bank erosion is reduced upstream and downstream, as would also be expected due to sedimentation and scouring.

Conclusions: Closing the three upstream side channels connecting to the Sibsa River has been proposed before. In this scenario the Sibsa is prevented from capturing the tidal prism located upstream of Mongla Port, allowing the Pussur to utilize its (presumably) original tidal prism. The model shows that closing the side channels has a strong impact at Mongla Port, causing the 2019-2029 simulated deposition to vanish, such that the Mongla Port behaviour becomes neutral compared to 2019, while the baseline shows significant sedimentation.

4.4.5 Scenario E: Adding regulators to the Sibsa connections

The idea of using regulators is to allow tidal flood discharges to be pulled in via the Sibsa and exit the corresponding ebb flows through the Pussur. Morphologically, this could be a less intrusive measure because incoming tidal flows are still allowed in the side channels.

Regulators will likely lead to increased salinity in Sibsa and in side channels and their surrounding floodplain. This is obviously problematic, but not considered in the analysis.

The scenario is similar to (D) the three side channels closed, but instead of closing them, they are regulated to allow incoming tide from the Sibsa and outgoing ebb through the Pussur. This should give a much stronger scouring effect than just closing the channels.

The simulation results are compared to the existing conditions as well as the case where the three channels are closed (D). This is done to demonstrate that the regulation increases the scouring effect at Mongla compared to just closing the channels.

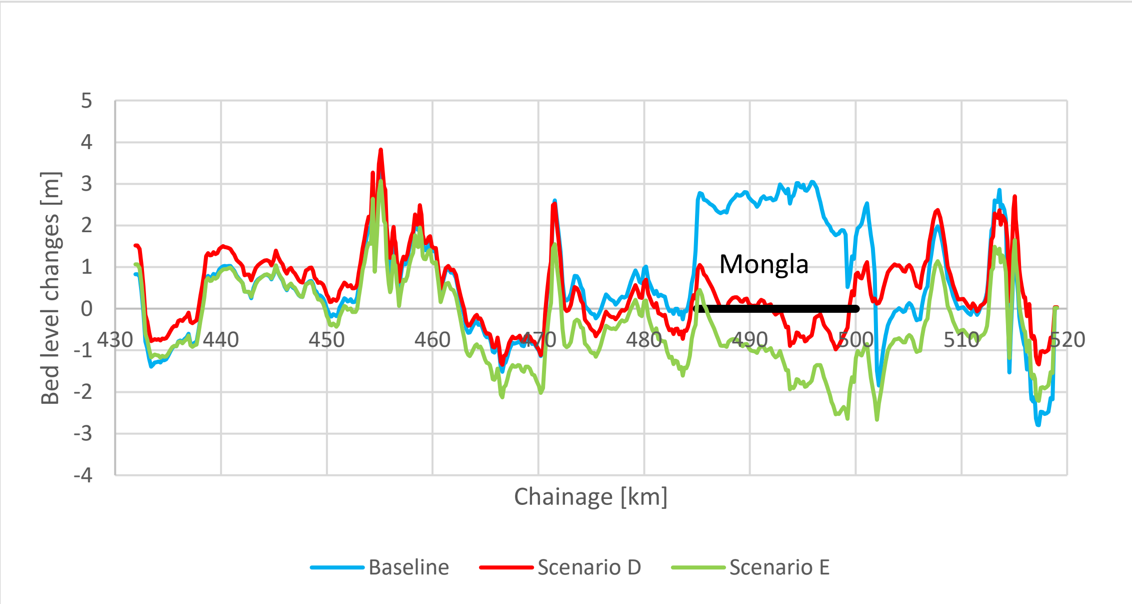

Figure 4-22 Simulated width-integrated bed level changes 2019-2029 for existing conditions, side channels closed (D), and side channels regulated (E).

The simulated width-integrated bed level changes are shown in Figure 4-22 for the three cases. It is clear from the figure that regulators cause additional bed level reductions compared to the case where the side channels are closed.

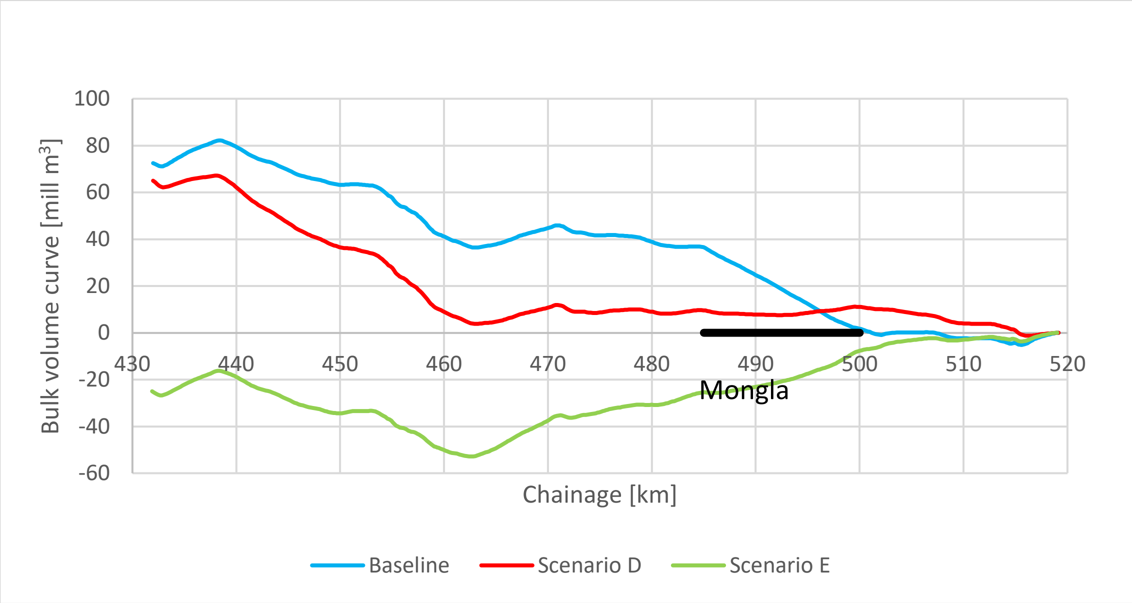

Figure 4-23 Simulated bulk volume curves 2019-2029 for existing conditions, side channels closed, and side channels regulated.

The best way to analyse the impact of regulators is to integrate the bulk volume curves, which are shown in Figure 4-23. The figure shows that the bulk volume curve with side channels regulated decreases along Mongla Port, while the bulk volume curve was neutral with side channels closed and increased for existing conditions. In other words:

- Mongla Port is depositional for existing conditions (A)
- Mongla Port is neutral with side channels closed (D)
- Mongla Port is erosional with side channels regulated (E)

This does not mean that the side channels need to be regulated to eliminate dredging at Mongla Port, and the results also do not mean that regulation of the side channels will eliminate the need for dredging. More thorough analyses are required to establish solid conclusions, while in this study the focus was conceptual.

If regulation of the side channels causes excessive erosion, it opens up for using the regulators only when necessary, i.e. the regulators can be operated only during periods when it is necessary to lower the bed elevation at Mongla Port.

Regulators were tested conceptually. It is not at all required that regulators be installed on all three side channels, and one single regulator, which it may even be possible to turn on and off, could be enough to give the flexibility to add extra scouring capacity at Mongla.

Different variants can be envisioned enabling a combination of regulators, channel closures and keeping some channels opens to achieve sufficient hydraulic dredging capacity at Monga Port with the least intrusive scheme. Only three variants were considered in the study, namely keeping all channels open, closing all channels and regulating all channels. Some combinations will be more problematic than others, i.e. regulators on all channels will give the highest salinity impact, while keeping some channels open could cause those channels to erode due to increased ebb flows to the Sibsa.

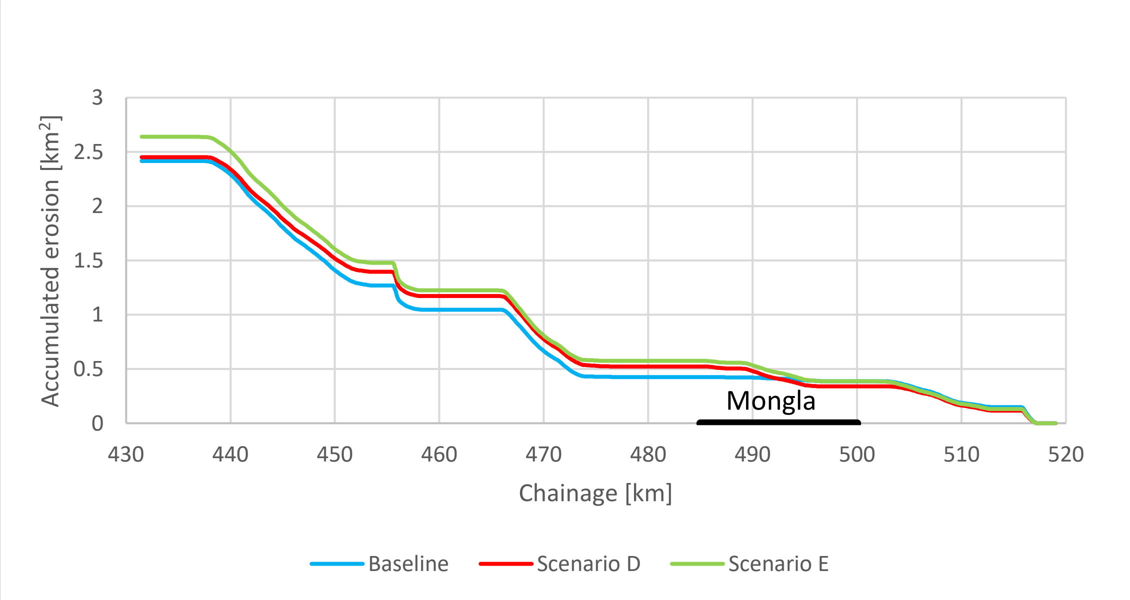

Figure 4-24 Simulated accumulated east bank area loss to bank erosion for 2019-2029 for existing conditions, upstream connections closed, and upstream connections regulated.

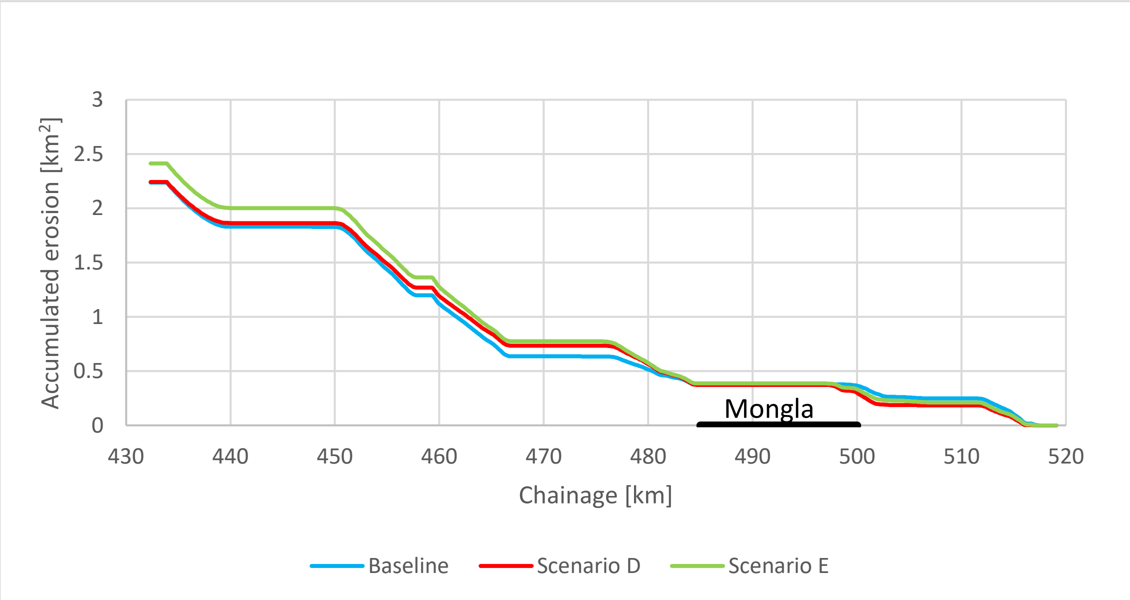

Figure 4-25 Simulated accumulated west bank area loss to bank erosion for 2019-2029 for existing conditions, upstream connections closed, and upstream connections regulated.

The impact on bank erosion was quantified by using the accumulated eroded area curves, see Figure 4-24 and Figure 4-25. The curves confirm that closing the channels does not lead to significant overall changes to bank erosion, while regulators will lead to increased erosion as a simple consequence of increased ebb flows. Regulators cause increased bank erosion mainly in the downstream end of Pussur, and the results yield 8% increased area loss along the west bank and 9% increased area loss along the east bank. These are not insignificant, but the increased area losses are concentrated downstream of Mongla Port.

Conclusions: Regulators were tested on the three side channels with the aim of allowing captured flood flows from Sibsa to add to the ebb flows going out through the Pussur. This will increase the erosion at Mongla Port due to the increased ebb flows, which was also verified using the model. The idea is to use the regulators to allow controlling the ebb flow scouring rates at Mongla Port in case closing the three side channels does not cause enough scouring. In the basic mode simulated with the model, the regulators will probably cause too much scouring, suggesting that the regulators can indeed be used for steering the scouring process at Mongla Port. The impact on salinity was not investigated with the model, but this should be considered, as the impact could be problematic in the area between Pussur and Sibsa along the three side channels.

4.4.6 Scenario F: Groynes at Mongla Port

Groynes at Mongla have been proposed before (IWM, 2015).

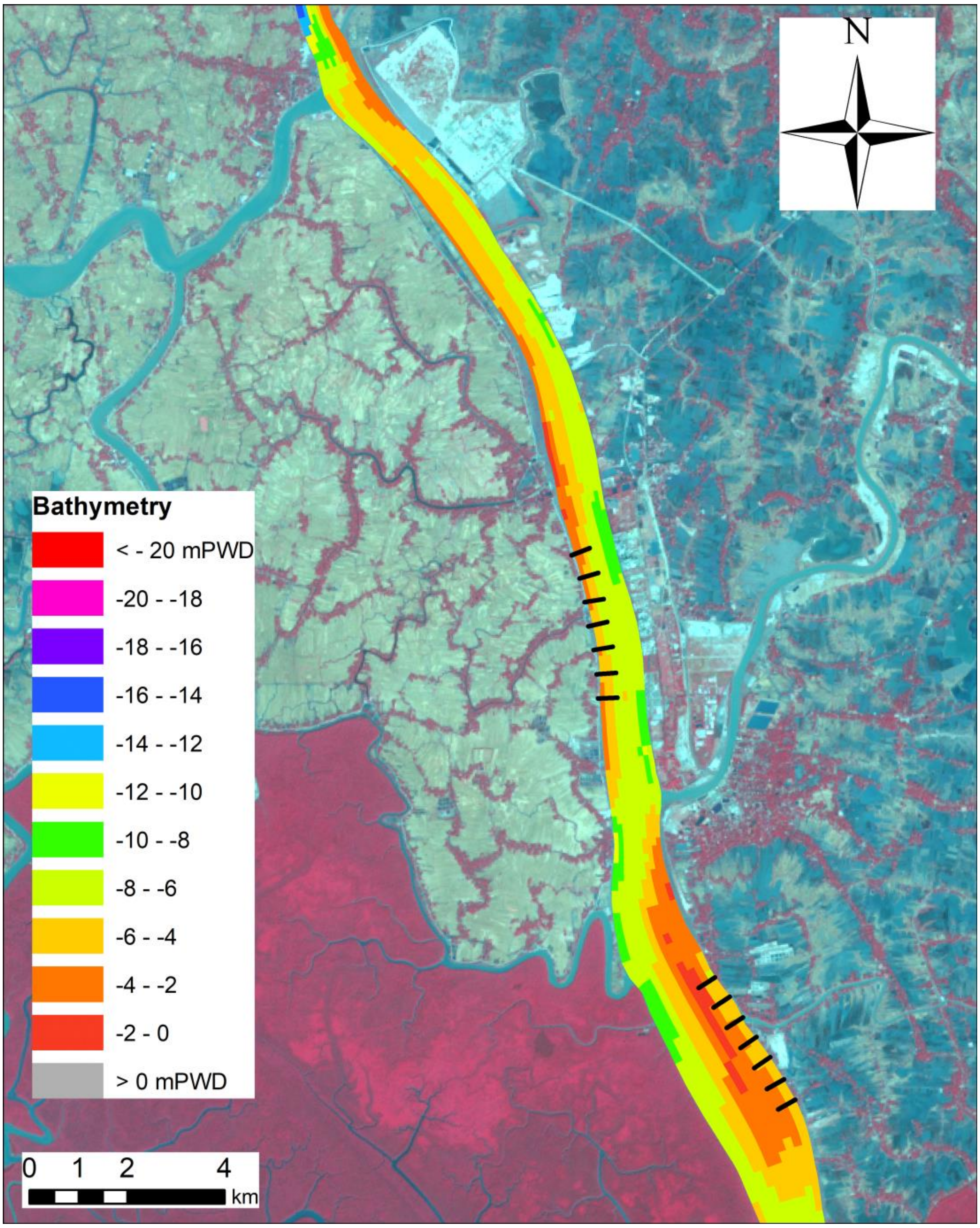

Figure 4-26 Groynes installed at Mongla Port.

The scenario is illustrated in Figure 4-26. The groynes were included based on the information provided by IWM (2015).

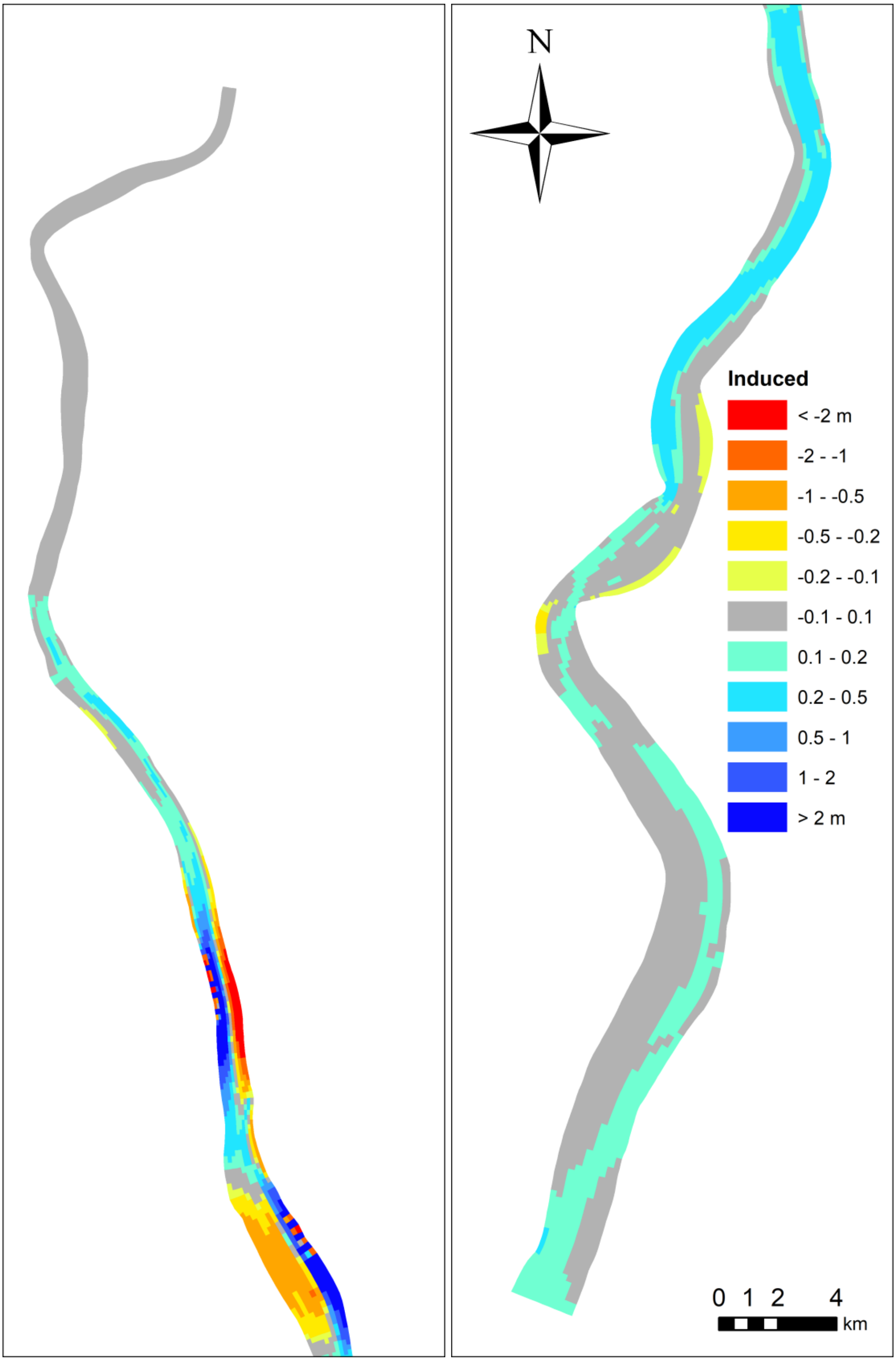

Figure 4-27 Induced bed level changes after 10 years associated with the groynes.

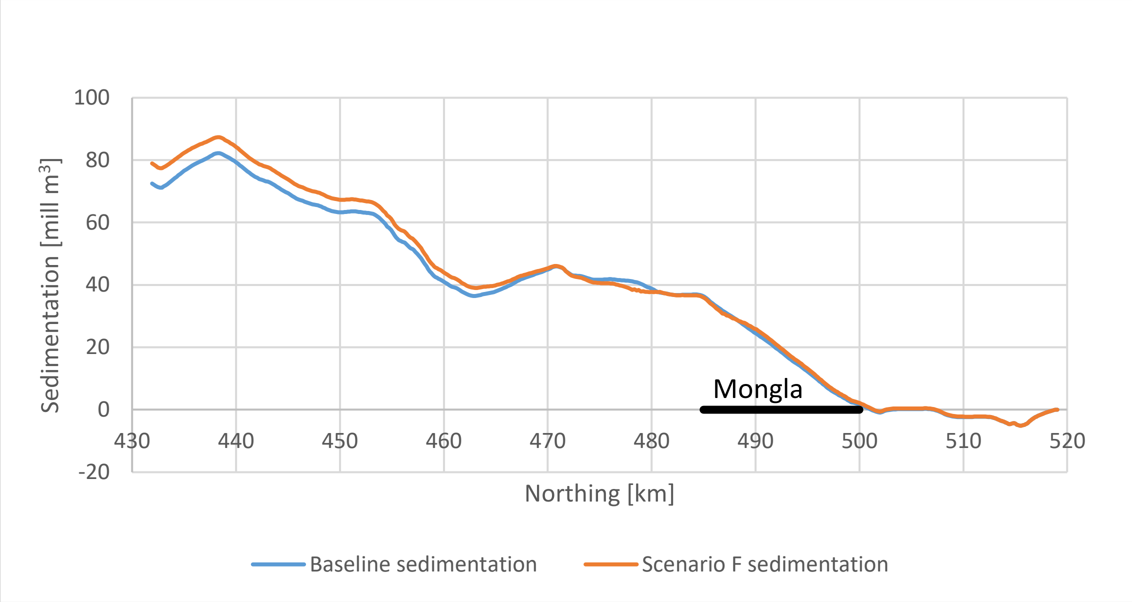

Figure 4-28 Calculated accumulated sedimentation curves 2019-2029 for existing conditions and with groynes installed at Mongla Port.

The simulated induced bed level changes after 10 years are shown in Figure 4-27.

The groynes reduce the bed levels significantly in the navigation channel, while deposition is induced in the area covered by groynes, as also expected. Further downstream the groynes cause increased sedimentation, which can be seen from Figure 4-28. The figure also shows that the groynes do not induce overall scour; they just redistribute sediment to allow for deeper channels along Mongla.

The groynes are clearly capable of reducing bed levels, but they also lead to increased sedimentation in Pussur River, which is probably due to reduced ebb flows caused by the added hydraulic resistance from the groynes.

As always, it is very instructive to observe how the Pussur River upstream of Mongla Port simply does not seem connected to Mongla Port, as seen from the induced bed level changes in Figure 4-27. The upstream part is controlled by Sibsa, and the groynes do not seem to have any impact upstream.

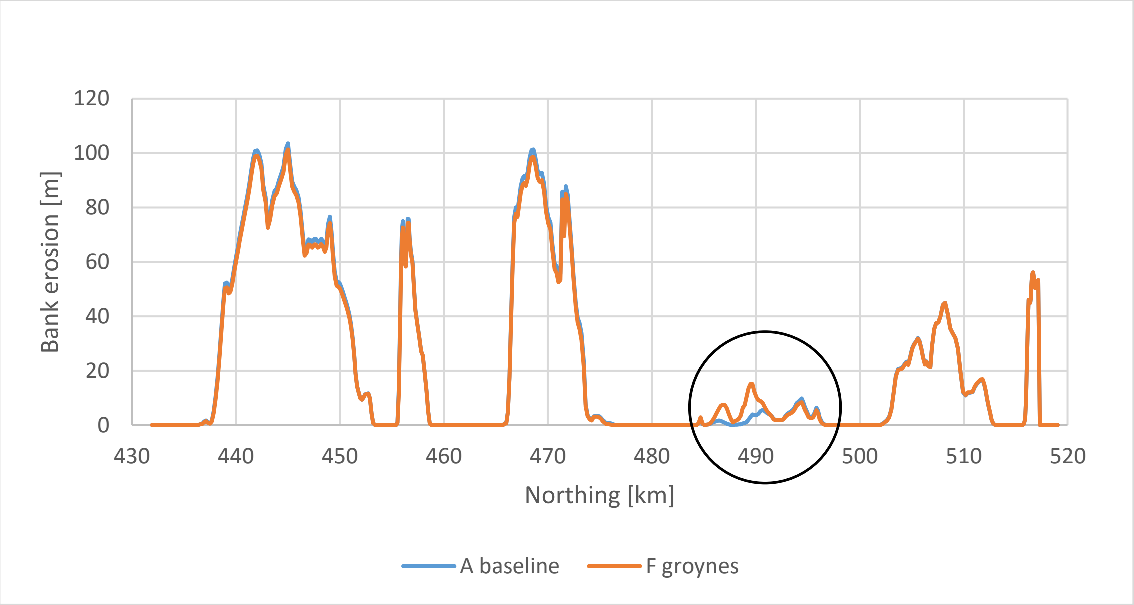

Figure 4-29 Simulated east bank erosion 2019-2029 for existing conditions and with guide bunds. The circle indicates the location along the east bank where the guide bunds located to the west will increase erosion along the eastern bank.

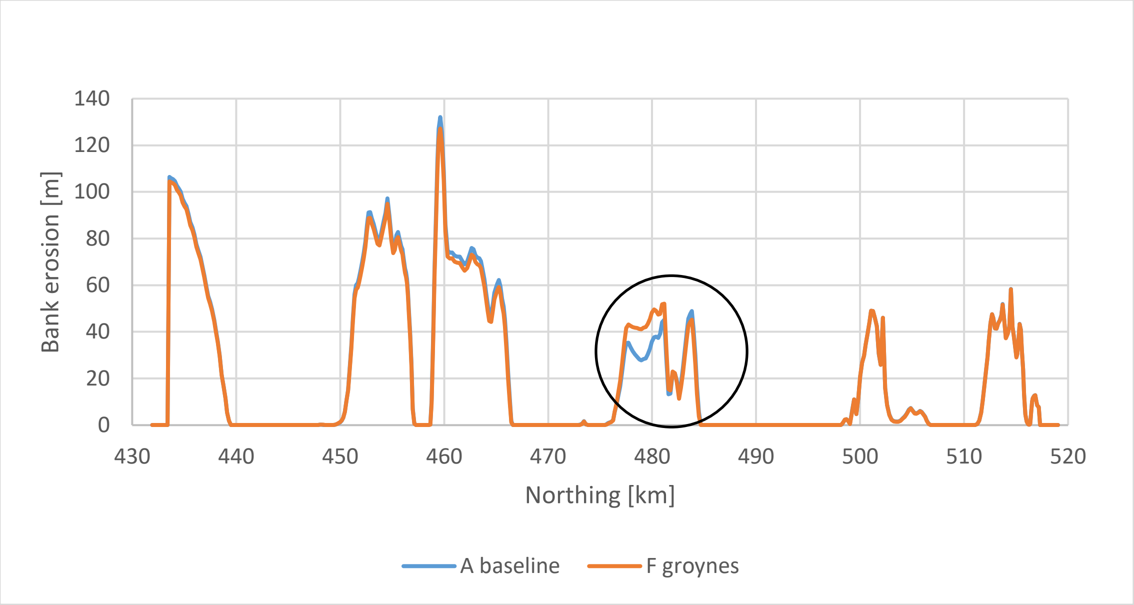

Figure 4-30 Simulated west bank erosion 2019-2029 for existing conditions and with guide bunds. The circle indicates the location along the west bank where the guide bunds located to the east will increase erosion along the eastern bank.

The impact on bank erosion is illustrated in Figure 4-29 and Figure 4-30. As expected, the deeper channels along the east and west banks lead to increased bank erosion, but the effect is relatively small.

Conclusions: The guide bunds at Mongla Port proposed by IWM (2015) were investigated using the morphological model. The model shows that the guide bunds will reduce bed levels in the channels opposite of the guide bunds, which should also not be difficult to achieve. The guide bunds will lead to increased sedimentation in Pussur River, downstream of Mongla Port due to the added hydraulic resistance from the guide bunds. The model also shows that the guide bunds will lead to increased bank erosion along the channels that are deepened by the guide bunds.

4.4.7 Scenario G: Apply TRM to Polder 33

Tidal basins have been proposed before, see e.g. IWM (2015). In this section the use of TRM for Polder 33 is investigated, which means a tidal basin effect is achieved along with sedimentation in the polder.

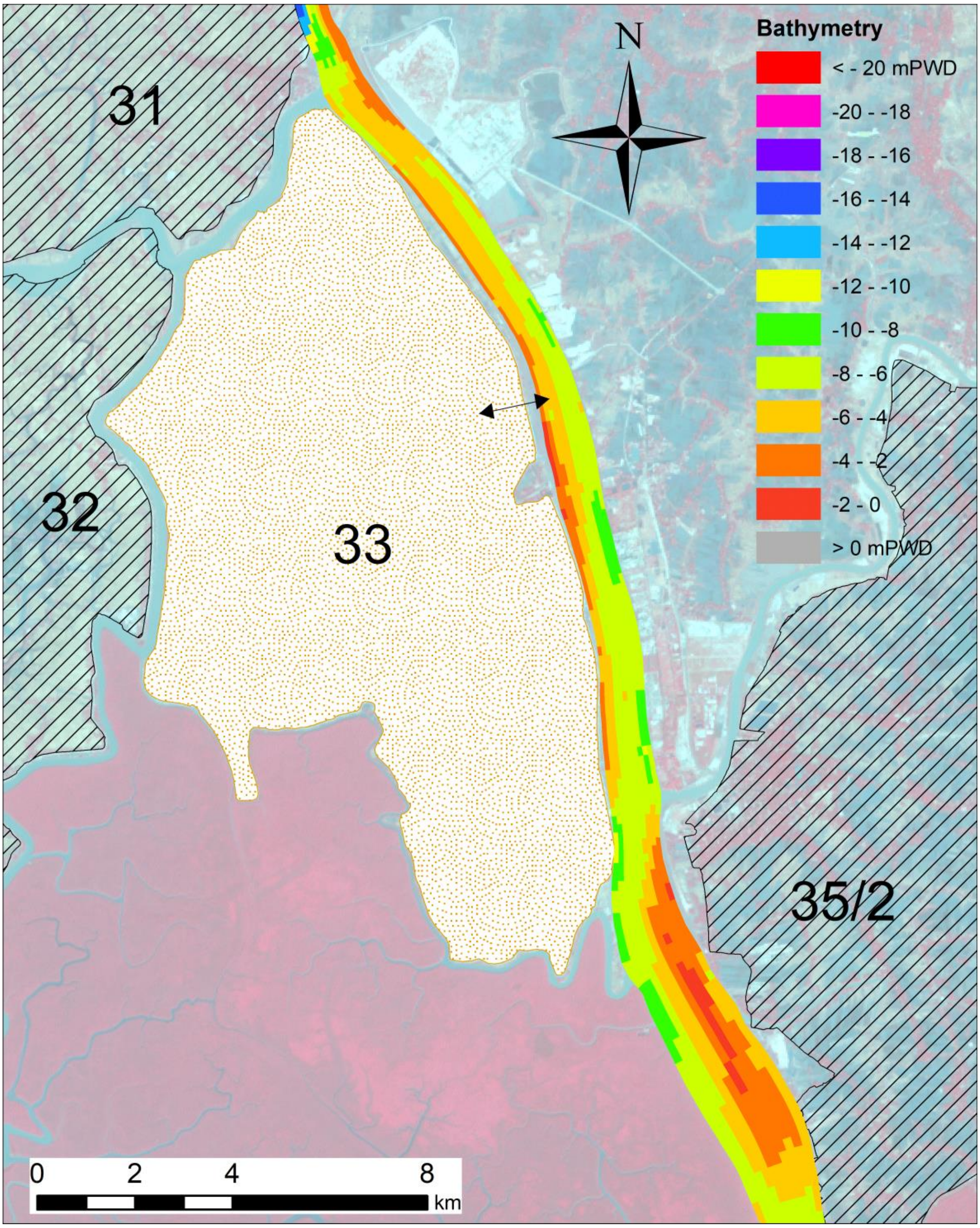

Figure 4-31 Application of Polder 33 for TRM.

Figure 4-31 shows the location of Polder 33, which in this scenario is connected to the Pussur to act like a tidal basin and also to bring sediment away from the Pussur. In this scenario the polder was connected to the Pussur River through a single channel.

Polder 33 has a surface area of 102 km^2. The polder was added to the SWRM to prepare boundary conditions for running the MIKE 21C model. The polder was then added to the MIKE 21C model as a boundary condition taking in water with the local sediment concentration for flow going to the polder and returning clean water from the polder. The polder obviously also changed other boundary conditions, which were extracted from the SWRM with the polder included.

The MIKE 21C simulations showed sizeable impacts of the polder, which also meant that the model results are not reliable after an estimated 5-year period due to too large changes in the Pussur River, which would ideally require updating of the SWRM boundary conditions caused by changes to the flow exchange with Polder 33. This was not done due to time constraints, and therefore the MIKE 21C model was only applied for a period of 5 years. Fortunately, the timescale over which TRM can be applied to a polder is no more than 5 years, so the limitations in the application of the model over time aligns with the timescale over which it can meaningfully be applied.

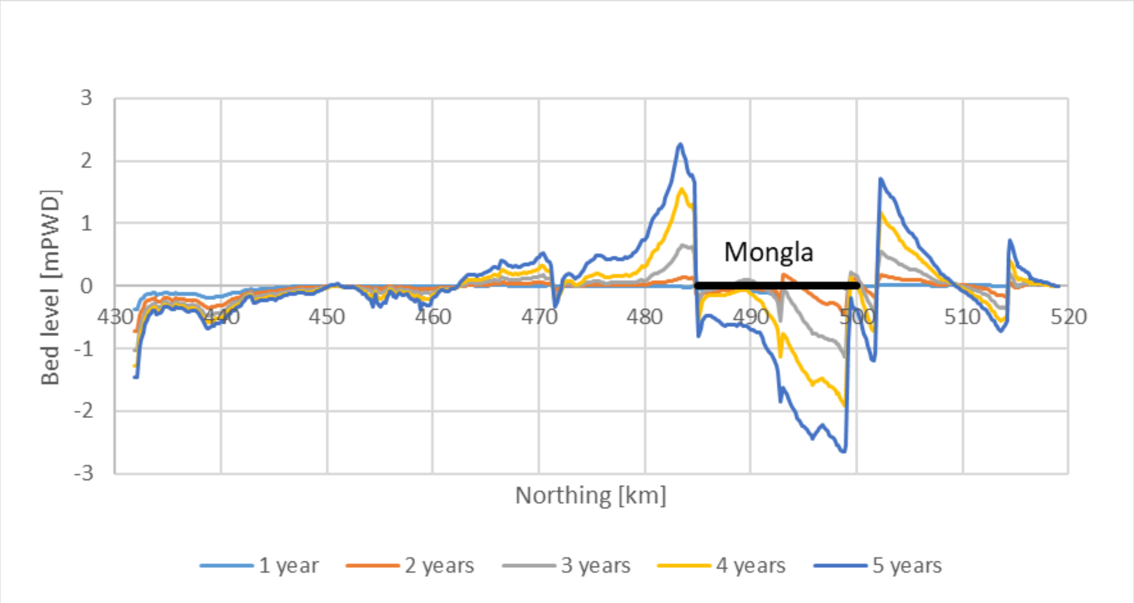

Figure 4-32 Simulated induced changes during the anticipated 5 years of operation.

The simulated induced bed level changes over time associated with the operation of Polder 33 as a tidal basin are shown in Figure 4-32. The results show that the operation of Polder 33 as a tidal basin is beneficial to the bed levels at Mongla Port, but also that the bed levels increase downstream of Mongla Port.

Induced scour at Mongla Port is a desirable outcome, but the increased sedimentation just downstream is problematic.

It does not appear as if the use of Polder 33 as a tidal basin can increase the tidal prism of the Pussur River. Hence, it is also not possible to induce consistent scouring in the river to improve navigation conditions at Mongla Port and downstream. The reason for this is not very complicated, namely that Sibsa is the underlying problem, and adding tidal basins to Pussur River just means that the Pussur tidal flows will exchange water with these basins, allowing Sibsa to capture more tidal prism from Pussur further upstream. This also manifests itself in the simulation in the shape of tidal discharges in Pussur River not actually increasing. The added tidal basin (Polder 33) simply replaces upstream tidal prism with tidal prism in Polder 33, while as a result the Sibsa tidal prism ends up increasing.

Variants of this scenario were considered, but not simulated. It is possible that more openings into Polder 33 could distribute the scouring impact over a longer distance in the Pussur River, especially elongating the impact further downstream. Ultimately, Polder 33 would only be a temporary fix, as the polder can only be used for a short period of time.

Conclusion: The potential application of TRM for Polder 33 was analyzed in the MIKE 21C model. Boundary conditions for the scenario were prepared using the SWRM, and it was found that the MIKE 21C model is not reliable beyond 5 years due to too large morphological changes ideally requiring updated SWRM boundary conditions (the tidal exchange between Pussur and Polder 33 would have to be updated). However, 5 years is a long timescale when considering TRM, so the analysis was only conducted for 5 years, while the Mongla Port scenarios generally considered 10 years in the study. The results show that TRM applied to Polder 33 can lead to reduced sedimentation at Mongla Port, but also to increased sedimentation downstream of Mongla Port, which means that TRM is not attractive. The tidal basin effect of Polder 33 is very illustrative for the fundamental problem with Mongla Port, namely that the added tidal basin does nothing for the Pussur tidal prism because the Sibsa will always be able to capture additional tidal prism upstream in scenarios aimed at adding tidal prism to Pussur downstream of the tidal divide located just upstream of Mongla Port.

4.4.8 Scenario H: Add tidal basins to Sibsa

Adding tidal basin(s) to Sibsa sounds counterproductive, but the purpose is to slow down the tidal propagation in Sibsa in order to help the Pussur capture more tidal prism upstream of Mongla.

This scenario was not tested, but it is mentioned due to its potential value.

5 Conclusions

The present report documents the development of the MIKE 21C model of the Pussur River.

Several historical bathymetry datasets exist for the Pussur River. However, the two most recent dataset were considered in the 2D model, as the older datasets do not have sufficient resolution for accurate 2D contouring of the bed elevation. The two most recent datasets are from 2011 and 2019 and have almost identical resolution, which means they constitute an excellent basis for hindcasting 2011-2019 of bathymetrical changes for model calibration.

Hydrometric data in the shape of water levels and discharges was used for calibrating the hydrodynamic model. No detailed flow velocity measurements were available for detailed calibration of the flow distribution in the models.

Some (21, although 3 were downstream of the model reach) bed samples were available. This is more than in any other river in this study, but 18 bed samples in a river of the size of Pussur River is still very few. The bed samples provide a lot of useful information with respect to the sediment in the river; notably it is clear that Pussur River is a sand-mud river with sandy bars and muddy channels. The data also shows a longitudinal variation with more sandy bars downstream compared to upstream. However, the data is not sufficient to make a reliable spatial distribution of the bed sediment sizes.

There is also a fair amount of suspended sediment data at three stations in the Pussur River, namely Rupsha (upstream), Mongla (roughly midway between upstream and downstream) and Akram Point (downstream). The data does not include particle size distribution, which is a major weakness, and it was therefore not possible to generate (detailed) boundary conditions for the model (only estimated order of magnitude) and to use the data for calibration of the model.

Historical bank lines were digitised from Landsat images 1988-2019. These showed very consistent and systematic bank erosion, typically 5-10 m/year with erosion taking place along the same bank locations. The observed bank erosion correlates extremely well with the bed levels, meaning that almost all bank erosion takes place along outer bends with deep bend scour.

Only limited information concerning the sediment size distribution in the riverbanks was available. Furthermore, only land surface samples were available, showing mud dominance on the land surface adjacent to the river. The bank material at eroding banks is a significant contribution to the sediment budget. However, without knowledge about the particle size distribution in the banks, there is a significant source of uncertainty.

The curvilinear grid (500x10 cells) was based on the 2011 bank lines digitised from the 2011 Landsat image, with the 2011 bathymetry contoured in the grid. A similar 2019 model was based on the 2019 bank lines and 2019 bathymetry data. The 2011 model was used in the model development process including calibration and validation, while the 2019 model was used for scenario simulations.

Hydrodynamic boundary conditions were provided by IWM from the SWRM for the period 2011-2019 (30 min time-step). The boundary conditions consisted of upstream discharge, inflow/outflow at several side channels and downstream water level time-series.

The sediment model was formulated as a 2-fraction model with sand and mud. The mud fraction represents the clay and silt, which were lumped together with one representative fall velocity and erosion function, making it difficult to hindcast both sediment concentrations and bed level changes. The mud was simulated using the exact same cohesive model parameters used for the other three models (Sibsa River, Baleswar River, Bishkhali River), which were shown to validate well against observed concentrations, but more importantly against observed bed level changes. The sand was treated with the same erosion model, and sand-mud interaction was added to the description.

Many calculations were made regarding the flow fields in the sharp bends of the Pussur River, especially in the downstream end.

There is no unique resistance calibration. The resistance models can have large spatial resistance variation, leading to different velocity distributions, but still generate the same water levels and discharges. There are no measured velocity profiles available for the sharp bends, which makes it difficult to identify the correct calibration.

The hydrodynamic model calibrated well to observed water levels and discharges with a constant Manning M=60 $m^{1/3}/s$. However, this resistance model causes high flow velocities over bars, even when the bars are quite shallow, and the flow can even accelerate over bars due to the inertia of the flow. Using a constant Manning M therefore makes it difficult to sustain bars in the morphological model because the high flow velocities will lead to sediment entrainment on the bars. Therefore, attempts were made to introduce a spatial varying resistance number in the morphological model.

Bed samples show that the point bars in the downstream end of the Pussur River are covered by sand. Using a regime predictor (van Rijn, 1984), it was shown that the conditions on the bars are exactly right for the formation of ripples (low flow velocities) and dunes on the bars, while the transition to upper plane bed does not seem to occur on the bars. Dunes produce very high form resistance and can easily give four times total resistance compared to skin friction. Dunes on the bars will therefore cause significant flow deflection from the bars, leading to much lower skin friction.

A dune module based on regime, dimensions and resistance predictors was tested for the Pussur River, but it caused problems due to the mixed sediment in the river. Dune models are generally developed for alluvial rivers, while the dominating sediment in Pussur River is silt, and sand is only found on bars. The total friction model of Engelund-Hansen (1967) was also tested, but this caused problems because it does not give control over the total resistance, which is essential for the model calibration.

A much simpler resistance model is available in MIKE 21C in which the total resistance is directly related to the local water depth. This can be used for modelling the high resistance on bars by indirectly taking advantage of the bars being shallow, while the deeper channels will have lower resistance. When using the resistance model, it is possible to make the Pussur River deflect flow away from the bars, while still generating the same water levels and discharges obtained in the hydrodynamic calibration with a constant Manning M. The different velocity distributions when using the alluvial resistance model will lead to significantly different bar formations. For constant Manning M the bars in sharp bends tend to erode, while high resistance on bars can lead to stable or even growing bars.

In practice, the depth-dependent resistance model turned out to be difficult to use in the model. There were two reasons for this. First, the resistance on bars depends on whether bars are sandy, and the data suggests that only the bars in the downstream end are sandy. In principle, this can be circumvented by using a spatially varying alluvial resistance coefficient, i.e. constant Manning M=60 $m^{1/3}/s$ appears to work well in the upstream end (no sand on the upstream bars, i.e. only skin friction), while strong flow deflection is required to correctly reproduce bars in the downstream end. Secondly and much more problematic, total flow resistance derived from the water depth is only partially correct, and when using the alluvial resistance model with strong flow deflection from shallow areas, the model can easily make bars grow too much, including in areas where there are no bars. It is clear that the high resistance on bars needs to apply only to the bars, and hence it cannot be estimated by using the water depth as a proxy.

Velocity distributions are not only influenced by the flow resistance. The well-known 3D momentum convection effect (Lien et al, 1999) associated with helical flow was investigated and was found to exchange momentum away from the shallow bars and into the deeper outer channels. It was concluded that it has negligible influence. Although the depth to curvature (h/R) of the Pussur River can be quite high, the width to depth ratio (B/h) is also very high, yielding a weak 3D convection effect.

Flow separation is also a candidate to consider for the flow distribution in areas with sharp bends. However, the investigations showed no tendency for flow separation.

Observed suspended sediment concentrations were assumed to contain significant amounts of clay, and it was observed that the calibrated cohesive sediment parameters lead to lower concentrations compared to observations, which is also to be expected if the observations contain a large (unknown) clay fraction. The mud erosion function is almost identical in the other studied rivers in the project (Sibsa River, Baleswar River etc).

The cornerstone of the morphological calibration is a morphological hindcast 2011-2019. For the Pussur River this can be conducted with very good reproduction of bed level changes in the period, even when suffering from uncertainties in the data and model inputs. Comparison to observed bed level changes is very convincing.

Bank erosion was simulated using almost the same formula as for the other rivers in the project. Bank erosion hindcasting 2011-2019 showed very good agreement with the observations, with the correct banks eroding and the magnitude correctly reproduced.

5.1 Recommended data collection for future model study

The current data situation for Pussur River does not allow 2-fraction models without making many assumptions. The following data can help reduce the need for making assumptions and reduce uncertainties in the model:

- Collection of ADCP data in bends to obtain depth-integrated velocity profiles.
- Sediment concentration, including particle size distribution at upstream model boundary (Rupsha).
- Sediment concentration, including particle size distribution at Akram Point.
- Mongla sediment concentration, including particle size distribution.
- Bank material particle size distribution.
- Bed samples processed into particle size distributions, at least 100 bed samples distributed over the whole riverbed. The bed samples can be collected from strategically selected locations allowing determination of the particle size distributions for various bed features (bar, channel etc.), including the longitudinal variation
- Identification of dunes from e.g. multibeam bathymetry data on the sand bars.

It is noted that IWM regularly collects ADCP data in the rivers. However, for convenience, the ADCP profiles are usually collected in straight reaches and processed into discharges. Hence the capability and expertise within ADCP data collection is already available, while the suggestion made in this report is to use the capability in a slightly different way by collecting the ADCP data in specific sharp bends with dune cover and post-process the ADCP data both into discharges (as usual) and depth-integrated velocity fields.

It is also noted that traditional single beam echo-sounder is normally adopted in the rivers, and that single beam is sufficient for the full bathymetries. However, local multibeam echo-sounder data is very valuable (especially for identifying dune fields, which cannot be done from single beam data perpendicular to the flow direction), and the capability is readily available at IWM.

5.2 Recommended model improvements

The model development had a lot of focus on the bends to get a good representation of bars, which is critically important for getting good predictions of bank erosion.

The current version of the Pussur River model opens for some questions about individual model components. Flow deflection from bars is not known in detail, and due to dunes, it could be much stronger compared to what is currently modelled. In the present version of the model, the bars are assumed to be erosion resistant due to sand-mud interaction, but stronger flow deflection can also explain the behaviour.

Measured velocity profiles are essential for the improvement of the model. Without measured velocity profiles, the unique calibration of the model in terms of flow resistance and sediment transport cannot be identified. Without measured velocity profiles, the model will have a range of calibrations.

Model improvements require more data.

5.3 Conclusions from the scenario simulations

The developed model was applied for the following scenario simulations:

- Bank erosion projection 30 years into the future
- Impact of climate change 30 years into the future
- Impact of bank protection on bed levels
- Mongla Port scenario simulations

Bank projection 30 years into the future showed no qualitative changes to the river bathymetry, while sedimentation would continue. The eroding banks will hence also not change in the future, and the projected planform 30 years into the future is driven mainly by erosion of banks that also erode today. The simulated future bank lines were processed into shape files that are available as part of the project submittal.

The impact of climate change was quantified using the MIKE 21C model over the period 2019-2049. The SWRM shows that climate change leads to increased tidal amplitude in the Pussur River without changing the net flows during the monsoon. The impact of bed levels is modest, and bank erosion will slightly increase upstream and downstream of Mongla Port, while a reduction in bank erosion was simulated at Mongla Port.

Bank protection will always lead to scouring due to the removal of eroded bank material from the sediment budget. It was established from data analysis - before even conducting modelling - that the Pussur River sediment budget is strongly influenced by bank erosion. Hence, it must be expected that bank protection in the Pussur River can cause significant induced bed level changes. To analyse the full potential, the extreme case where all banks are protected from erosion was considered. The model showed that bank protection would cause induced scouring up to 2 m upstream and increasing to 4-5 m in the downstream end of Pussur River. The largest induced scour correlates with the bed levels, such that deeper channels will exhibit the largest increase in depth due to bank protection.

The Pussur River model was also applied to investigate scenarios to alleviate sedimentation at Mongla Port. Several scenarios were tested, many of them already tested in less ambitious models in previous studies. Indeed, some of the investigated scenarios have been on the table since the 1990s and maybe even before. The following scenarios A-H were investigated:

A Existing conditions (baseline)

B Ganges Barrage

C No bank erosion

D Close upstream connections to Sibsa

E Regulate upstream connections to Sibsa

F Install groynes at Mongla Port

G Apply TRM for Polder 33

H Add tidal basins to Sibsa River (not tested)

The impacts of scenarios were quantified by comparison to the baseline. Conclusions from the scenario investigations are summarized in the following.

B: Ganges Barrage has been proposed to reduce saline intrusion in the SW region. Boundary conditions were extracted from the SWRM model where Ganges Barrage has been included. The model results showed that Ganges Barrage will lead to increased sedimentation at Mongla Port.

C: The no bank erosion scenario was conducted as an easy means to quantify the impact of bank erosion on the Mongla Port sedimentation. Eroded bank material plays a significant role in the sedimentation of the Pussur River. The hypothetic scenario in which bank erosion is eliminated in Pussur River would lead to a somewhat (1/3) reduced sedimentation rate at Mongla Port, but sedimentation would not be halted. Considering how expensive bank protection is and how much of Pussur River runs through the Sundarbans without polders to protect, the scenario is not viable.

D: Closing the three side channels connection to Sibsa River upstream of Mongla Port has been on the table as an option for a long time. It is not known to the present study whether DHI's Pussur-Sibsa study from 1993 was the first time the option was investigated, but it was tested in that study. In this scenario, the Sibsa is prevented from capturing the tidal prism located upstream of Mongla Port, allowing the Pussur to utilize its (presumably) original tidal prism. The model shows that closing the side channels has a strong impact at Mongla Port, causing the 2019-2029 simulated deposition to vanish, so that the Mongla Port behaviour becomes neutral compared to 2019, while the baseline shows significant sedimentation.

E: This does not seem to have been investigated before. Regulators were tested on the three side channels with the aim of allowing flood flows from Sibsa to add to the ebb flows going out through the Pussur. This will increase the erosion at Mongla Port due to the increased ebb flows, which was also verified using the model. The idea is to use the regulators to allow controlling the scour rates at Mongla Port in case closing the three side channels does not lead to enough scouring. In the basic mode simulated with the model the regulators will probably cause too much scouring, suggesting that the regulators can indeed be used for steering the scouring process at Mongla Port. The impact on salinity was not investigated with the model, but this will be important to consider, as the impact could be problematic in the area between Pussur and Sibsa along the three side channels.

F: The groynes at Mongla Port proposed by IWM (2015) were investigated using the morphological model. The model shows that the groynes will reduce bed levels in the channels opposite of the groynes. The groynes will lead to increased sedimentation in Pussur River, downstream of Mongla Port, due to the added hydraulic resistance from the groynes. The model also shows that the groynes will lead to increased bank erosion along the channels that are deepened by the groynes.

G: The potential application of TRM for Polder 33 was analyzed in the MIKE 21C model. Boundary conditions for the scenario were prepared using the SWRM, and it was found that the MIKE 21C model is not reliable beyond 5 years due to too large morphological changes ideally requiring updated SWRM boundary conditions (the tidal exchange between Pussur and Polder 33 would have to be updated). However, 5 years is a long timescale when considering TRM, so the 5 years simulation used for this scenario is considered adequate, while the other Mongla Port scenarios considered 10 years in this study. The results show that TRM applied to Polder 33 can lead to reduced sedimentation at Mongla Port but also to increased sedimentation downstream of Mongla Port, which does not make TRM attractive.

The tidal basin effect of Polder 33 is very illustrative for the fundamental problem behind the sedimentation at Mongla Port, namely that the added tidal basin mainly increases the tidal prism in Sibsa while the Pussur tidal prism remains largely unchanged.

H: Adding tidal basins to Sibsa may increase the tidal prism in the Pussur by delaying the Sibsa flood tide. Such a scenario was not tested, but listed as Scenario H for emphasis.

6 References

Ahmadi, M. M., Ayyoubzadeh, S. A., Namin, M. M., & Samani, J. M. V. (2009). *A 2D numerical depth-averaged model for unsteady flow in open channel bends.* Journal of Agricultural Science and Technology, 11(4), 457-468.

Brownlie, W. R. (1981). *Prediction of flow depth and sediment discharge in open channels, Report No. KH-R-43A*. W. M. Keck Laboratory of Hydraulics and Water Resources, California Institute of Technology, Pasadena, California, USA, 232 p.

DHI (1993). *Mathematical Model Study of Pussur-Sibsa River System and Karnafuli River Entrance, Executive Summary*. Final Report

Engelund, F., & Hansen, E. (1967). *A monograph on sediment transport in alluvial streams*. Technical University of Denmark, Ostervoldgade 10, Copenhagen K.

Engelund, F., & Fredsøe, J. (1976). *A sediment transport model for straight alluvial channels*. Hydrology Research, 7(5), 293-306.

Fredsøe, J. (1982). *Shape and dimensions of stationary dunes in rivers*. Journal of the Hydraulics Division, 108(8), 932-947.

Fredsøe, J., & Deigaard, R. (1992). *Mechanics of coastal sediment transport.* Vol. 3, p. 369. Singapore: World scientific.

Galappatti, R. (1983). *A depth integrated model for suspended transport*. Communications on hydraulics, 1983-07.

Hasegawa, K. (1989). *Universal bank erosion coefficient for meandering rivers*. Journal of Hydraulic Engineering, 115(6), 744-765.

Hossain, M. B., Sakai, T., & Hossain, M. Z. (2011). *River embankment and bank failure: a study on geotechnical characteristics and stability analysis*. American Journal of Environmental Sciences, 7(2), 102.

Islam, M. S., Khan, A. J., Siddique, A., Kabir, R., & Nasrin, S. (2014). *Performance evaluation of riverbank protection using jute geotextiles*. In National Seminar on Jute Geo-textiles, Organized by Jute Diversification Promotion Centre (JDPC), Dhaka, Bangladesh (pp. 35-48).

IWM (2015). *Monitoring the Performance Dredging in/c Hydrological & Morphological Impacts by Mathematical Modeling & Assessment of Effectiveness of Dredging in the Harbour Area of Pussur River of Mongla Port*. Mongla Port Authority

Krumbein, W. C. (1934). *Size frequency distributions of sediments*. Journal of Sedimentary Petrology. 2 (4).

Kumar, A., Ramanathan, A. L., Prasad, M. B. K., Datta, D., Kumar, M., & Sappal, S. M. (2016). *Distribution, enrichment, and potential toxicity of trace metals in the surface sediments of Sundarban mangrove ecosystem, Bangladesh: a baseline study before Sundarban oil spill of December, 2014*. Environmental Science and Pollution Research, 23(9), 8985-8999.

Lien, H. C., Hsieh, T. Y., Yang, J. C., & Yeh, K. C. (1999). *Bend-flow simulation using 2D depth-averaged model.* Journal of Hydraulic Engineering, 125(10), 1097-1108.

Mitchener, H., & Torfs, H. (1996). *Erosion of mud/sand mixtures*. Coastal engineering, 29(1-2), 1-25.

Mehta, A. J., Hayter, E. J., Parker, W. R., Krone, R. B., & Teeter, A. M. (1989). *Cohesive sediment transport.* I: Process description. Journal of Hydraulic Engineering, 115(8), 1076-1093.

Mosselman, E. (1995). *A review of mathematical models of river planform changes*. Earth Surface Processes and Landforms, 20(7), 661-670.

Niemann, S. L., Fredsøe, J., & Jacobsen, N. G. (2011). *Sand dunes in steady flow at low Froude numbers: Dune height evolution and flow resistance.* Journal of Hydraulic Engineering, 137(1), 5-14.

Olesen, K. W. (1987). *Bed topography in shallow river bends*. Communications on Hydraulic and Geotechnical Engineering, 87. Delft University of Technology, Delft.

Rubey, W. W. (1933). *Settling velocity of gravel, sand, and silt particles*. American Journal of Science, (148), 325-338.

Tjerry, S., & Fredsøe, J. (2005). *Calculation of dune morphology.* Journal of Geophysical Research: Earth Surface, 110(F4).

van Ledden, M. (2003). *Sand-mud segregation in estuaries and tidal basins* (p. 221). Sydney: University of Technology.

van Rijn, L. C. (1984). *Sediment transport, part III: bed forms and alluvial roughness.* Journal of hydraulic engineering, 110(12), 1733-1754.

Waeles, B., Le Hir, P., Lesueur, P., & Delsinne, N. (2007). *Modelling sand/mud transport and morphodynamics in the Seine river mouth (France): an attempt using a process-based approach.* Hydrobiologia. 588(1), 69-82.

Wright, S. and Parker, G. (2004). *Flow resistance and suspended load in sand-bed rivers: simplified stratification model*. Journal of Hydraulic Engineering, 130(8), 796-805.

APPENDICES

Joint Venture of

The expert in WATER ENVIRONMENTS

&

Enabling Delta Life

in association with

Water Environment & Climate

University of Colorado, Boulder, USA
Columbia University, USA

APPENDIX A – Flow fields over the sandbars in the Pussur River

Joint Venture of

The expert in WATER ENVIRONMENTS

&

Enabling Delta Life

in association with

Water Environment & Climate

University of Colorado, Boulder, USA
Columbia University, USA

A Flow fields over the sandbars in the Pussur River

The simulated flow fields are critically important for the simulated development of the sandbars.

The flow fields are influenced by several factors:

- Bathymetry and planform
- Secondary (helical) flow and its effect on the velocity profiles
- Dunes and ripples (flow resistance)
- Vegetation (listed for the sake of completeness; it is not relevant in Pussur River)

A.1 Secondary flow convection of longitudinal momentum

MIKE 21C can optionally include the secondary flow convection of longitudinal momentum, which is a well-known effect described by Lien et al. (1999), Ahmadi et al. (2009), and Olesen (1987). Olesen (1987) concluded that the effect is only important for high h/R and low B/h. Wide rivers with low curvature have no influence from 3D. The present project has many rivers with high h/R up to around h/R=0.05, but the B/h values are also high, so the 3D effect is simply not important.

The effect of 3D momentum convection on the velocity fields is quantified later in this appendix to verify that it is indeed not important.

A.2 Dunes forming on the bars in the Pussur River

The purpose of this section is to explore whether the bars in the Pussur River can be expected to be dune covered. The bars are very similar to elevations around -5 mPWD, while the available bed samples suggest that the bars downstream are sandier and upstream bars are muddier. This also explains the higher planform curvature downstream; the bars downstream will deflect more flow, which will increase the planform activity due to the interaction.

The adopted Manning M=60 $m^{1/3}/s$ yields very weak flow deflection from bars, which would dramatically change with dune covered bars. This also has significant implications for the simulated bed morphology.

The bed form regime can be determined for various bed surfaces in the Pussur River by using the van Rijn (1984) regime predictor developed for uni-directional flow. If dunes exist as per the regime predictor, dimensions (length and height) can be calculated along with the total flow resistance.

In areas of the river bathymetry covered by sand, the bed samples show that the dominating sand size is 0.125 mm. To use the van Rijn (1984) regime predictor, the first step is to calculate the non-dimensional grain size D* corresponding to the median sand size:

$$D^* = d\left(\frac{(s-1)g}{\nu^2}\right)^{1/3}$$

This results in D*=3.56 for d=0.125 mm and a viscosity of 0.836×10^{-6} m^2/s corresponding to a 28 degrees water temperature. For this particular value of D*, low flow velocities will form ripples, and higher velocities will form dunes, which will wash out for even higher flow velocities.

The second parameter in the van Rijn regime predictor is the non-dimensional Shields parameter:

$$T = \frac{\theta'}{\theta_c} - 1$$

The critical Shields parameter is calculated from Brownlie (1981) as follows:

$$\theta_c = 0.22\ Re^{-0.6} + 0.06 \cdot 10^{-7.7\ Re^{-0.6}}$$

Yielding θ_c=0.07, where Re is the grain Reynolds number related to D*:

$$Re = (D\ *)^{1.5}$$

The skin friction shear stress associated with the flow velocity is estimated by using M=60 $m^{1/3}/s$ and a water depth of 5 m (the Manning M number is reasonable for the skin friction with a grain size of 0.125 mm, and the water depth corresponds to 0 mPWD water level and -5 mPWD bed level).

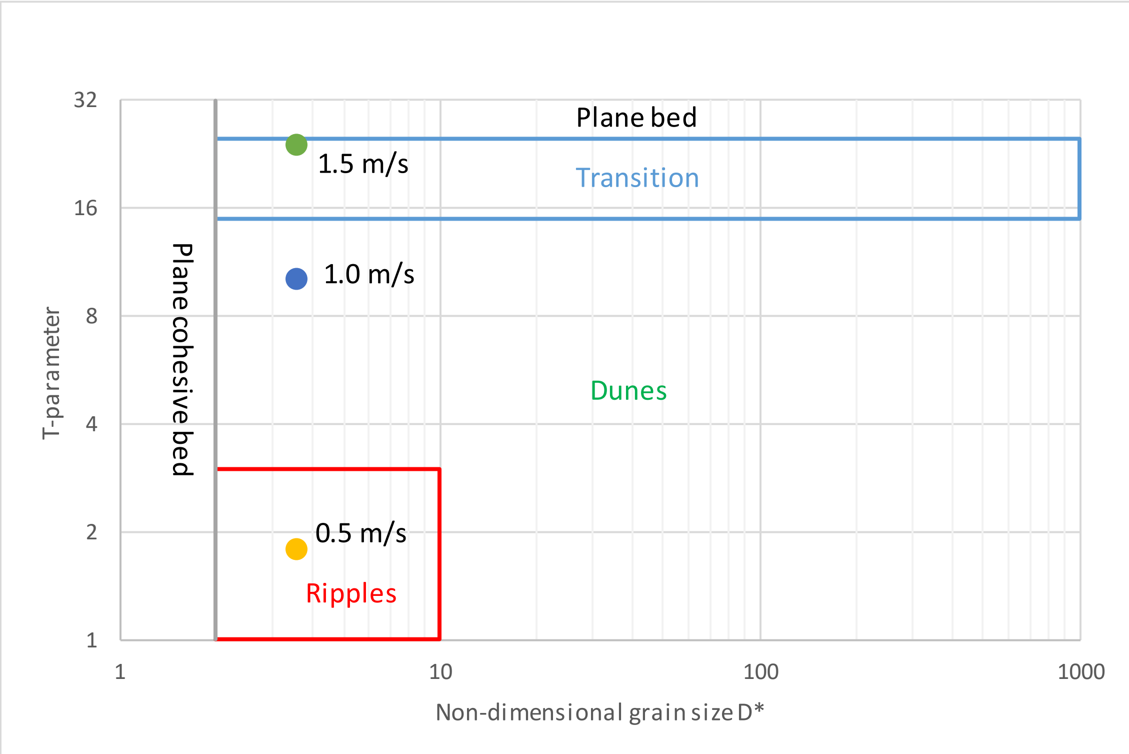

Figure A 1 van Rijn regime predictor for 0.125 mm sand in the Pussur River. The three calculation points for 0.5 m/s, 1.0 m/s and 1.5 m/s show how the flows in Pussur River will form ripples, dunes or transition to upper plane bed.

The van Rijn diagram is shown for the 0.125 mm sand in Figure A 1. Flow velocities in Pussur River can be up to 1.5 m/s, although not on bars. Hence the upper transition to plane bed regime is not really found on the bars, suggesting that the dune fields on bars are stable over time, i.e. dunes are not washed out for high discharges. Dunes obviously only exist for a sandy bed, as the D* value for mud is much too low to form dunes. Sandy bed conditions are found predominantly on bars in the downstream end of the river according to bed samples, while there are no bed samples showing sandy main flow channels.

These simple regime calculations suggest that the Pussur River bars will be dune covered when the bars are sandy. The flow velocities are in the appropriate range for dunes, although the D* is fairly small leading to the well-known fact that very fine sand will form ripples for low flow velocities and dunes for higher velocities (expressed in the van Rijn diagram).

Flow resistance involves form resistance on the bars due to sand waves (dunes and ripples). This is very compelling because the bars are sandy, while the deep channels are muddier, so it is plausible that the bars will be dune covered, while the deep channels will have plane bed. Dunes can significantly increase form resistance to 3-4 times higher than skin friction, see Parker (2004).

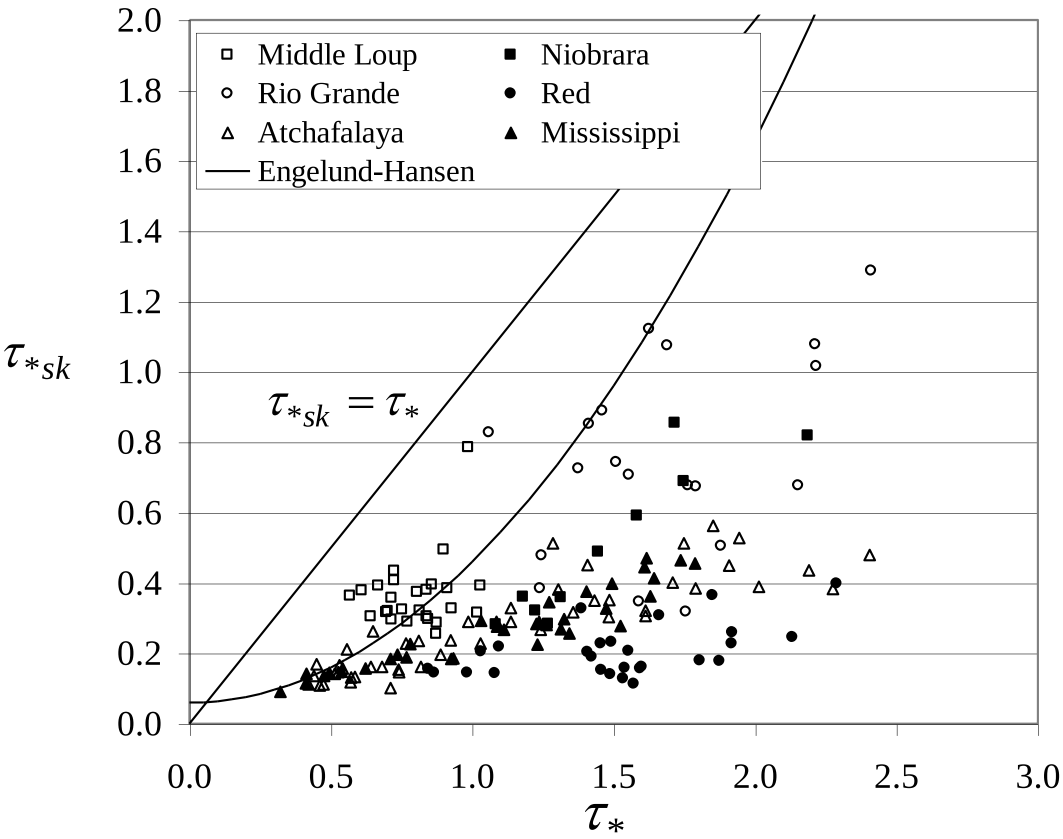

Figure A 2 Classic total friction versus skin friction, from Parker (2004), Engelund-Hansen (1967) compared to data. The data shows that the total friction is easily 4 times higher than the skin friction. This can be used for guiding an alluvial resistance model.

A dune model was explored by using the Engelund-Hansen (1967) resistance model (also shown in Figure A 2):

$$\theta' = 0.06 + 0.4\,\theta^2$$

When using this, the skin friction (θ') is known from the skin friction shear stress, while the total resistance (θ) has to be calculated from the expression. However, this turned out to be problematic because direct control cannot be exerted over the total resistance when calculating the total resistance from Engelund-Hansen or from Wright & Parker (2004). The total resistance is important because the model must above all reproduce observed discharges and water levels, which are controlled by total resistance. Clearly the total resistance must be high for a dune covered bed, but also unaffected for a bed without dune cover, becoming equal to the skin friction over the silt bed. These considerations suggest that the total resistance over a silt bed should reflect skin friction, probably represented well by a Manning M=60 $m^{1/3}$/s, while the total flow resistance on a dune covered sandbar should be maybe four times higher than the skin friction predicted on the sandbar from the skin friction (0.125 mm).

The impact of sediment composition is not included in the predictors for total flow resistance, which made it difficult to directly apply the predictors in the model.

The calculations in this section suggest that the bars in the Pussur River will be dune covered if the bars are sandy, which in general appears to be the case in the downstream end of the river, but not upstream (upstream bars appear muddy). The dune cover significantly influences the flow resistance and must be included to obtain the correct flow resistance and hence sandbar elevations.

A.3 Alluvial resistance model

A much simpler model allowing flow deflection from bars is already available in MIKE 21C. Bars are shallow and channels deep, so the resistance variation can be primitively modelled by using the depth as proxy and apply the expression for the Chezy number:

$$C = ah^b$$

In fact, the Manning resistance is already in this form:

$$C = Mh^{1/6}$$

The alluvial resistance model in MIKE 21C allows stronger variation of the resistance with the water depth compared to the standard Manning formulation. The advantage of the alluvial resistance model over a dune model is that the total resistance can be controlled better, especially in deep channels, which are important for tide propagation.

When adopting the alluvial resistance model, it is necessary to ensure that the model still calibrates to water levels and discharges. At first glimpse this might seem problematic with increased bar resistance, but if the deep channel resistance is lowered to compensate the increased resistance on the bars, calibration to water levels and discharges is still possible. This also leads to an important conclusion: It is possible to calibrate to water levels and discharges using different spatially varying resistance numbers, i.e. there is no unique calibration. Ultimately the same water levels and discharges can be obtained with very different velocity profiles, which also underlines a major weakness faced in the project: There are no ADCP velocity profiles, so the spatial resistance variation is not directly measured, although it can be indirectly (albeit with uncertainties) estimated from bed samples and regime predictors.

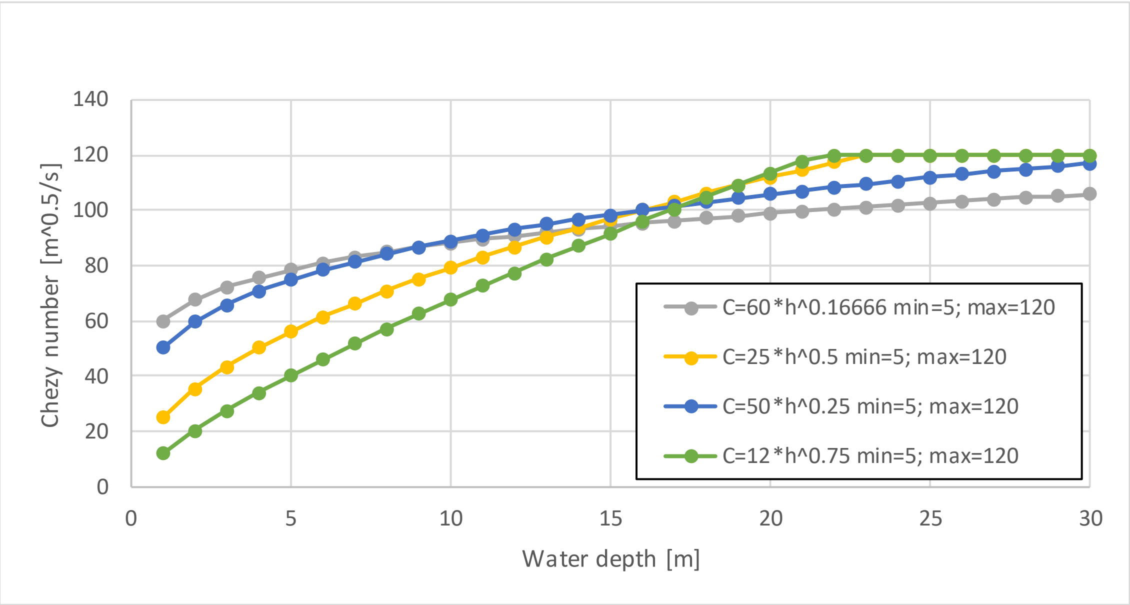

Figure A 3 Alluvial resistance models tested for Pussur River. The higher the b-exponent in the formula, the more bar deflection, while still ensuring correct low friction for large water depths (a-coefficient). These variations were explored during the model development.

Some of the explored alluvial resistance models are shown in Figure A 3. The alluvial resistance model is very simple and is generally easy to adopt in a model without significantly changing the flow fields, except that the bars deflect the flow. The reason for this lies in the way the alluvial resistance model can be tuned to yield high resistance for shallow water and low resistance for deep water, which is also what is generally expected in the Pussur River due to dunes forming on the bars and plane bed predominantly in the channels. The simplicity of the alluvial resistance model is compelling, but it can cause problems because it only relates resistance to depth and not bed surface composition.

Figure A 3 shows that for e.g. b=0.75 with a curve approaching the Manning M=60 $m^{1/3}/s$ curve for deep water, the alluvial resistance Chezy number for 5 m water depth will be halved compared to M=60 $m^{1/3}/s$. This means that the total resistance will be four times higher than skin friction (supposedly represented by M=60 $m^{1/3}/s$), and this is not an unrealistic increase in total resistance when looking at the theory for dunes, see e.g. Fredsøe (1982) and Fredsøe & Deigaard (1992).

The alluvial resistance model is still a simplification compared to using a dune model. Several problems were experienced using very strong alluvial resistance variations (large b-exponent) in which some bars, especially downstream, would be better represented, while upstream bars would grow more than observations. Also, when using the alluvial resistance model, shallow water in general, and not just bars, can develop into bars due to the variation of the resistance with depth. The van Rijn (1984) dune predictor strongly suggests that the bars should be dune covered, but only when they are sandy, and it is not known in detail which bars are sandy. The data and the experience with the alluvial resistance model suggest that bars in the downstream end are sandy, while the upstream bars are muddy, and therefore the upstream bars produce much less flow deflection, which should be accounted for.

It is possible to account for dunes only in the downstream end by using the alluvial resistance downstream and e.g. fixed Manning M upstream. However, the lack of data for the bars makes this problematic, and a model can easily become subjective due to the forced sediment composition implicitly assumed when imposing a fixed resistance model.

A.4 Flow deflection tested in a local model covering the sharpest bend

The flow deflection from bars into the deeper (outer) channels can be explained based on the following mechanisms:

- Flow resistance (topographical steering)
- 3D effects (transverse momentum convection)
- Flow separation due to the sharp bends

With the calibrated Manning M=60 $m^{1/3}/s$, topographical steering is weak, while it can be increased significantly using the alluvial resistance model.

In the following, hydrodynamic calculations are conducted for the following cases:

- MIKE 21C: Constant Manning M, 3D effect included, alluvial resistance model
- MIKE 21C versus MIKE FM
- MIKE FM 2D versus 3D

For illustrative purposes, steady state was applied with a discharge of 20,000 m^3/s and downstream water level equal to 0 mPWD.

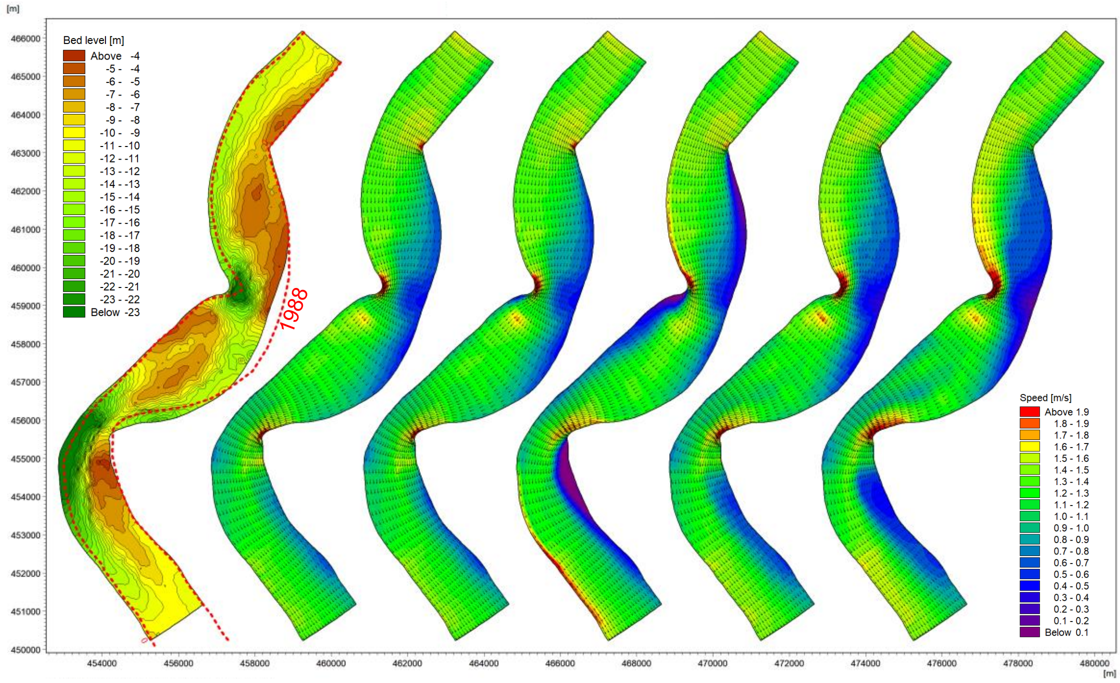

Figure A 4 MIKE 21C results (note the different colour scales for the bathymetry and speed contours). From left: 1) bathymetry, 2) Manning M=60 $m^{1/3}/s$, 3) 3D included, 4) 3D x10 included, 5) $C=25h^{0.5}$, 6) $C=12h^{0.75}$. The 1988 bank line is shown for reference (red dotted line) to illustrate the eroding and accreting banks (1988 is better graphically than 2011 and 2019).

MIKE 21C results are shown in Figure A 4. It is seen that the basic case M=60 $m^{1/3}/s$ does not deflect much flow from the bars; the highest flow velocities are in fact found on the bars. The 3D convection of momentum is very weak (higher curvature h/R but also high width to depth B/h); the effect needs to be much stronger and was increased tenfold to really see an impact, which is obviously not realistic. The alluvial resistance model needs to have a steep variation of the Chezy number with the water depth to give enough deflection (to sustain bars); b=0.5 is not enough, so b=0.75 is needed to really make a difference, but morphological simulations strongly discourage the use of such high b-exponents, as the river morphology becomes too sensitive and starts exhibiting braiding tendencies because even small bars tend to deflect the flow.

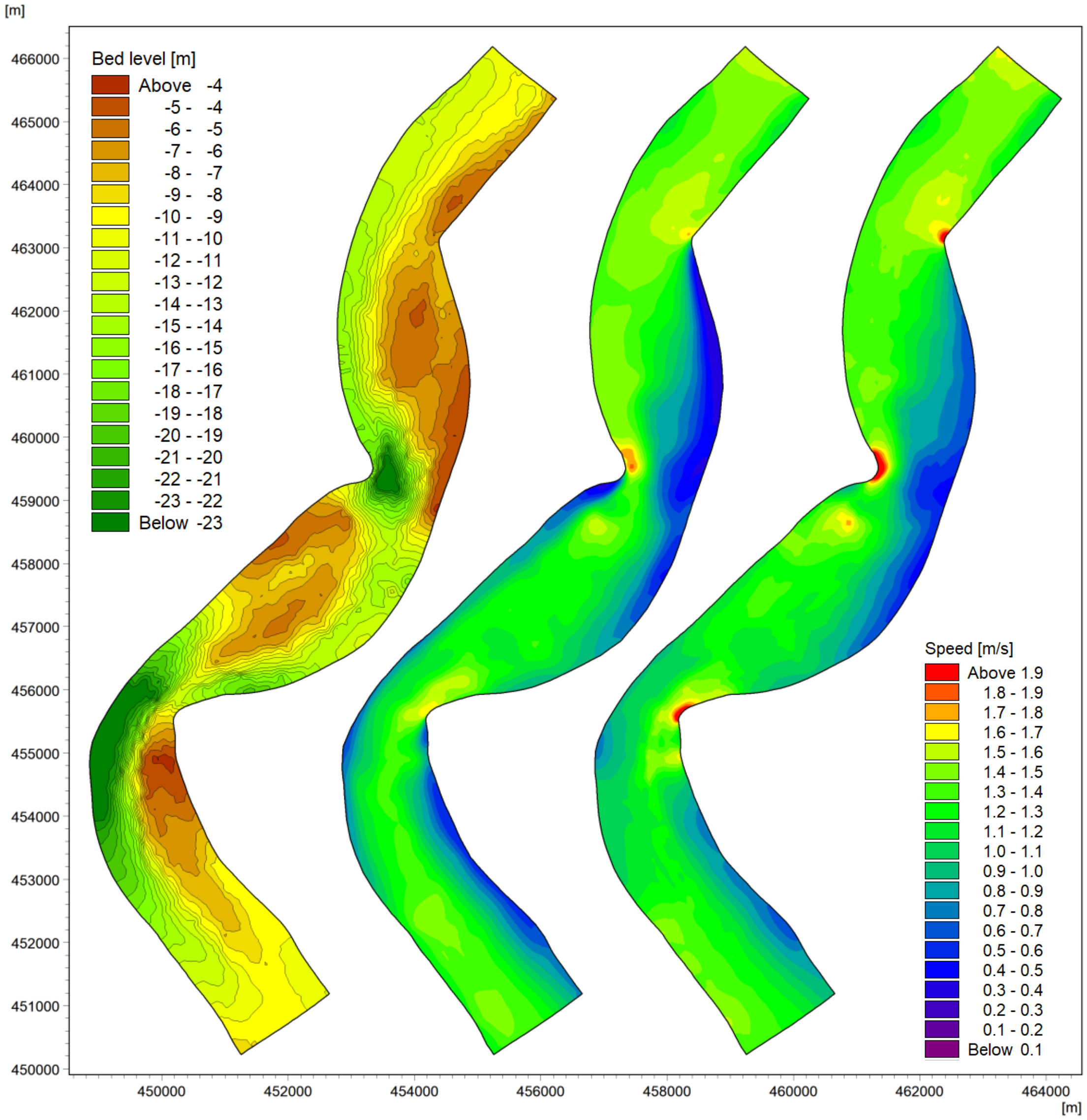

Figure A 5 Comparison of MIKE 21C and MIKE FM, showing only speed contours because the velocity vectors in MIKE FM cannot be plotted in the same manner as in MIKE 21C. From left: 1) bathymetry, 2) MIKE FM, 3) MIKE 21C.

Figure A 5 shows a comparison of MIKE 21C and MIKE FM. The results are similar, but there are also differences between the models, especially at the banks. It is not known how MIKE FM handles the friction terms at the banks, but the results imply that there is extra friction, which could originate from the schematization in the FM model. MIKE 21C does not include any sidewall friction, so the velocity cannot decrease at the bank; this effect is relatively small because the grid size is larger than the water depth (typically 30 m deep at the bank and grid size 100 m).

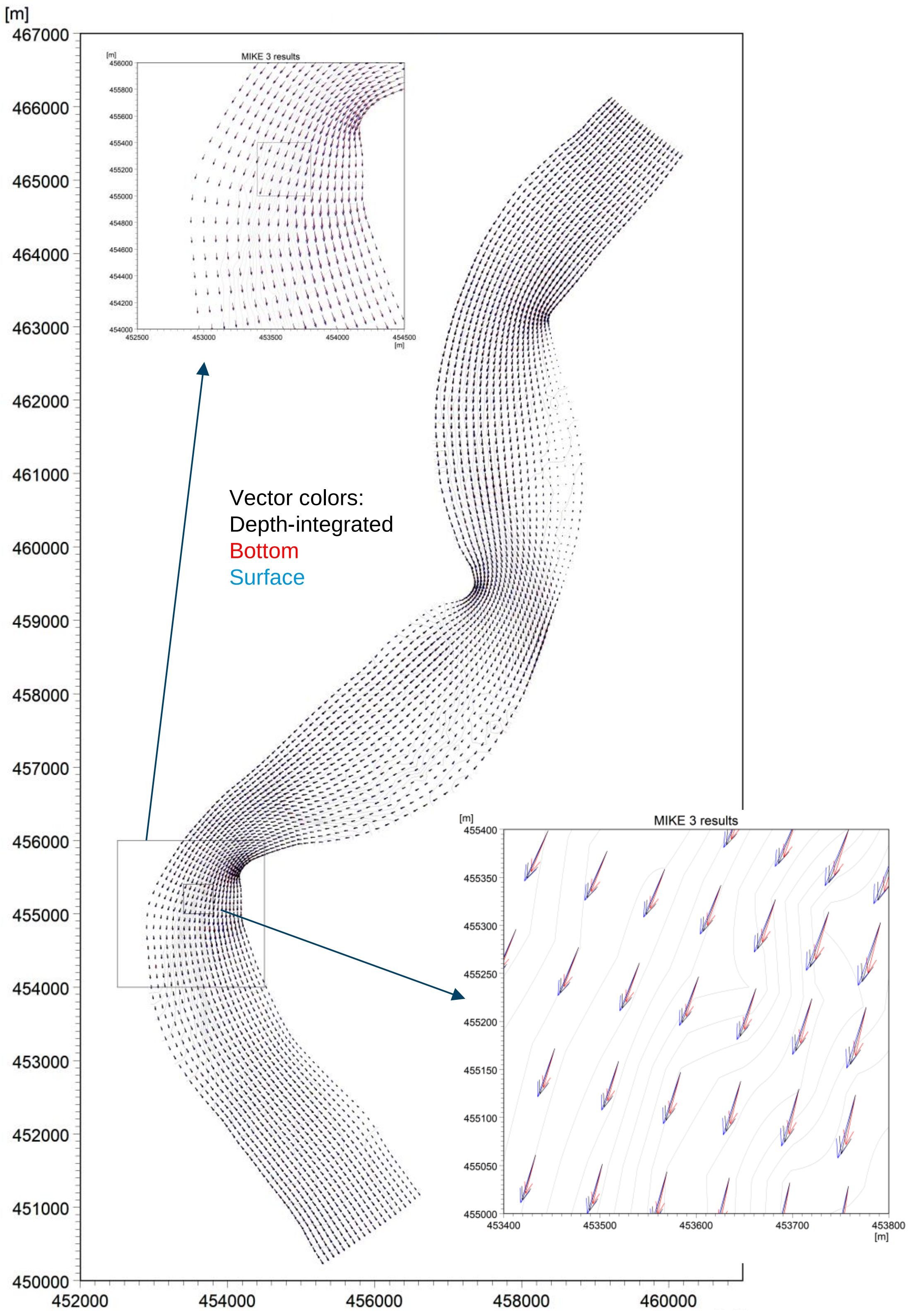

Figure A 6 MIKE FM 3D results shown with details in the bends.

MIKE FM 3D results are shown in Figure A 6. It is observed that the depth-integrated flow fields are very similar to the 3D depth-integrated solution, so the results confirm that 3D effects do not have a significant impact on the flow fields. Also note how the helical flow can be observed if zooming into the sharp bend downstream, although the flow fields must be inspected carefully.

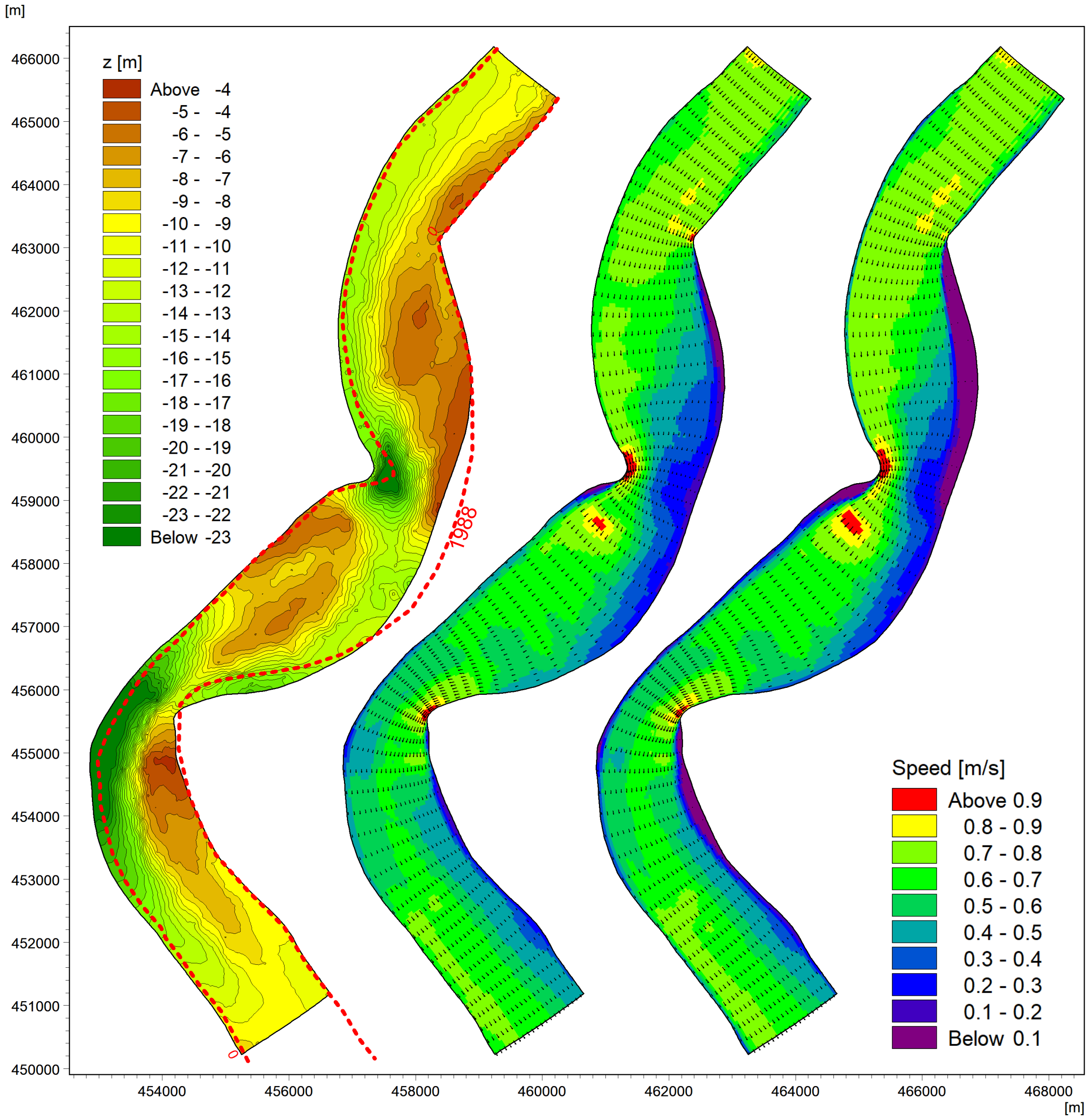

Figure A 7 Flow fields calculated on fine grids (40 grid points across) using the quasi-steady HD solver with a QUICK scheme for the convective terms (Tjerry & Fredsøe, 2005). From left: 1) bathymetry, 2) flow field, 3) flow field with sidewall friction included. The discharge was 10,000 m^3/s and the water level 0 mPWD. The red dotted line is the 1988 bank line shown for reference to highlight the eroding (and accreting) banks.

One sure way to concentrate flow along the outer bends in the sharp bend reach is by flow separation. To address this, simulations were also conducted on fine grids using a QUICK scheme for the convective terms in the quasi-steady HD solver (Tjerry & Fredsøe, 2005). It is known that flow separation can be difficult to reproduce, see Tjerry & Fredsøe (2005) and Niemann & Fredsøe (2011). To further facilitate flow separation, sidewall friction was added to represent the turbulent boundary layer (reducing near-bank momentum). By assuming that the sidewall friction has the same Manning M as the bed, the Manning M can be modified in the cell adjacent to the bank:

$$M' = M\sqrt{\frac{\Delta n}{h + \Delta n}}$$

This is a simple modification based on the total flow area including bed and sidewall, where h is the water depth in the cell and Δn the transverse grid spacing at the bank. In addition, fine grids were used to better resolve the boundary layer.

A finer grid with 40 grid cells crosswise was used, which gave down to 10 m transverse grid spacing at the bank in the deep channels just upstream of the sharp bends. With 10 m transverse grid spacing and 30 m depth (typical for the deep channels), the modified Manning M' at the bank becomes M=30 $m^{1/3}/s$, while M=60 $m^{1/3}/s$ is used for the model.

The results are shown in Figure A 7. It is observed that the velocities are reduced at the banks, while there is very little impact in the general flow pattern; the flow velocities are still very high on the bars.